HUNGARIAN AGRICULTURAL ENGINEERING

HUNGARIAN ACADEMY OF SCIENCES

Hungarian Agricultural Engineering

N° 27/2015

PERIODICAL OF THE COMMITTEE OF AGRICULTURAL ENGINEERING OF THE HUNGARIAN ACADEMY OF SCIENCES

Published by

Szent István University, Gödöllő
Faculty of Mechanical Engineering
H-2103 Gödöllő, Páter K. u. 1.

Gödöllő
2015

Published online: http://hae-journals.org
HU ISSN 0864-7410 (Print)
HU ISSN 2415-9751(Online)

PREFACE

In the name of the Comittee of Agricultural and Biosystem Engineering of the Hungarian Academy of Sciences we would like to welcome everyone who is interested in reading our journal. The Hungarian Agricultural Engineering (HAE) journal was published 28 years ago for the very first time with an aim to introduce the most valuable and internationally recognized (in these years already DOI numbered) Hungarian studies about mechanization in the field of agriculture and environmental protection. Initially the "Hungarian Institute of Agricultural Engineering" was responsible for the publication of the magazine which was mostly based on the articles and the presentations of the annually organized International Mechanization Conference. Later on – thanks to these international meetings – we were able to publish the researches of experts from different international universities. Basically we used the printed paper form to publish our journal and distributed it amongst the libraries of well-known Hungarian and international research centers and everyone who subscribed for it. In the year of 2014 the drafting committee decided to spread it also in electronic (on-line) edition and make it entirely international. After that the Szent István University's Faculty of Mechanical Engineering took the responsibility to publish the paper in cooperation with the Hungarian Academy of Sciences. Our goal is to occasionally report the most recent researches regarding mechanization in agricultural sciences (agricultural and environmental technology and chemistry, livestock, crop production, feed and food processing, agricultural and environmental economics and energy) with the help of several authors. The drafting committee has been established with the involvement of outstanding Hungarian researchers who are recognized on international level as well. All papers have been selected by our editorial board and double blind reviewed by prominent experts, which process could give the highest guarantee for the best scientific quality. We hope that our journal provides with accurate information for the international scientific community and serves the aim of the Hungarian agricultural and environmental engineering research and development - from 2015 twice a year.

Gödöllő, 20.12.2015.

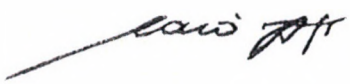

Dr. István SZABÓ
editor in chief

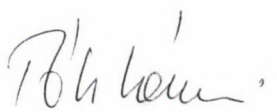

Dr. László TÓTH
editor in chief

HUNGARIAN AGRICULTURAL ENGINEERING
N° 27/2015 5-13
Published online: http://hae-journals.org/
HU ISSN 0864-7410 (Print) / HU ISSN 2415-9751(Online)
DOI: 10.17676/HAE.2015.27.5

PERIODICAL OF THE COMITTEE OF AGRICULTURAL AND BIOSYSTEM ENGINEERING OF
THE HUNGARIAN ACADEMY OF SCIENCES
and
SZENT ISTVÁN UNIVERSITY
Faculty of Mechanical Engineering

MODELLING THE STIRRING PROCESS OF BIOGAS PLANTS USING MIXED MATERIALS

Author(s):
Z. Bártfai – L. Tóth – I. Oldal – I. Szabó – J. Beke – N. Schrempf

Affiliation:
Szent István University, Faculty of Mechanical Engineering, 1.Páter K. street. Gödöllő, H2100

Email address:
bartfai.zoltan@gek.szie.hu, toth.laszo@gek.szie.hu, oldal.istvan@gek.szie.hu, szabo.istvan@gek.szie.hu, beke.janos@gek.szie.hu, schrempf.norbert@gek.szie.hu

Abstract

Among the possible energetic usages of biomass, producing biogas is the most compatible with the environment, while also ecologically correct. Fermentation technology to create biogas is mainly defined by the secondary and tertiary (leftovers and waste) biomass variants to be processed. The aftercare of such substances is required almost unilaterally, since there are environmental causes to be taken into consideration (f.e. diseases, damages to groundwater, etc.). During the process of biogas fermentation, the various substances become acceptable for environmental standards. Once the process is completed, useful heat and electric energy is produced, while fermented leftovers don't negatively impact the environment, furthermore, are in some cases, have soil enriching and reinvigorating effects.

Keywords

biogas, substrate stirring, modelling stirring method.

1. Introduction

Our research analysed a biogas plant, which has definitive differences between the variations of materials used and their relation to each other. Usually, we use primary biomass, and (secondary) waste variants from husbandry in agriculture [1, 2]. These plants operate adequately, if proper material supply is assured, since the composition of materials is static. Technology used to process excess slurry is a different group among purification establishments, where the composition of the material can be similarly standardised.

The share of slurry in the substrate of our researched object may reach up to 55-65%. Since said slurry comes from the sewage of 8-10 settlements, both the quantities and compositions of imported materials are very different. Also due to the 10-15% share of varied profile / composition foodstuff wastes, the substrate requires re-balancing.

The facility, producing ~2,0 MWp electric power is operated by a modern system. Figure 1 shows the system's structure.

The SDM container is responsible for preparing – mixing and grinding – bovine manure, which also has straw in it, and corn silage. This is where it's put into the pre-digester (FF). The primary mixing of thin manure, sully and other fluids happens in the pre-container (WM) which can be heated as well. Various foodstuffs past their expiration dates, and other waste (kitchen waste, fatty materials from cleaning, depleted oil, fats from fat collectors, etc.) go into the grinder (WM). At this place, grinding and selection of various foodstuff wrappings (W) also happens, while thin materials are lead into the autoclave, kept at 70°C at least, for sterilising purposes.

GO biogas plants always aim to produce constant electric and heat energy production, which can be calculated as early as possible, which requires constant, undisturbed gas production [3]. There exists a prior report commitment for the static quantity (for the next 24 hours) of electric energy to be transferred (scheduling), and differences are sanctioned by the Hungarian energy system, and if said difference is over 20%, a 15-18% fine in the purchase price is given [4].

These plants have to deal with various operation factors impeding gas yield, which was a result of foam in the digesters. Our goal was to increase gas yield, and get rid of the impeding factors.

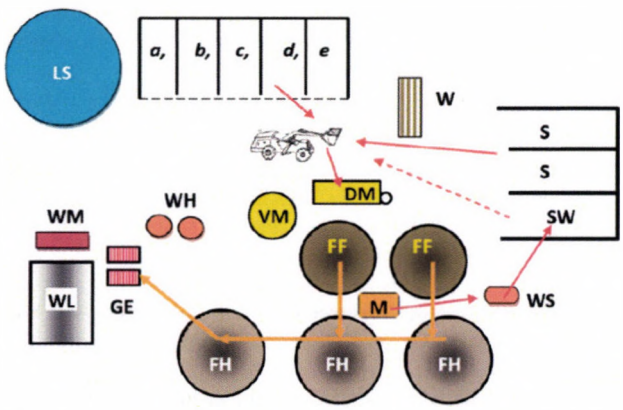

Figure 1. Arrangement of various facilities
W = Evaluation of inbound materials, a, b, c, d = Temporary containers for various materials, S = Silage container SW = Separated terminal product container, LS = Terminal containment of thin material (lagoons), VM = Pre-container and mixer for fluids, DM = Mixing, grinding and containment of dry materials, WH = Sanitizer, W = Waste container, GE = Gas-propelled blocks FF, FF = Pre-digesters, FH, FH, FH = Post-digesters, M = Suction-pump station, WS = Separator

Generally, systems using similar mixed materials and slurry have an amount of 10-15%. In our case, from an agricultural soil management, but also an energy gain perspective, using (putting in) 40-60% (non-contaminated) substance is quite descriptive [5].

In Hungary, up to 500.000 tons of slurry is generated annually, 58-65% of which goes to agriculture, 20-22% to waste dumps (depositories), 1-2% to combustion, and the remaining portion is more-or-less unknown. In 2015, 390.000 tons of slurry go to agriculture (dry materials / year, 65%). Using biogas produced by fermenting slurry, a conservation of energy can be achieved, which decreases the costs of wastewater purification. By placing the fermented slurry in the agriculture, ecologic state of soil can be improved, since minerals and trace elements needed by plant life can be used for that purpose. This is why processing sewage slurry in fermentation systems important [6]. It's obvious that getting to know, and fixing the processes and problems of fermentation improves efficiency, and soil nutrition management in agriculture acquires an important resource (147/2010. (IV. 29.) Gov. enactment.).

2. Overview of literature

The following environmental factors have an impact on methane production: substrate concentration, adaptation of bacteria, pH value, ammonia concentration, and temperature [7].

The negative impact on gas yield - which also means efficiency - is caused by both biological and technological errors, f.e. the frothing of the reactors.

If the composition of the substrate injected into the digester changes, the composition of the micro-biologic population follows suit [8]. The numbers of some micro-organisms increase and their biological activity also hastens, while other micro-organisms go through the exact opposite change. These changes may happen together with the changes in chemical and enzymatic properties of the micro-biologic population, which results in the new micro-biological population's ability to decompose the new substrate. This adaptation is not short-term, but happens over a longer timeframe, dependent on the reproduction speed of the population. If bacteria are put into a different environment, a certain amount of time passes before they adapt to the new circumstances, which is almost always longer than their generational timeframe. During the new period, bacteria adapt to the new environment (via changes in metabolism), after which they begin to reproduce again [9].

Possible reasons of errors that might come up

Kougias et al. [10] state that these problems - similarly, frothing as well - happened in the 16 facilities they analysed, to different degrees. The timeframe was usually 1-21 days, during which a gay yield loss of 20-50% was documented.

According to analyses in the Lemwig (Denmark) biogas plant, the main reason of decreased gas yield and frothing was both the composition of the substrate used and improper mixing attributes [11, 12].

Their measurements state that the bacteria colony didn't have an effect on frothing, by which they pointed out the indifference of the filamentosus (unlike other authors) in their co-substrate-based reactor. However, they also stated that other bacteria (Gordonia, Microthrix, Parvicella) can result in errors of operation with sewage slurry fermentation. Multiple authors state that the feeding overload of the reactor, and the over-production of acetyl causes f.e. intensive frothing [13], where they worked with a 10% slurry load in the substrate at best. Load was gradually increased (for about 30 days), but due to avoiding frothing, slurry was re-circulated during the putting the system in operation, and pH values were stabilised using liming.

According to McCarthy [14], slurry as a substrate has all the nutrients required for bacteria, if 60-75% of the dry material component is organic. Oláh et. al. state that putting incoming organic waste into the digesters without any prior examination has dangers, since the unknown composition may end up in overload. This overload is shown via the strong frothing and the methane content of the gas produced suffering a serious decrease, merely 30 minutes after the fact.

What sources think the reasons of reduced gas yield and frothing are, and what their solutions might be:

- If the composition and specific quantity of used organic nutrition mix is close to static, there are almost no notable problems - this results in a balanced micro-biological population (at most, for 4kg / day / m3 reactor volume) [15].
- The C / N ratio is important, since to build proteins, nitrogen is required. If there's not enough nitrogen, the amount of carbon processed decreases, and if there's too much, there will be too much ammonia, which inhibits methane generation. A C / N value of 15-30 litres is optimal, which can be set via properly mixing the base materials [15].
- The optimal pH value of bacteria causing hydrolysis or fermentation is 4,5-6,3, and 7-7,5 for methanogens (a value below 6,8 in digesters might be a bad impact) [13].
- By mixing the material properly, we can improve effectiveness, and the efficiency of fermentation [16].
- If there's an erratic temperature change in the substrate, methane production decreases, and this common temperature difference breaks biochemical equilibrium [9].
- The optimal environment for mesophile bacteria is at 35-40°C. This temperature has to be kept stable in the entire reactor.
- The most important factor is the dry component ratio, which defines the system's load. Quantity and concentration both define the proper input data.
- Organic volatile acid content has to be monitored at all times, just like HCO3 content and its ammonium ion concentration. Keeping the volatile acid content below 1000mg of acetyl / l average is optimal [15].
- The FOS / TAK value is usually optimal at 0,3-0,4 kg in the reactor (however, it can only be defined via frequent system-specific, longer duration measurements). The value is between 0,2-0,3 in the post-digester and the lagoons. A FOS / TAK value below 0,2 signifies that not enough organic material is present, however, if it goes above 0,4, there's too much organic material [17].

By checking the presented data [18], and incorporating them, the system can be stabilised, but will worsen, if the system requires mandatory changes due to mechanical errors, or transport times of materials are delayed, mixing – after input, or in-between – isn't done, etc.

3. Source and method

Requirements of input

The technology took using various materials into consideration, the composition of which may differ during transport. Variations used continually and always:

- Silo corn,
- Bovine manure,
- Thin manure,
- Sewage slurry* (from 12 sources, in different compositions).

Less frequent materials:

- Foodstuff leftovers,*
- Oil- and fat slurry,*

–Foodstuffs over expiration date (meat, chips, ice cream, etc.),*
–Depleted oil, and oil past expiration date.
* Note: quite different, with unknown composition when arriving.

To keep efficiency as good as possible, the manager can set the composition in the pre-mixer using the data he got from composition estimations before input, while the reactor substrate's temperature and composition spread can only be influenced with the inner mixers. As for the latter, it has to be taken into consideration during planning, meaning the system's specs define f.e. the level of grinding, the equality in composition spread for the entire inner area, and the same for temperature homogeny [19, 20].

We can create "recipes" for input, meaning we can almost completely optimise the composition (CN ratio, pH value, FOS / TAK, etc.) [21].

Attributes of sewage slurry types

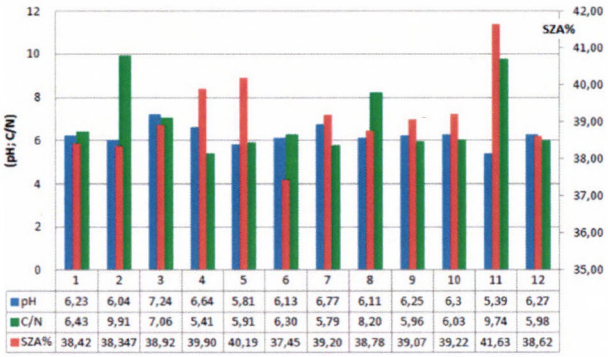

	1	2	3	4	5	6	7	8	9	10	11	12
pH	6,23	6,04	7,24	6,64	5,81	6,13	6,77	6,11	6,25	6,3	5,39	6,27
C/N	6,43	9,91	7,06	5,41	5,91	6,30	5,79	8,20	5,96	6,03	9,74	5,98
SZA%	38,42	38,347	38,92	39,90	40,19	37,45	39,20	38,78	39,07	39,22	41,63	38,62

Figure 2. Dry material content, pH value and C / N ratio of the 12 sewage slurry samples (avg. values)

The samples arriving from 12 different places were analysed, some of the more important results are shown in Illustration 3. The dry material volume in some samples are quite different, but the carbon amount for dry material is roughly the same [22, 23]. The biggest problem is that some samples have quite the different pH values, and the C / N ratio is also quite varied, which have to be equalised by other materials, which however generates other imbalances to equalise in turn (Figure 2). There was a substantial difference in energy volume of some samples. A higher energy content means in a lower ash content, which showed some samples held a high amount of minerals, probably due to the mechanical errors in the water purifier's sand partitioning systems.

Heavy (granular) minerals cause an efficiency decrease in stirring, increase energy requirement, and lead to the wearing of blades due to their quick decanting. Manure which contains straw also has a high concentration of sand, which doesn't only cause blades to wear, but does the same to the percussion hammers of the grinding machine, and due to their wearing, the grinding effect decreases almost to zero, thereby resulting in long straws (cellulose) entering the reactor, where they stick to the blades, reducing their stirring effect, or even causes the blades to break in some cases [24].

The efficiency of stirring was evaluated with samples from before and after said stirring happened (temperature, pH value, amount of organic material), but we didn't see any big differences, which is why we ran a check on the stirring system, its arrangement, and level of activity.

Stirring system

Requirements of proper management [25, 26, 27, 28, 29]:

A Adding thicker or thinner material has to allow setting the density for the entire mass.
B A static pH value and temperature level has to be possible for the entire volume (making heat extractable from the heating bodies, and evenly distributable).
C Micro-organisms have to be in a forced connection with the nutrients.
D The entire volume is effective, there aren't any so-called dead spaces. Material components which inhibit the process have to be thinned.
E The decanting of the substrate isn't allowed, which homogenises nutrition content.
F. Materials which change position relative to each other leave the bacteria, enter the gas material, and cause bubbles to appear via their so-called velocity shear.

Stirring possibilities [3]

– Via mechanical method (various bladed mixers),
– Via recirculation of the entire substrate and fluid phase, including the slurry (fluid beam made via pumps),
– Via gas bellowing (layer swap),

Biogas plants use various mechanical mixers. There are two common variations shown on Illustration 3.

A

B

Figure 3. A - horizontal axis, spiral bladed mixer, B - slanted axis propeller mixer

Solution at the analysis' site

There are four mixers found in the pre-digesters, and three in the post-digesters at the complex we analysed. The stirring process

is more important at the pre-digesters, meaning analysing and modelling was done for that one. As for the pre-digesters, there's 1800-2000 tonnes of material in case of an 80% load, to which adding 14-20 tonnes of extra material doesn't cause a substantial increase in temperature (0,6-0,8oC) in either spring or autumn, but not even in summer. Even for the non-extraordinary winter season, the difference isn't that much, if the heating system operates properly (1,0-2,0oC). In case of a lower outside temperature, even 6-8oC isn't that unusual after input.

The cross-section of the pre-digester, and the three variable and one fixed mixers can be seen on Figure 4, 5 and 6.

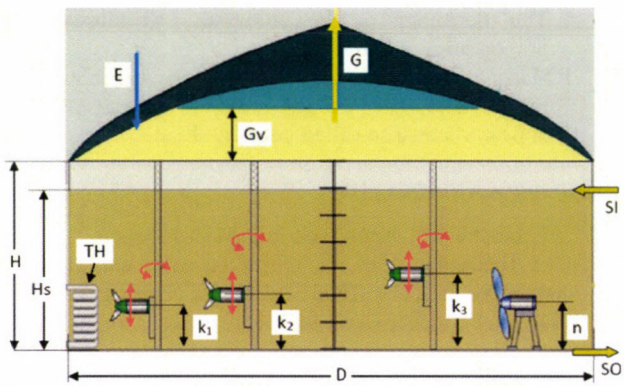

Figure 4. Mixers of the digesters
Abbreviations: D –diameter of the reactor, H – height of the reactor wall, Hs – height of suspension in the reactor, TH – tube heating on the walls, E – entry of air, area of removing sulphur, G – gas drain, Gv – gas volume and its changes, SI – substrate input, SO – substrate output, k_1, k_2, k_3 – mixers with variable height and angle, n – fixed big mixer.

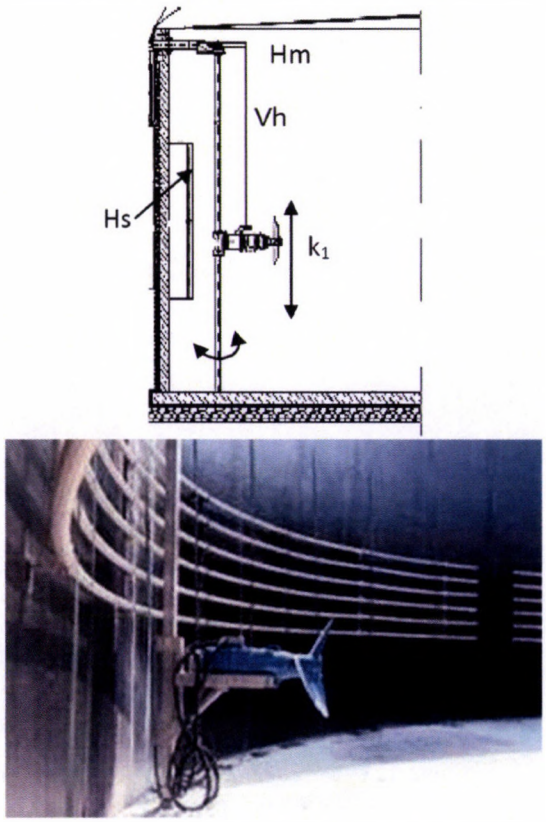

Figure 5. Small mixers (k_1) and installation scheme
Vh – vertical setting, Hm – horizontal setting, Hs – heating tubes

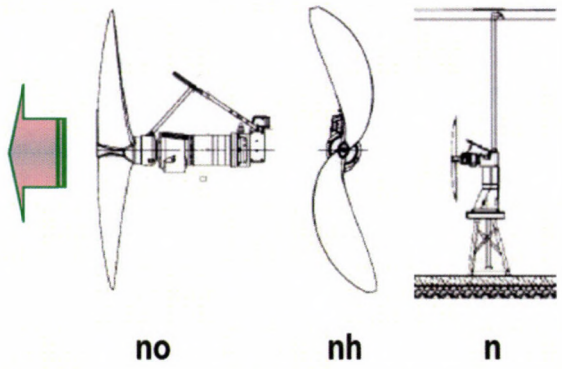

Figure 6. Large-diameter fixed mixer
no – large mixer (side view), nh - large mixer (front view), n – large mixer installation schematic

How substrates react to stirring

The substrates in the reactor can be considered viscous fluids if they contain 10-14% of organic matter. In the case of viscous fluids' flow, fluid parts which have a difference in velocity cause shear stress (Figure 7). In case of continuously parallel flow fluid layers, there's an inner friction force (F) contradictory to the direction of movement, which is directly proportional to the area sizes (A) causing the friction (moving on each other), and the velocity gradient (du/dy). The ratio factor is none other than the static describing the material quality of the fluid, in other words, the dynamic viscosity (η = Pa s):

$$\eta = \frac{A}{F}\frac{du}{dy}$$

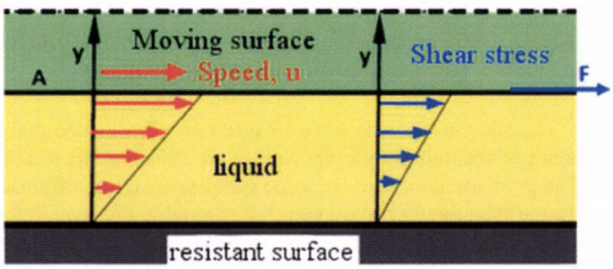

Figure 7. Description of the shear stress
(u - velocity, y – fluid thickness)

Using the F/A physical quantity, we can write shear stress using the law τ, [N/m^2]:

$$\tau = -\eta\frac{du}{dy}$$

Where the velocity gradient, or velocity shear [s^{-1}] is as follows:

$$\dot{\gamma} = \frac{du}{dy}$$

Newton's viscosity law states that the shear stress between various layers is directly proportional to the velocity gradient. This isn't directly proportional in case of non-newtonian fluids, meaning there's a more complex formula between shear stress and velocity gradient.

Dynamic viscosity (η) can be defined as the quotient of shear stress and velocity shear [kg m^{-1} s^{-1}, or Pa s]:

$$\eta = -\frac{\tau}{\dot{\gamma}}$$

Therefore, shear stress in the fluids depends on the shear gradient. This function is directly proportional for Newton's and Bigham's fluids, but non-newtonian fluids give a convex or concave function, in other words, different to linear change.

Materials which have about 10% dry material content used by biogas fermentation aren't Newton's fluids, and are rather pseudo-plastic in nature. Maier et al. [29] analysed a substrate, for which velocity shear was reduced by an increase in viscosity. The shear factor exists due to the interaction between the fluid, and the hard molecules in the material. Molecules often break the continuity of the flow, which impact the mixing of various elements. Björn et. al. [30] state that the reactor substrates' dry material content, dynamic viscosity and their related factors offer no easy to state relation, while rheological attributes are important for the efficiency of mixing. Getting to know these relations is important when designing mixing systems. In the case of sewage slurry variants, raising the dry material content also increases the limit of dynamic viscosity, the rate of which depends on the size of granules in the material, to be precise, their increase causes a decrease in said statistics. Sinking due to granule size has an effect on velocity shear, and the rate of material stirring.

Homogeny is dependent not only on the attributes of the fluid, but also the configuration of the tank, and the attributes of mixer performance [21].

When viscosity increases, the velocity shear gradient usually follows suit. In the case of lighter material parts, a greater decrease in viscosity is required, compared to more heavy ones, to breate the same velocity gradient. However, the behaviour of the sediment and the slurry showed differences (Figure 8).

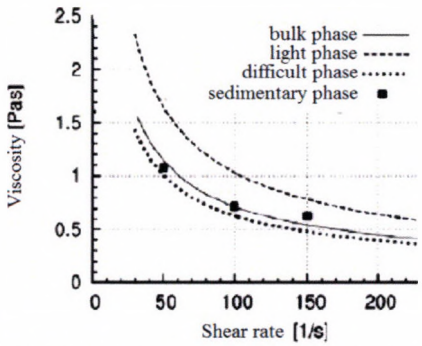

Figure 8. Relations between viscosity and velocity shear [4]

Shear performance is related to performance put into stirring, which means the values of velocity shear are greatly dependent on the attributes of the mixing machinery (drive performance, peripheral speed, shape attributes).

As for a different analysis, in case of given materials and also taking various consistencies into consideration, running the simulation on relations resemble Figure 9.

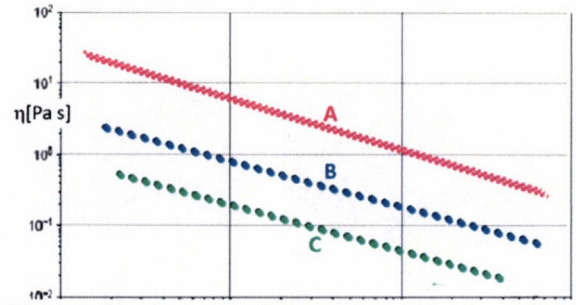

Figure 9. Rheological attributes of the substrate according to measurements of designated materials by the Oswal-de Waele relation (logarithmic scale) [25] Materials being: A- corn silage, B – sewage slurry, C - organic waste

According to the processed sources, we can state that materials in the biogas digesters can be defined by three phases: light (ascending), heavy (sinking), and floating (colloid and smaller) granules. The proper homogeny of these three attributes inside the internal volume - taking the whole mass into consideration - can only be maintained via stirring.

To reach a favourable gas yield, there are huge differences in both the number of times stirring is required, and the timeframe of stirring for the various reactor types and mixer solutions (according to authors researching the topic). The general practice is to stir 3-6 times a day, 0,5-3 hours each.

4. Model analyses

In the system we selected to model, by rotating the 3 small mixers (k), we see the activation area by moving it to the maximum value (R), and the theoretic motion volume by moving the conical beam (RSn). Similarly, there's a static fluid beam in the case of the big mixer (n) (Figure 10).

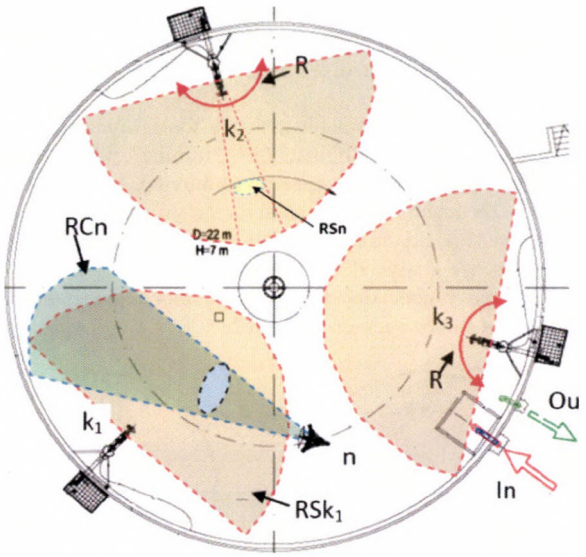

Figure 10. Arrangement of mixers, and effect areas in the pre-digester k1, k2, k3 – variable height and angle mixers, n – fixed big mixer, R – level and direction of rotation, In / Ou – input and output of substrate, RSk – area of effect for small mixers (only as an indication), RCn – conical area of effect of the big mixer, RSn – conical area of effect of the small mixers

We chose the CFD method to model, while taking the framework conditions obtained by the measurements, and possible solution methods into considerations [14]. The viscosity of the "mixture" in the biogas reactor, which has a 10-12% dry material content is 300-1000fold compared to that of water at 20°C, 1,0020 cP, which means it's 300-1000 cP, meaning 0,3-1,0 Pa.

Of course, realistic circumstances differ greatly, since the material isn't homogenous, it contains both bits and pieces, and fibrous parts.

In our first approach, we did the calculations with water, to get the flow directions and movement data of water molecules at various mixer positions without any disturbance. This means the models didn't designate velocity values as important, but instead focused on the movement of the matter molecules compared to each other in space. Figure 11 shows possible main positions.

According to the illustration:

– mixers k_1. k_2 és k_3 were defined by 9 basic positions each (3 height – v_1-v_3 – and 3 heights each - h_1-h_3).

– Each could take either position not related to each other, but altogether, all triad positions have to be different. This makes the number of possible configurations 9×8×7=504.

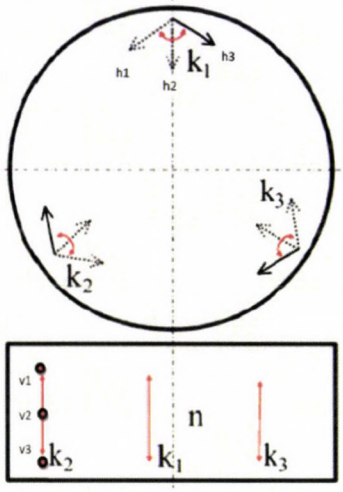

Figure 11. Small (k) and large (n) mixers (the position of which can't be changed, it's installed in a static manner)

If we chose different positions to the designated ones, the number of possible combinations is "infinite", which is why we analysed the ones most specific to stirring, by giving border values. The results were checked for the suspension forecast, and an extra 10% dry material content as well. After running the program, we analysed 192 variations (for the given viscosity, water, and higher density). The positions presented in our document can be seen on Figure 12.

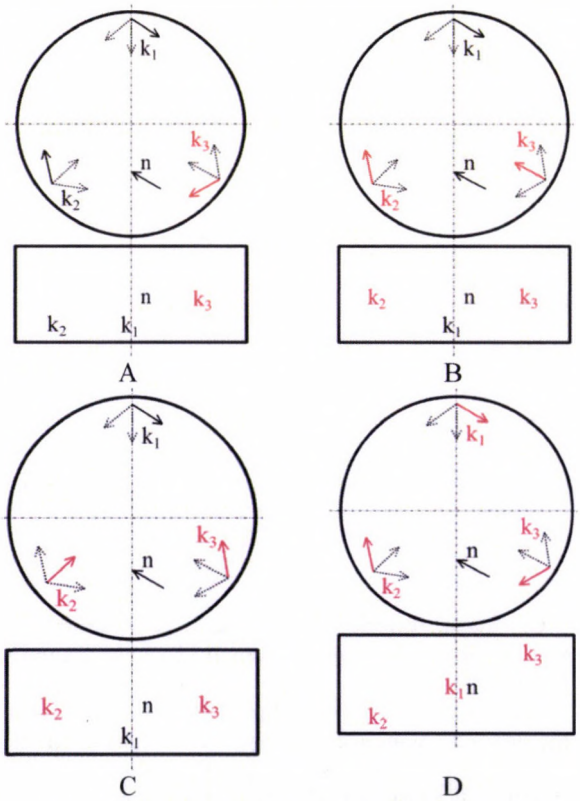

Figure 12. Blade positions selected for showing the model ("with border values")

A All (k) mixers stirring in the same direction, one in middle height.

B One (k) mixer down, two in mid-height, one stirring radially.

C One (k) mixer down, two in mid-height, but different directions, one stirring radially.

D All three in different heights, but stirring in the same direction.

Velocities in the direction of the flow are presented on Figure 13, 14, 15, 16.

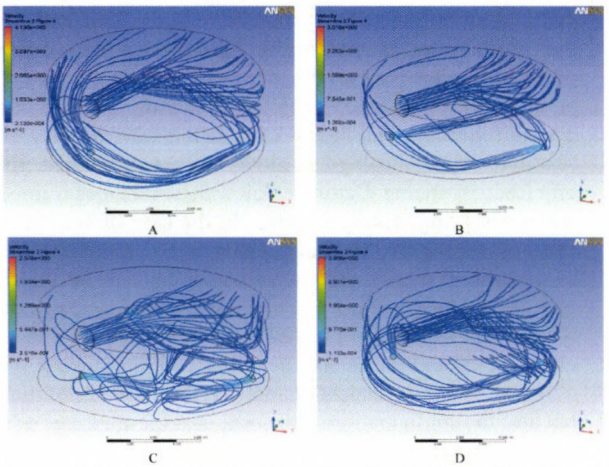

Figure 13. Velocity starting from the mixers, in the direction of the flow Highest value is for A (1-2m/s), lowest for C (~0,0 m/s)

The velocity lines of the big mixer extend to the wall facing it, and generate an upward draft after crashing into it. The small mixers generating the other flow are concentrated near the wall if the transport is in a single direction, and only turn towards the surface in case of a crash. Facing flows are impossible to calculate, and becomes chaotic. Radial guidance helps the flow upward, but isn't beneficial for heat exchange, since their flows don't reach the wall.

Flow on the upper and lower levels of the fluid

After analysing these layers, variations A and D are more beneficial, since there's a balanced, and sufficient flow circling around the wall, meaning heat exchange for heating is beneficial. However, inside the planes, intensity is higher, and areas almost static are less in number. Variation C isn't recommended, since movements satisfy almost no requirement at all.

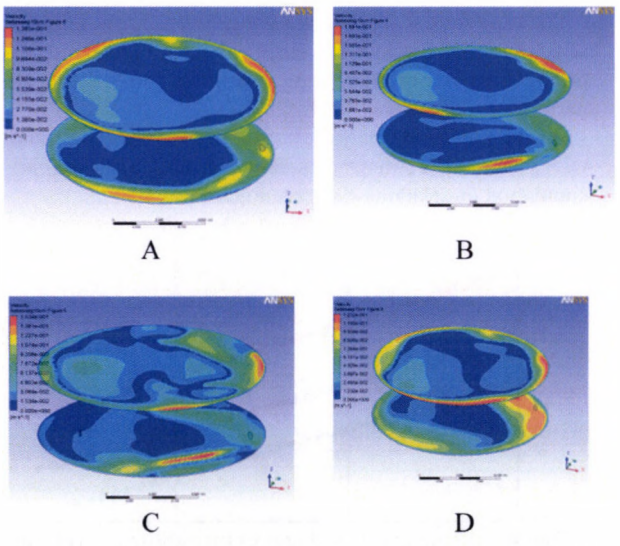

Figure 14. Motion deciphered in an area for the 0,1m surface and lower level plane of the material inside the reactor Highest velocity: 1,8m/s Lowest velocity: ~0,0m/s

Our notes for the upper and lower planes are supported by the section in the middle area as well. The consistent flow near the walls is the most important here, since the heating pipe system is also at this height (see Figure 5 above).

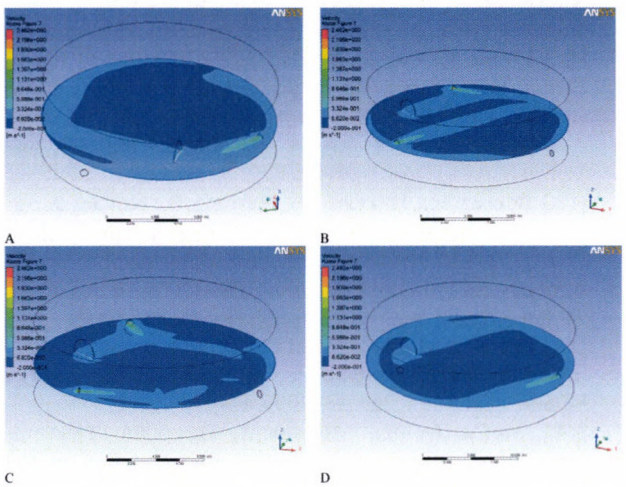

Figure 15. Motion deciphered in the horizontal middle plane of the material inside the reactor

Highest velocity: on the blade's deformed side ~2,1-2,6 m/s, and 2-3 meters away from the blades (directly after the blade, it reaches up to 4,0 m/s). Lowest velocity in the flow is ~0,12m/s.

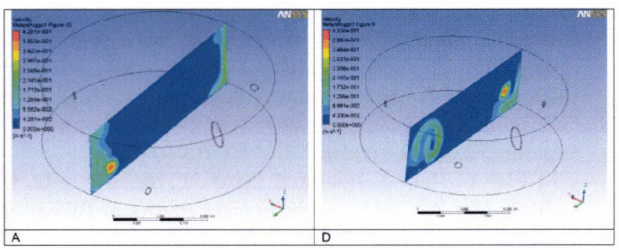

Figure 16. Motion deciphered in the vertical middle plane of the material inside the reactor

Variation A shows the most beneficial movement on vertical sections, which shows that there's intensive movement near the heat exchanging walls. This has an importance in the winter season, when outside temperature is low, and the material put in follows suit, and a need for intensive heating, and heat exchanging arises. Variation D shows an intensive vertical whirlpool, which extends to the wall at variations C and B more, while at A, less. The highest velocity can be observed on the blade's deformed side - ~2,1-2,6m/s - which remains even 2-3m away from the blades. The lowest velocity is ~0,2m/s.

5. Results

Main conclusions:

- The total amount of material in the digesters can't be put into motion consistently in the current system. Theoretically, there's no need to do so, since heat exchange near the heat expending surfaces can only be done with a stronger material flow.
- Due to incorrect stirring directions set in the system, masses not in motion can also develop meaning there's a need to validate beneficial variations suggested by the modelling, via inserting thermometers.
- The timeframe of stirring cycles, their number and intensity can only be validated by measuring gas yield.
- It seems to be obvious that after the material input, a more intensive stirring period is required, which can be realised by raising the rotational speed of the mixers, or in other words, improving the transport mass-flow. Keeping the higher intensity isn't required, since life support of the methanogene bacteria is reduced by a higher velocity shear between matter molecules. More intensive stirring also helps in creating thermal homogeny of the material mass, and shortening the time needed for general homogeny. To reach this effect, it's important to supply the mixers with rotation frequency adjusters, which makes it possible to get close to optimal material movements.
- Time required for stirring increases, and requires more energy consumption, if the substrate contains much more dense granulates. In the case of sewage slurry, transportation companies should check the proper operation of sand partitioning systems.
- The optimum of time spent between stirring tasks can only be set via evaluating gas yield.

First actual plant results to validate calculations and modelling

While doing experiments for 5 months, we were trying to – as much as we were able to – reach the best mix for input, and match stirring to the model. This was often problematic to do professionally, due to mechanical errors, constipations, and the fact that some materials weren't present when they were required. As for the latter, we can learn that there should be capacity to stock up, which can help avoid errors due to lack of materials, meaning we should make materials always ready to use.

The amounts (m^3) of materials put in from the 3 main points of input were shown on Figure 9. The pre-container serves to provide mainly thin manure, sewage slurry, and materials used to thin taken from the lagoons. The mass input changes, since separation also happens, and equalising the separated mass' volume happens from the pre-container. The quantity of this volume is a fundamentally defining factor for the system. The silo and straw manure is put in from the dry grinder, and sometimes, the quantity of fermented and separated dry material (in smaller quantity) can be kept constant. The Higi (AC) area offers input for various foodstuff waste in sterilised form, and the materials contained in the fat container (their percentage isn't that high though).

As a result of model-like implementation, the gas yield for nutrients put in was improved. Electric and heat energies were taken into consideration in a 40/60% ratio (Figure 17). During almost 3 months, the volume of energy increased from 61,2% to 68,7% (Table 1). This proves that our thoughts were correct. By improving the stirring, efficiency will probably improve even further.

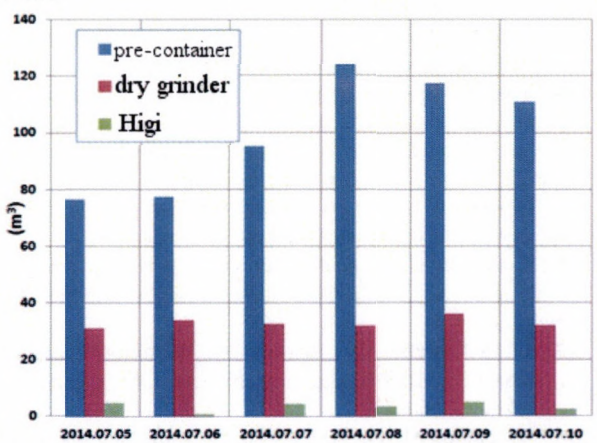

Figure 17. Current load on the system regarding electric energy

Table 1. The Volume of Energy

Internal performance of the generator P_m [MWh/month]	Energy derived from nutrients ** $[P_{t2}]$[MWh/month]	Energy derived from nutrients * $[P_{t1}]$[MWh/month]
1480,56	1 017,6	916,2
	$(P_{t2}/P_m)100$	$(P_{t1}/P_m)100$
100%	68,7%	61,2%

Notes: * input farther from the recipe
** input closer to the recipe

6. Conclusion

Our article showcased how one element of a biogas plant works. These plants will be more and more typical as we see them, since it's both a government aim, and the European Union also supports biogas plants linked to sewage water purifiers. The plant can be built right on the purifier's grounds (using mixed materials), but it's beneficial to build it in the vicinity of multiple purifiers, which are similar to the one we introduced in our article. Usually, the biggest management problem is the varied physical nature of incoming materials, and the differences in content of various transported goods. Operations without problems can only work if so-called "input recipes" are made for the materials, which are selected by the most important parameters (shown in our research). Consequent input and stirring (homogenising) improves the gas yield by nutrients on average (m3/kg). Hungary produces up to 500.000 tonnes of sewage slurry, only 20% of which is delivered to a biogas facility for fermentation (most of it is poured into deponies), while anaerobic fermentation is the most optimal, and ecologically beneficial solution, since energetic end products (electricity, heat) are not the only benefits - another example would be bio-manure useful for soil management.

Acknowledgements

This work was supported by: TÁMOP 4.2.2.D-15/1/Konv-2015-0011 számú "Interdiszciplináris nemzetközi kutatói teamek létrehozása Békés megyében" (Creating inter-disciplinary international research teams in Békés county)

References

[1.] Bayerische Landesanstalt für Landwirtschaft (LfL).: 2006. Biogastechnologie zur umweltverträglichen Flüssigmistverwertung und Energiegewinnung in Wasserschutzgebieten

[2.] Tóth L., Fogarassy Cs.: 2012. Low-carbonenergiaellátási rendszerek a gyakorlatban. A megújuló energiatermeléstechnológiái Magyarországon. Szaktudás Kiadó Ház Zrt., Budapest, 2012 ISBN:978-615-5224-37-9 p. 112-156

[3.] Berglund M., Börjesson P.: 2006. Assessment of energy performance in the life-cycle of biogas production, Elsevier, Biomass and Bioenergy Volume 30, Issue 3, March 2006, pp 254–266. http://dx.doi.org/doi:10.1016/j.biombioe.2005.11.011

[4.] Tóth L. -Beke J - Sembery P. - Hajdú J.: 2012. The role of biomass in Hungarian energy supply, Hungarian Agricultural Research, Journal of the Ministry of Rural Development Hungary, Vol. 21, Nr. 4. ISSN 1216 4826. 14-19 p.

[5.] Domahidy L. Gy.: 2013 A szennyvíziszapra vonatkozó hazai szabályozás tervezett változtatásai Budapest

[6.] Kovács et all.: 2003. A szennyvíziszap-kezelés és hasznosítás jogi, gazdasági, műszaki, környezetegészségügyi feltételrendszere.

[7.] Oláh J., Palkó Gy., Szilágyi M., Barabás Gy., Gyarmati I., Tuba L.: 2010 Rothasztók üzemeltetése, Magyar Szennyvíztechnikai Szövetség

[8.] Gerardi, M. H. 2003. The Microbiology of Anaerobic Digesters, John Wiley & Sons, Inc., Publication, 11 – 57

[9.] Gruber, W. 2007. Biogasanlagen in der Landwirtschaft. Aid infodienst Verbraucherschultz, Ernährung, Landwirtschaft e.V. Bonn. 1453.

[10.] Kougias P. G., Boe K., Thong S. O, Kristensen L. A. and Angelidaki I.: 2014. Anaerobic digestion foaming in full-scale biogas plants: a survey on causes and solutions, ISWA publishing

[11.] Loum A., Fogarassy Cs.: 2015. The effects of climate change on cereals yield of production and food security in Gambia. Applied Studies in Agribusiness and Commerce – APSTRACT Vol. 9. No. 4. pp. 83-92. http://dx.doi.org/10.19041/APSTRACT/2015/4/11

[12.] Borocz M., Horvath B., Herczeg B., Kovacs A.: 2015. Greener cement sector and potential climate strategy development between 2015-2030 (Hungarian case study). Applied Studies in Agribusiness and Commerce – APSTRACT Vol. 9. No. 4. pp. 65-74. http://dx.doi.org/10.19041/APSTRACT/2015/4/9

[13.] Boe K. et al.: 2008 Serial CSTR digester configuration for improving biogas production from manure. Water Research Volume 43, Issue 1, January 2009, Pages 166–172

[14.] McCarthy K., Murphy J. D.: 2005. The optimal production of biogas for use as a transport fuel in Ireland Renewable Energy, Elsevier Volume 30, Issue 14, November 2005, Pages 2111–2127. http://dx.doi.org/doi:10.1016/j.renene.2005.02.004

[15.] Zehnsdorf A., L. Moeller , K. Görsch, V. Beer. Bernburg.: 2010. Schaumbildung in Biogasanlagen, Hemholtz, Zentrum für Umweltforschung UFZ, 30. November

[16.] Shen Fei; Tian, Libin; Yuan, Hairong; Pang, Yunzhi; Chen, Shulin; Zou, Dexun; Zhu, Baoning; Liu, Yanping; Li, Xiujin.: 2013. Improving the Mixing Performances of Rice Straw Anaerobic Digestion for Higher Biogas Production by Computational Fluid Dynamics (CFD) Simulation, Applied Biochemistry & Biotechnology; Academic Journal. EBSCO Publishing is a division of United States, Vol. 171 Issue 3, p 626 http://dx.doi.org/doi:10.1007/s12010-013-0375-z

[17.] Tóth L., Beke J., Bártfai Z., Szabó I., Hartdégen G., Oldal I., Blahunka Z.: 2014. Technological Features of Biogas Plants Using Mixed Materials, HUNGARIAN AGRICULTURAL ENGINEERING, N° 26/2014 39-46, Published online: HU ISSN 0864-7410 (Print) / HU ISSN 2415-9751(online) http://dx.doi.org/doi:10.17676/hae.2014.26.39.

[18.] Esteves S., Miltner M., Fletch S.: 2013. Folyamatos ellenőrzési útmutató a biogáz és biometán üzemek megfelelő működtetéséhez, Intelligent Energy Europe

[19.] Banks C. J., Chesshire M., Heaven S., Arnold R.: 2011. Anaerobic digestion of source-segregated domestic food waste: Performance assessment by mass and energy balance Bioresource Technology, Volume 102, Issue 2, January 2011, pp.612–620. http://dx.doi.org/10.1016/j.biortech.2010.08.005

[20.] Fantozzi F., Buratti C.: 2011 Biogas production from different substrates in an experimental Continuously Stirred Tank Reactor anaerobic digester.

[21.] Seyssiecq I., Ferasse J. H., Roche N.: 2003. State-of-the-art the rheological characterization of waste water treatment sludge. Biochemical Engineering Journal, Vol.16, pp. 41-56. http://dx.doi.org/doi:10.1016/s1369-703x(03)00021-4

[22.] Fogarassy Cs., Horvath B., Kovacs A.: 2015. Cross-sector analysis of the Hungarian sectors covered by the Effort Sharing Decision – Climate policy perspectives for the Hungarian agriculture within the 2021-2030 EU programming period. Applied Studies in Agribusiness and Commerce – APSTRACT Vol. 9. No. 4. pp. 17-24. http://dx.doi.org/10.19041/APSTRACT/2015/4/2

[23.] Fogarassy Cs., Horvath B., Szoke L., Kovacs A.: 2015. Low-carbon innovation policy with the use of biorenewables in the transport sector until 2030. Applied Studies in Agribusiness

and Commerce – APSTRACT Vol. 9. No. 4. pp. 45-52. http://dx.doi.org/10.19041/APSTRACT/2015/4/6

[24.] Wu B.: 2013. Advances in the use of CFD to characterize, design and optimize bioenergy systems. Computers and Electronics in Agriculture 93(0), 195-208. http://dx.doi.org/doi:10.1016/j.compag.2012.05.008

[25.] Brehmera M., Kraumea M.: 2012. Mixing Performances In Biogas Plants, Technische Universität Berlin, 14th European Conference on Mixing, Warszawa, 10-13 September.

[26.] Kaparaju P., Buendia I., Ellegaard L., Angelidakia I.: 2008. Effects of mixing on methane production during thermophilic anaerobic digestion of manure: Lab-scale and pilot-scale studies, Bioresource Technology Volume 99, Issue 11, pp. 4919–4928. http://dx.doi.org/doi:10.1016/j.biortech.2007.09.015

[27.] Kardos L.: 2012. A szennyvíztelepi biogáz termel_ fermentációs folyamatok nyomonkövetése kémiai és biokémiai módszerekkel Eötvös Loránd Tudományegyetem, Természettudományi Kar, Bp. Környezettudományi Doktori Iskola pp. 113-114.

[28.] Lindmark, J., Thorin, E., Bel Fdhila, R., Dahlquist, E.: 2014. Effects of mixing on the result of anaerobic digestion: Review. Renewable and Sustainable Energy Reviews 40(0), 1030-1047. http://dx.doi.org/doi:10.1016/j.rser.2014.07.182

[29.] Maier C., Weichselbaum W., Schlerka M., Harasek M.: 2010 Development of Agitation Systems in Biogas Plants: Investigation of Mixing Characteristics, Improvement of Energy Efficiency and Scale-up using CFD Getreidemarkt 9/166-2, 1060 Vienna, Austria www.aidic.it/cet/10/21/200.

[30.] Björn A., Segura de La Monja P., Karlsson A., Ejlertsson J., Bo J., Svensson H. B.: 2012. Rheological Characterization, Biogas, ISBN: 978-953-51-0204-5, InTech, http://dx.doi.org/doi:10.5772/32596

HUNGARIAN AGRICULTURAL ENGINEERING
N° 27/2015 14-19
Published online: http://hae-journals.org/
HU ISSN 0864-7410 (Print) / HU ISSN 2415-9751(Online)
DOI: 10.17676/HAE.2015.27.14

PERIODICAL OF THE COMITTEE OF AGRICULTURAL AND BIOSYSTEM ENGINEERING OF
THE HUNGARIAN ACADEMY OF SCIENCES
and
SZENT ISTVÁN UNIVERSITY
Faculty of Mechanical Engineering

THE ADAPTABILITY OF DISCRETE ELEMENT METHOD (DEM) IN AGRICULTURAL MACHINE DESIGN

Author(s):
Á. Kovács – K. Kotrocz – Gy. Kerényi

Affiliation:
Department of Machine and Product Design, Budapest University of Technology and Economics, Műegyetem rkp. 3., Budapest, H-1111, Hungary

Email address:
kovacs.adam@gt3.bme.hu, kotrocz.krisztian@gt3.bme.hu, kerenyi@eik.bme.hu

Abstract

This study focuses on the adaptability of discrete element method (DEM) in agricultural machine design.

Laboratorial three point bending, compression and dynamic cutting tests were conducted to define the main mechanical parameters and behaviour of corn stalks.

For the DEM simulations of the laboratorial tests Timoshenko-beam bonded model was selected. With modifications of the geometry structure and the input parameters of the contact model, during an iteration process, the right assembly was found.

The findings of the study clearly demonstrate that DEM capable of simulating the interactions, among the plants, the parts of the machine, and the appeared loads during agricultural processes.

Keywords

DEM, maize, stem, agricultural machine design

1. Introduction

The increasing demand for high-quality agricultural products presents a big challenge for the developers of agricultural machinery. Due to the seasonal nature of agricultural products in situ tests of new constructions are limited in time and often prove to be very expensive. In the field of agricultural machine design numerical methods are not available which could properly replace field tests.

The utilization of corn plants and crops is remarkable worldwide, the corn production in the world is almost 1000 million tons. In 2014 almost 10 million tons of corn were harvested by farmers in Hungary (HCSO, 2015), which demonstrates the significance of the plant in the agriculture of the country.

This study focuses on the adaptability of discrete element method (DEM) in agricultural machine design in connection with maize product.

The paper builds around a literature review on the industrial or agricultural applications of the discrete element method. DEM is used to investigate bulk agricultural materials widely.

Keppler et al. calibrated the micromechanical parameters of a sunflower DEM model based on odometer tests so that the model can sufficiently approach the macro mechanical behaviour of the real bulk material. [1.] Földesi et al. investigated the pressure relations of an oil press by DEM simulations. [2.]. Tamás et al. examined the soil-tool interaction and the relations in cohesive soil by using the DEM [3.].

In connection with string materials fewer literature can be found. Kemper et al. investigated the iteration among grass stalk and rotation mower by DEM [4.].

To calibrate a DEM model, in situ and laboratorial test are indispensable. Qin Tongdi et al. investigated the effect of different production fields on three point bending behaviour of the same maize species [5.]. Sun Zhong-Zhen et al. examined the effect of moisture content on three point bending behaviour of maize stalks [6.]. M. Azadbakht et al. accomplished in situ dynamic cutting test by a modified Charpy impact test to analyze the resistance against dynamic cutting force of maize stalks [7.].

Based on the findings, the agricultural product (maize) and its typical loads (compressive, three point bending loads and dynamic cutting) were determined giving the research a more concrete and better focus.

2. Material and methods

Discrete element method (DEM) is developed to investigate bulk materials which contains separate parts. The definition of a DEM model is the following [8]: It contains separated, discrete particles which have independent degrees of freedom and the model can simulate the finite rotations and translations, connections can break and new connections can come about in the model.

Based on harvest and product processes of mature maize stalks the main loads of the stalk were determined. Root, leaves and ears of the plant were neglected in our study. First of all the physical properties of the stalks (mass, length, diameter, shape) were measured and noticed. After that laboratorial three point bending, compression and dynamic cutting tests were conducted to define the main mechanical parameters and behaviour of corn stalks.

The examination of the available contact models was the first step of the modelling. After that the models were compared and the Timoshenko-beam bonded model, which is based on the Timoshenko-beam theory, was selected for the study.

In the next step the possible DEM geometry formations of the real plant geometry was analysed. To select the right geometry model that can simulate the mechanical and physical properties and behaviour of the plant most accurately, DEM simulations of the laboratorial tests were conducted.

With modifications of the geometry structure and the input parameters of the contact model, during an iteration process, the right assembly was found.

3. Measures

For the measures the maize stalks were divided in determined parts. The first node above the air root was marked 1st node and after the first node the first internode was marked 1st internode. Following this logic the entire stalk was divided as seen on Figure 1.

Before each measure the necessary specimens were prepared. During the preparation leaves and ears were pruned from the stalk and after that the necessary physical parameters were measured. Finally the stalks were cut to the right size for the mechanical measures.

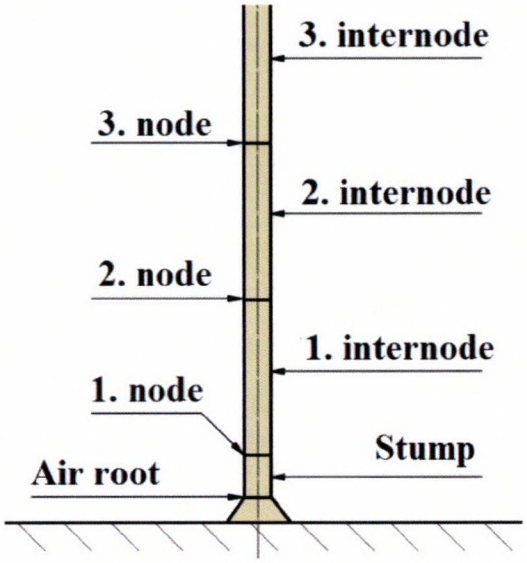

Figure 1. Dividing of the maize stalks

Analyses were conducted for the first internode so hence the results of the study are in relation to the first internode.

During the measurement of the physical parameters 8 plants were investigated. Moisture content, diameter, length and mass of the first internode were measured (Table 1.).

Table 1. Physical parameters of the first internode

Parameters	Results
Average moisture content	64,67 %
Average diameter	24,80 mm
Average length	120,63 mm
Average mass	42,52 g

The aim of the three point bending test was to define the resistance against bending of the first internode. During the measure a zero point was defined by touching the specimen with the bending tool. Then the crosshead of the machine was moved with 200 mm/min to 50 mm displacement. Five specimen were measured, the results were calculated with statistical methods from the measured data (Figure 2.) in order to calibrate the DEM model of the first internode. The bending diagram has three different sections: the linear section where the relation is linear among the force and displacement, the contraction section where the diagram reaches the maximum force and the bended cross-section of the internode is flattening, and finally, the plastic joint section where the bended cross-section is crashed so the resistance against the bending is decreasing gradually until the end of the bending test.

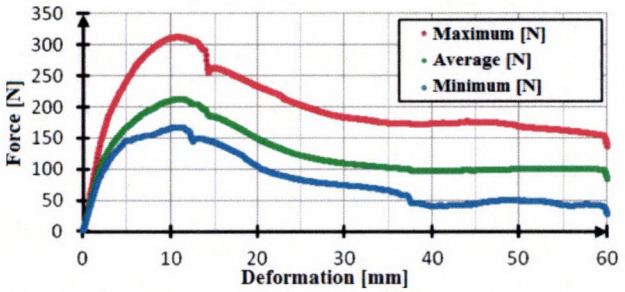

Figure 2. Three point bending test results of the first internode

The aim of the compression test was to determine the side pressing resistance of the first internode and the crossway and residual sideway deformation over the stalk length. After the prepared specimens were placed in the clamp jaws the crosshead of the machine compressed them with 100 mm/min pace. Five specimens were measured, the aim of the evaluation was to determine an average deflection - resistance force diagram to calibrate the DEM model of the first internode (Figure 3.).

On this figure two different sections can be observed: the constant section which goes up to 30% deflection where the resistance force is close to constant, the exponential section that goes from 30% to 75% deflection where the resistance force is exponentially increasing.

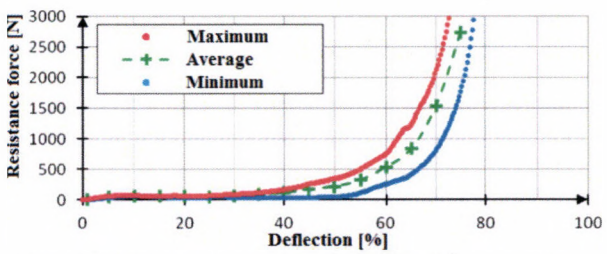

Figure 3. Compression test results of the first internode

The aim of the dynamic cutting test was to determine the cutting work of the first internode. A Charpy impact test was revised for the measurement by a special cutting blade and fixing apparatus (Figure 4.). The position of the gripper and the cutting apparatus was adjusted to minimize the gap among the cutting edge and the fixing apparatus. After a specimen was fixed the test was carried out with 3,47 m/s cutting speed. Five specimens were investigated, and based on the evaluation of the results the average cutting work was 17,57 J.

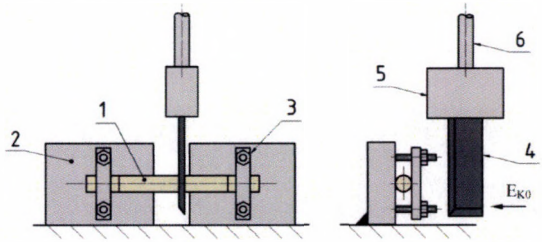

Figure 4. Sketch of dynamic cutting test (1: Measured sample 2: Stalk gripper 3: Fixing unit 4: Cutting blade 5: Blade gripper 6: Flywheel arm)

4. Physical model of corn stalk

In the geometry model of the first internode the following neglects were used: the shape of cross-section was a standard circle instead of an ellipse, over the length of the internode the

size of the cross-section was constant, any other special feature of the internode was also neglected.

The smallest unit of the DEM geometry model is the particle. Basically this unit in the EDEM 2.7 software has a sphere shape but any special shapes can be created through the combination of the different spheres. For a better distribution of the external loads the shape of the bark was chosen for a cylinder that is made up by two sphere shapes (Figure 5. a.). For determining different cross-sections in the pith simple spheres were used (Figre 4. b.).

The size of the particles were based on the measured size of the plant and the geometry structure of the DEM geometry. The radius of the spheres was chosen for r=2,57623 mm in consideration of the high accuracy.

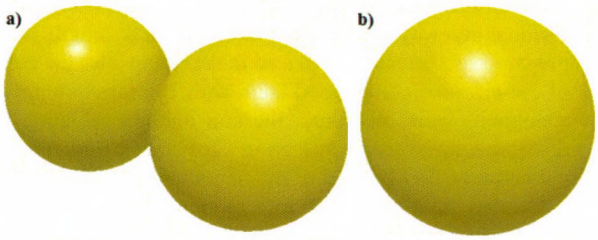

Figure 5. a) Shape of the particles in the bark b) Shape of the particles in the pith

The second largest unit of the geometry is the module that consists of a couple of particles in a determined structure (Figure 6.). The particles of the bark (light and dark green particles) have a special offset structure similar to a fastener to better disperse the external loads to the particles of the pith. The particles of the pith (yellow and orange particles) formed segregated cross-sections side by side.

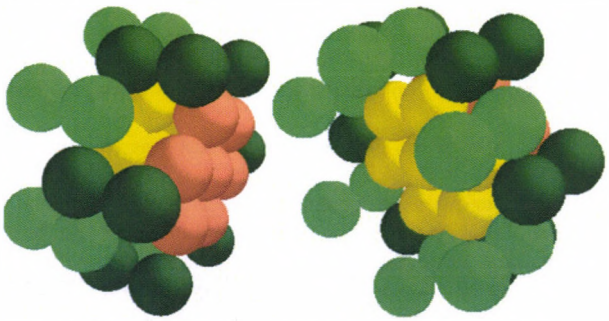

Figure 6. The geometrical structure of a module

The complete geometry model of the internode, which represents a standard cylinder geometry, is built up from several modules one after the other (Figure 7.).

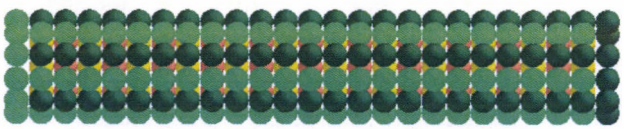

Figure 7. DEM geometry model of the first internode

5. Connection system of the model

Different connections were determined in axial and tangential directions of the bark and the pith, and another connection was defined between the pith and the bark.

The particles in the pith and in the bark have different mechanical parameters (Table 2.).

Table 2. Mechanical parameters of particles

	Particles of bark	Particles of pith
	P1&P2	P3&P3
Poisson's ratio [-]	0,25	0,25
Shear stiffness [Pa]	1,00E+08	1,00E+06
Density [kg/m^3]	2650	2650

During an interaction among the different particles of the stem or among the particles and the parts of the geometry special connection parameters were defined (Table 3.).

Table 3. Mechanical parameters of interactions

	Among particles of stem	Among particles of stem and geometry
Coefficient of friction [-]	0,3	0,3
Coefficient of rolling friction [-]	0,01	0,01
Coefficient of restitution [-]	0,5	0,5

In the bark in tangential (P1:P2) and axial direction (P1:P1 & P2:P2) different connections were defined to simulate the different behaviour of the stalk in these directions. (Figure 8.) (Table 4.).

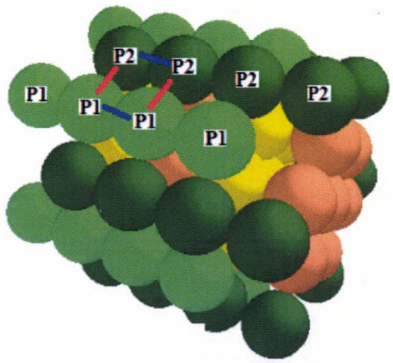

Figure 8. Connection model of the bark

Table 4. Mechanical parameters of connections among the particles of bark

	P1:P1 P2:P2	P1:P2
Coefficient of damping [-]	0,5	0,5
Young-modulus [Pa]	1,00E+08	1,00E+08
Poisson's ratio [-]	0,15	0,15
Max. compression stress [Pa]	7,50E+06	3,75E+06
Max. tension stress [Pa]	10,00E+06	5,00E+06
Max. shear stress [Pa]	5,00E+06	2,50E+06
Coefficient of variation [-]	0	0
Radius multiplicator [-]	1,00	1,00

In the pith in tangential (P3:P3 and P4:P4) and axial direction (P3:P4) similar different connections were defined to simulate the different behaviour of the stalk in these directions. (Figure 9.) (Table 5.).

For the better load distribution in the model a connection was defined among the particles of the pith and the bark (P1:P3; P2:P3; P1:P4; P2:P4) (Figure 9.) (Table 6.).

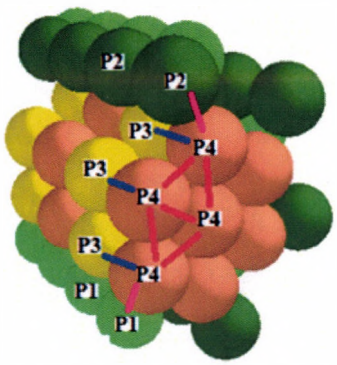

Figure 9. Connection model of the pith

Table 5. Parameters of connections among the particles of pith

	P3:P4	P3:P3 P4:P4
Coefficient of damping [-]	0,5	0,5
Young-modulus [Pa]	1,00E+07	1,00E+06
Poisson's ratio [-]	0,15	0,15
Max. compression stress [Pa]	2,00E+07	1,00E+04
Max. tension stress [Pa]	3,00E+07	1,00E+06
Max. shear stress [Pa]	1,50E+07	5,00E+05
Coefficient of variation [-]	0	0
Radius multiplicator [-]	1,00	0,50

Table 6. Parameters of connections among the particles of pith and bark

	P1:P3 P2:P3 P1:P4 P2:P4
Coefficient of damping [-]	0,5
Young-modulus [Pa]	1,00E+08
Poisson's ratio [-]	0,15
Max. compression stress [Pa]	1,30E+07
Max. tension stress [Pa]	2,00E+07
Max. shear stress [Pa]	1,00E+07
Coefficient of variation [-]	0
Radius multiplicator [-]	0,50

6. Results

The model was evaluated with quantitative and qualitative evaluation methods. With the quantitative method the real measure diagrams were compared with the simulation diagrams. With the qualitative method cross-section deformations, crashes, breaks of the model were compared with the measured experiences of the real specimens.

The result from the three point bending simulation test is shown on Figure 10. The sudden changes of the diagram came from the DEM geometry, because the sudden connection breaks and sudden movements of the particles resulted in the observed changes on the chart. From this reason a sixth grade polynomial trend line was fitted on the results to correct the sudden changes (Figure 10). The simulated results are between the minimal and maximal results of the measure. The linear section, the contraction section and the plastic joint section of the simulation data approached the measured data very well.

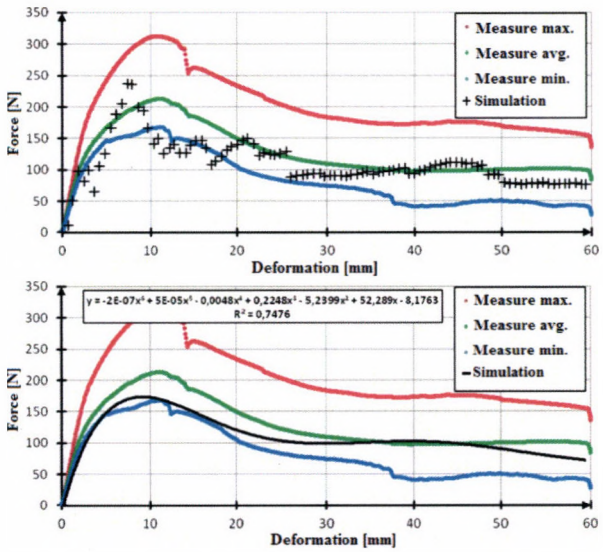

Figure 10. Results of three point bending test simulation

The simulation data of the compression test are above the measured data of the real specimens (Figure 11.). To fit an exponential trend line it was necessary to create an average point of the gradually increasing sections of the data. These data approach the measured data from above up to 60% deflection, then a nearly vertical section of the chart can be observed that is sharper than the measured characteristic.

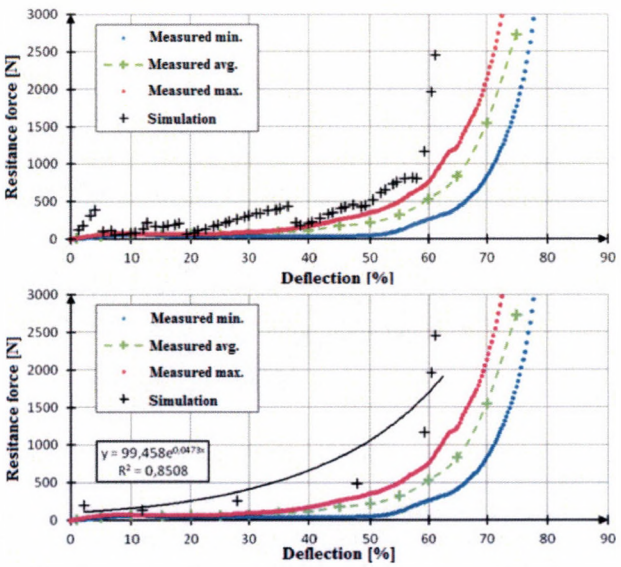

Figure 11. Results of compression test simulation

The simulation result of the dynamic cutting is a cutting force – time chart as opposed to the results of the measures (Figure 12.).

To compare the different results the area, that is limited by the data points, was calculated by the classic trapeze integration rule and was multiplied by the constant cutting force (3,47 m/s). The simulated dynamic cutting work was 19,15 J, so the difference from the measured results is only 9%, which is a very good accuracy.

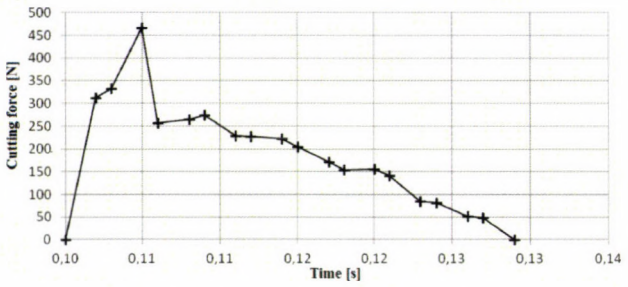

Figure 12. Result of dynamic cutting simulation

During the qualitative evaluation of the three point bending moment the deformation of the cross-section under the bending edge and the residual deformation were analyzed.

The bended cross-section deformation of the model approaches the real deformation of the internode very well, however the simulated deformation is less than the real deformation (Figure 13.).

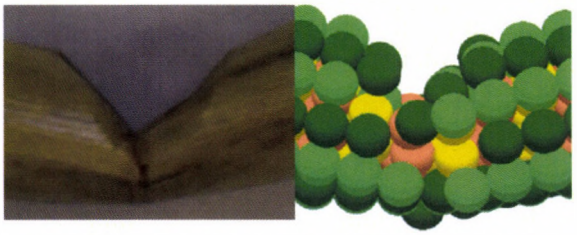

Figure 13. The real and simulated bended cross-section deformations

The residual deformation of the model approaches the real deformation of the internode well, but the simulated internode is demaged during the simulation (Figure 14.). The right side of the simulated internode was cracked in axial direction and thanks to this the threads of the pith appeared. This phenomenon wasn't observed during the measures.

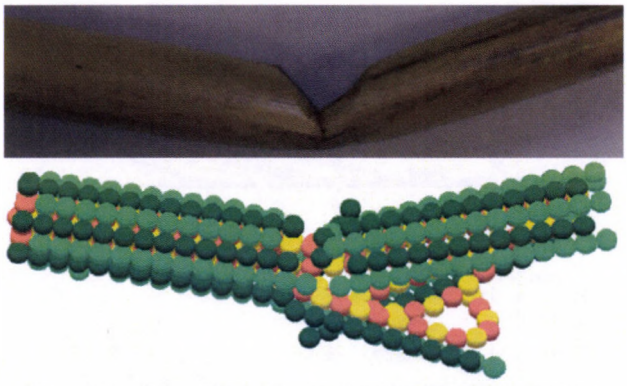

Figure 14. The real and the simulated residual deformations

During the qualitative evaluation of the compression test the deformations and the damages of the cross-section were analyzed.

The deformation and condition changes of the simulated internode appeared earlier during the compression process and were more effective (Figure 15.). On the first picture the initial conditions can be observed. On the second figure the deformation of the simulated internode is bigger than the real observed but the crashed condition of the two samples is the same. On the last figure huge deformations can be noticed in connection with both internodes, but the crashed condition of the simulated sample is completely different. During the real compression test the bark is still embracing the pith during the whole test, but in the simulation the bark is crashed and from this reason the geometry structure completely broke and the functions of the bark were lost. In this case the behaviour of the model internode during the compressing test is still acceptable.

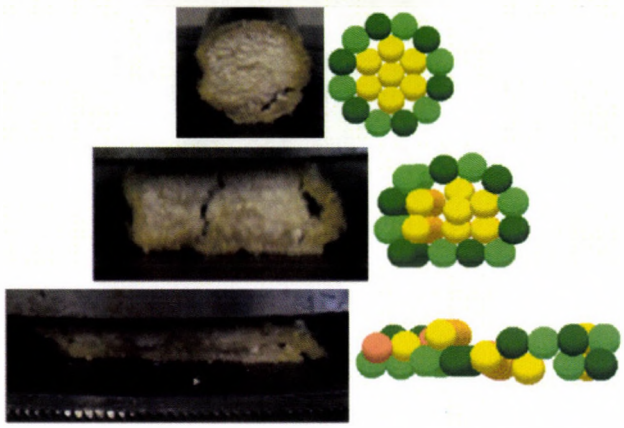

Figure 15. The real and simulated compression process of the first internode

During the qualitative evaluation of the dynamic cutting test the cutting surface was analyzed.

Due to the geometry structure of the model (fastener structure of the bark) the perfectly flat cutting surface cannot be expected. Even so the simulated cutting surface converged the real surface very well (Figure 16.). The threads of the bark show crashed behaviour similar to the real internode and the pith demonstrate a perfectly flat, straight cutting surface. Thanks to the structure of the bark several particles flew off due to the strong impact.

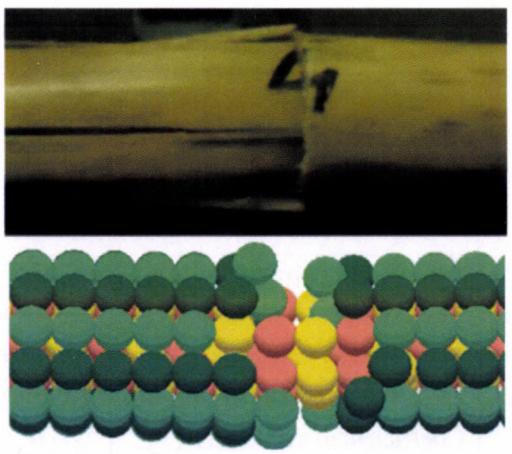

Figure 16. The real and the simulated cutting surface

5. Conclusion

The DEM model of the first internode, which is based on the Thimoshenko beam theory, showed reassuring results in connection with the three point bending, compression and dynamic cutting test. The quantitative and qualitative evaluations

clearly demonstrate that the discrete element method (DEM) is capable of simulating the interactions, among the plants, the parts of the machine, and the appeared loads during agricultural processes.

To increase the accuracy of the simulations a viscous-elastic connection model is essential to simulate the real relations between the stress and strain conditions and the changing of the Young-modulus during the simulations.

Acknowledgements

We would like to thank Katalin Gaál from the Institute of Agricultural Engineering at Gödöllő, Dr. Gábor Szebényi from the Department of Polymer Engineering at BUTE, Dr. Imre Obrulov from the Department of Material Science and Engineering at BUTE and Dr. Tibor Poós from the Department of Building Services and Process Engineering at BUTE for their valuable and constructive help.

References

[1.] Keppler I. Kocsis L., Oldal I., Csatár A.: 2011. Determination of the discrete element model parameters of granular materials, Hungarian Agricultural Engineering, No 23/2011, pp.30-32, HU ISSN 0864-7410

[2.] Földesi B., Rádics J. P., Tamás K., Jóri I. J.: 2011. Determining pressure relations of vegetable oil press using discrete element method simulation, Hungarian Agricultural Engineering, No 23/2011, pp. 33-36, HU ISSN 0864-7410

[3.] Tamás K., Jóri. J. I.: 2011. 2D DEM simulation of the soil-tool interaction in cohesive soil, Hungarian Agricultural Engineering, No 23/2011, pp. 45-49, HU ISSN 0864-7410

[4.] S. Kemper, T. Lang, L. Frerichs.: 2014, The overlaid cut in a disc mower – results from field tests and simulation, Landtechnik 69(4), pp. 171-175, ISSN 0023-8082

[5.] Tongdi Q., Yaoming L., Jin C.: 2011. Experimental study on flexural mechanical properties of com stalks, New Technology of Agricultural Engineering (ICAE), 2011 International Conference on. pp. 130-134, http://dx.doi.org/doi:10.1109/ICAE.2011.5943766

[6.] Zhong-Zhen S., Huan-Xin J., He-Ping C., Qiu-Sheng Y., Li-Xin L., Li W., Guo-Lin C..: 2013. The Viscoelasticity Model of Com Straw under the Different Moisture Contents, Mathematical Problems in Engineering, Volume 2013. http://dx.doi.org/doi:10.1155/2013/320207

[7.] M. Azadbakht, E. Esmaeilzadeh, M. Esmaeili-Shayan.: 2015. Energy consumption during impact cutting of canola stalk as a function of moisture content and cutting height, Journal of the Saudi Society of Agricultural Sciences, Vol. 14, Issue 12, pp. 147-152. http://dx.doi.org/doi:10.1016/j.jssas.2013.10.002

[8.] Cundall P. A., Hart R. D.: 1992: Numerical modelling of discontinua. Engineering Computations, Vol. 9, Issue 2, pp. 101-113. http://dx.doi.org/10.1108/eb023851

HUNGARIAN AGRICULTURAL ENGINEERING
N° 27/2015 20-23
Published online: http://hae-journals.org/
HU ISSN 0864-7410 (Print) / HU ISSN 2415-9751(Online)
DOI: 10.17676/HAE.2015.27.20

PERIODICAL OF THE COMITTEE OF AGRICULTURAL AND BIOSYSTEM ENGINEERING OF
THE HUNGARIAN ACADEMY OF SCIENCES
and
SZENT ISTVÁN UNIVERSITY
Faculty of Mechanical Engineering

CHANGES OF METHANE CONTENT OF LANDFILL GAS WITH REGARD TO DIFFERENT WIND SPEED INTERVAL

Author(s):
T. Molnár – F. Farkas

Affiliation:
University of Szeged Faculty of Engineering, Technical Institute
Mars str. 7., 6724, Szeged, Hungary

Email address:
molnart@mk.u-szeged.hu, farkasf@mk.u-szeged.hu

Abstract

In the recent years in Hungary the continuous increase of solid waste, as a result of private consumption, has become a serious issue. In Hungary currently about 23 million m3 solid urban waste is formed annually. Sixty-two percent (62%) of this waste is household waste and the remaining is waste produced at institutions or service providers which can be treated together with the household waste. Waste management plays a key role in the quality of environment, protecting natural resources and developing environmental security. There can be two basic environmentally harmful effects of waste disposal. The problem of landfill gas from the decomposition of communal waste got into the focus of attention since it was proved that on the Earth the natural and anthropogen methane and the carbo-dioxide emmission contribute to the so-called glass-house effect [1, 2].

Keywords

landfill gas, methane content, wind speed interval, greenhouse gas.

1. Introduction

The quality and quantity of biogas presumably depends on the weather parameters of the refuse dump, the technical parameters of the bio gas recovery system and the organic matter content, typical of the Hódmezővasárhely region. Because of that our objective is to define the the quality and quantity parameters of landfill gas at the refuse dump with regard to the weather parameters, operational factors and the organic matter content. In accordance with the assumption environmental impact can influence directly or indirectly the quality and quantity parameters of the produced landfill gas. Besides the examination of the connection between environmental conditions and gas production it is appropriate to examine the organic matter content of the waste as legal requirements regulate the biodegradable proportion of it. Our objectives are the following under the following headings:

The current relevance and significance of the topic is that by the use of modern, state-of-the-art techniques in accordance with EU standards, we could use alternative forms of energy instead of fossil energy sources for both electric and thermal energy production which has both economic and environmental benefits [3, 4, 5, 6].

2. Material and methods

The communal solid waste refuse dump of the „A·S·A Hódmezővásárhely Köztisztasági Ltd." Is located on the outskirts of Hódmezővásárhely on the area No. 01957/1. The refuse dump is situated south of Hódmezővasárhely, west of no. 4414 road, about 5-6 kilometres from the centre. In terms of public service obligation the communal solid waste of Hódmezővásárhely and six other settlements is taken to the refuse dump (Mindszent, Mártély, Földeák, Békéssámson, Nagyér), its area of responsibility is 100.000 people [7, 8, 9, 10].

The elements of landfill gas extracting system are the following: gas wells, gas collecting pipes, gas controller unit, compressor unit, torch, container with gas engine, meteorological station. The collection of landfill gas is with the help of gas wells.

At the beginning there were low drainage gas wells used at the refuse dump but because of their sinking and deformation the effectiveness of gas extraction was impeded. They converted to upper drainage gas wells which are only built after the dump is completely filled or reached a certain height. It does not interfere with the operation and good quality landfill gas is attainable [11, 12, 13].

When preparing the measuring system three measuring points were established (Figure 1.) Measuring point 1 is the two measuring cones, one for measuring the applied depression [mbar] and the other is for measuring the quality compound of the landfill gas (methane [%], carbon dioxide [%], oxygen [%]) and the opening angle of the sluice valve [°]. Measuring point 2 is situated at the vacuum pump. Pressure values can be measured in front of and behind the pump, and thus the amount of the pressure difference can be calculated. [8, 9]. From the pressure difference flow rate of the extracted landfill gas without pipe friction can be calculated and then, with the pipe diameter, the amount of the produced landfill gas. Measuring point 3 is located at the meteorological station of the refuse dump. It provides the weather parameters: tk: external temperature [°C], φ: air humidity [%], vsz: windspeed [m/s], h: rainfall intensity [mm/day], Ph: local atmospheric pressure (QFE).

Evaluating data, statistical methods, measuring instruments: for diagnosing the degradation process in the refuse dump and optimizing energy recovery I used a GA2000 type NDIR (Non Dispersive Infra Red) analyzer, working in the medium infrared region.

The data was statistically processed with SPSS for Windows 11.0 program was used. The data was processed by the method

of analysis of variance. Homogeneity was examined with the Levene-test. When comparing the group-couples Tamhane test (in case of heterogeneity), and LSD test (in case of homogeneity) were applied. The tightness between variables was determined by linear regression analysis. In our examinations we calculated the necessary number of data by using a method by Sváb [14]. In order to be able to determine the necessary number of data in a sample you have to be aware of the standard deviation (s), you have to provide the permissible estimation of errors (h), have to give the P% significance level or the likelihood of error.

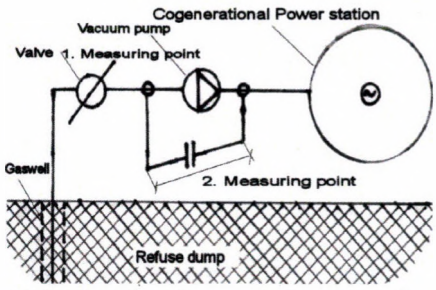

Figure 1 The location of measuring system at the refuse dump [8, 9, 10]

If we know the standard deviation in the unit of measurement of the data and the permissible estimation of errors are given in the same unit of measurement the sample size of the data can be calculated:
n: number of items, tp%: critical element of the „t"test, s: standard deviation, h: estimation of errors

$$n = \frac{t_{P\%}^2 \cdot s^2}{h^2} \qquad (1)\ [15, 16]$$

In case standard deviation is known in percentage (coefficient of variation) and the permissible estimation of errors is also given in percentage then the number of necessary elements can be defined by the following formula:
n: number of items, tp%: critical element of the „t"test, s%: standard deviation percentage (coefficient of variation) (%), h%: estimation of errors percentage (%)

$$n = \frac{t_{P\%}^2 \cdot s\%^2}{h\%^2} \qquad (2)\ [15, 16]$$

We made the calculations for a P=3% and P=5% probability level. According to our results in the case of h%=3% estimation of error the sample size for the statistical analysis of the results and drawing the relevant conclusions is n=363 pieces, in the case of h%=5% estimation of error the necessary sample size is n=131 pieces. On this basis we have concluded that the data we collected (n=517) is sufficient to carry out the appropriate statistical examinations and analysis. Even though we carried out the Levene test, by which we concluded which test to use at the comparison of group pairs (Tamhane or LSD) I found it important to calculate the CV% (coefficient of variation) as well. We would like to present the standard deviation within each group by the analysis of coefficient of variation, which was specified by the following formula:

$$s\% = CV = \frac{s}{\overline{X}} \cdot 100 \qquad (2)\ [15, 16]$$

CV: coefficient of variation [%], s: standard deviation, x: average of dataline

During the examinations we created measuring groups, definition of group establishment is in Table 1.

Table 1. Definition of group creating and their operating parameters

Wind speed groups	Wind speed interval [m/s]
1. group	v_{sz}<=0,6
2. group	0,6 > v_{sz} <=1
3. group	1 > v_{sz} <=1,3
4. group	1,3 > v_{sz} <=1,8
5. group	1,8 > v_{sz} <=2,4
6. group	v_{sz} >2,4

During the statistical process we examined what connection can be found between the average temperature interval, relative humidity, barometric pressure, wind speed interval precipitation changes and the quantity and quality parameters of landfill gas in the case of all and each gas well. We found significant differences between group pairs on the basis of the methane content of the pairs. The connection examinations between the variables of the gas wells were made by regression analysis. The results we got through the calculations are presented in charts, graphs and diagrams [12, 17, 18, 19]

3. Results

During our examination we tried to find relationships between the different wind speed intervals and the methane content values of the landfill gas recovered from the refuse dump. During the construction of a landfill site the heights of the retaining walls can be as high as 15-30 meters. At this height we can assume that the wind conditions might have the effect that despite extraction methane can dissipate from the top layers of the dump. This mostly happens during the loading of the dump when the height of the 3m wide and 2m high ramparts on the outside edge of the retaining walls gets higher than the height of the waste in the refuse dump. As a result the methane content of the recovered landfill gas can significantly decrease and have higher oxygen content.

The results are in Table 2. where methane content changed between 1-68%. The most favorable value, 51,78% methane content was measured in the 2nd group in 0,6m/s>vsz≤1m/s interval, with n=99 sample size. The least favorable value, 47,30%, was found in the 1st group – contrary to what I assumed – in the vsz≤0,6 wind speed interval and in the 6th group, 49,53% in the vsz>2,4m/s wind speed interval. From the results it can be seen that in groups 3,4,5 and 6 changes of wind speed shows small difference in methane content so it is necessary to examine the connection between the volume of gas recovery and prevailing wind speed. Variation of coefficient is CV%=22,81% in the wind speed interval of the 2nd group (0,6>vsz≤1). We measured the most favorable methane content value in this case and the minimum and maximum values were between 14-66% methane content.

Table 2. Results of the relationships between wind speed intervals and methane content

Wind speed group	Wind speed interval [m/s]	n [db]	CH_4 mean [%]	Coefficient variation CV% [%]	Std. deviation [%]
1. group	$v_{sz} \leq 0,6$	88	47,30	31,22	14,771
2. group	$0,6 > v_{sz} \leq 1$	99	51,87	22,81	11,832
3. group	$1 > v_{sz} \leq 1,3$	99	49,81	30,45	15,169
4. group	$1,3 > v_{sz} \leq 1,8$	99	48,65	30,58	14,880
5. group	$1,8 > v_{sz} \leq 2,4$	66	50,95	29,26	14,908
6. group	$v_{sz} > 2,4$	66	49,53	28,79	14,260
	Total	517	49,67	28,82	14,319

Table 3. Results of wind speed group pairs and methane content differences

Wind speed group	Wind speed interval [m/s]	1. group	2. group	3. group	4. group	5. group	6. group
1. group	$v_{sz} \leq 0,6$	-	*	-	-	-	-
2. group	$0,6 > v_{sz} \leq 1$	4,571	-	-	-	-	-
3. group	$1 > v_{sz} \leq 1,3$	2,512	2,059	-	-	-	-
4. group	$1,3 > v_{sz} \leq 1,8$	1,351	3,219	1,161	-	-	-
5. group	$1,8 > v_{sz} \leq 2,4$	3,650	0,920	1,138	2,299	-	-
6. group	$v_{sz} > 2,4$	2,232	2,338	0,279	0,881	1,418	-

* = P<5%, ** = P< 1%

During the homogeneity tests of the group pairs the samples showed homogeneous results so at the statistical process we used the LSD test, results can be seen in Table 3. We found the largest difference between 2.-1. Group pairs with 4,57% methane content. Between group pairs the analysis of variance showed significant difference only between group pairs 2.-1. P<5% .

For all the gas wells we carried out a linear regressive examination taking both methane content changes and wind speed intervals into account (Figure 2.). The relationship between the methane content changes of a particular gas well and the wind speed intervals can be calculated by the following equation: y=-5,28369x+56,452, R2=0,1699. The coefficient of correlation is r=0,48 so the closeness of relationships shows moderate correlation between the change of the methane content in all gas wells and the changes of wind speed intervals at the refuse dump. On the basis of the linear regressive examination we can conclude that the changes of wind speed interval might decrease the methane content of the landfill gas.

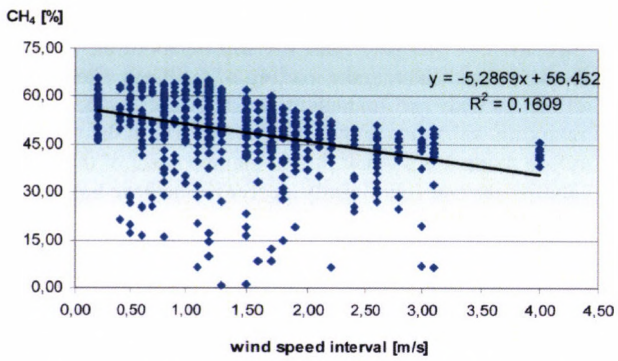

Figure 2. Changes of the methane content of landfill gas in different wind speed intervals [7, 10]

During our examination we were looking for relationships between the characteristic methane content values of each gas well and the characteristic wind speed intervals at the refuse dump. So we combined all the 8 gas wells' methane content values and their belonging wind speed values. The results can be found in Table 4. From the results it can be seen that the least favorable value was found at the 5th gas well between 1.-6. wind speed interval group, 23,63-37,57%, the value of average methane content was 32,53%. The most favorable methane content value was found at the 6th gas well between geoups 1.-6. (58,06-63,85%), the average methane content was 61,12%.

During the statistical evaluation we found a relationship between the methane content values which characterize each gas well and the wind speed interval groups. The results can be seen in Table 5. The homogeneity test was carried out by the Levene test and we used the LSD test in all the cases as the samples were homogeneous. We found significant differences, P<5%, between 3.-1. group pairs at the 1st gas well, between group pairs 2.-1. at the 3rd gas well, between 6.-2. and 6.-5. group pairs at the 4th gas well and between 3.-1. and 5.-1. group pairs at the 6th gas well. At number 2,5,7,8, gas wells the analysis of variance did not show significant differences.

Table 4. Methane content values of each gas well with regard to wind speed groups

Wind speed group	1. gas well	2. gas well	3. gas well	4. gas well	5. gas well	6. gas well	7. gas well	8. gas well
1. group	39,28	34,06	37,68	55,11	49,59	58,06	49,99	60,34
2. group	49,00	37,57	48,04	57,63	53,06	59,32	55,01	60,61
3. group	48,74	33,39	41,90	54,07	48,07	63,10	52,52	57,62
4. group	52,94	23,63	45,71	48,18	54,54	61,37	54,31	55,24
5. group	38,95	33,87	41,27	57,82	53,13	63,85	52,20	61,38
6. group	51,63	33,67	45,35	44,32	52,00	61,80	49,67	60,05
Total	47,10	32,53	43,45	53,03	51,67	61,12	52,50	58,99

Table 5. Results of the statistical processes of each gas well.

	Results of homogenity examination	Significant differences between group pairs in *P<5% level	Significant differences between group pairs in **P<1% level	Methane content differences CH_4 [%]	
				*P<5%	** P<1%
1. gas	homogeneous	3.-1.	-	13,66%	-
2. gas	homogeneous	ns	ns	-	-
3. gas	homogeneous	2.-1.	-	10,36%	-
4. gas	homogeneous (LSD)	6.-2. 6.-5.	-	13,31% 13,49%	
5. gas	homogeneous	ns	ns	-	-
6. gas	homogeneous (LSD)	3.-1. 5.-1.	-	5,03% 5,78%	-
7. gas	homogeneous	ns	ns	-	-
8. gas	homogeneous	ns	ns	-	-

For all the gas wells we carried out a linear regressive examination taking both methane content values and wind speed values belonging to wind speed intervals into account. The relationship between the methane content changes of a particular gas well and the wind speed intervals can be calculated by the following equation (Table 6). From the processed data we can see that the effect of the wind speed interval changes on methane content in the cases of gas wells 4,5,7 correlation coefficient changed between r=0,57-0,66, the closeness of relationship shows moderate correlation. In the cases of gas wells 1,2,3 there are loose correlation relationships and correlation coefficient is between r=0,12-0,33. In the cases of gas wells 6 and 8 there is tight correlation and correlation coefficient is r= 0,74-0,76. On the whole we can say that the changes of wind speed intervals in a particular area influences the methane content of the produced landfill gas since the airflow on the side of the landfill causes vacuum on the top of the dump and pulls the valuable methane out of the waste dump so methane content can decrease.

Table 6. Coefficient of correlation changes by gas wells with regard to methane content and wind speed intervals

	Linear equation	R^2	r
1. gas well	y = -1,5841x + 48,555	0,0152	0,1232
2. gas well	y = -5,3454x + 43,672	0,0643	0,2535
3. gas well	y = -3,3061x + 50,314	0,1117	0,3342
4. gas well	y = -7,9509x + 63,502	0,4232	0,6505
5. gas well	y = -4,642x + 57,368	0,3338	0,5777
6. gas well	y = -6,1143x + 64,857	0,5621	0,7497
7. gas well	y = -5,7277x + 60,316	0,4445	0,6667
8. gas well	y = -6,8312x + 64,912	0,5902	0,7682

4. Discussion

We diagnosed how the different wind speed intervals at the refuse dump influence the methane content of landfill gas where coefficient of correlation is r=0,48. Between the variables there is negative correlation which means that when wind speed values increase methane content values decrease. This process can increase during the raising of the landfill site when the height of the 3m wide and 2m high ramparts on the outside edge of the prisms gets higher than the height of the waste in the refuse dump. By that the methane content of the recovered landfill gas can decrease and have higher oxygen content. After linear regression examination (Table 6) we found a moderate negative correlation in the cases of 4, 5, 6, 7 and 8 gas wells. In the cases of the other gas wells we found loose negative correlations. All things considered we can state that the wind speed intervals at the refuse dump influence the methane content of landfill gas.

5. Conclusion

Based on the statistical processes with regard to wind speed interval tests we concluded that the wind speed changes specific for the landfill site affect the methane content of the landfill gas. Relationships between wind speed changes and methane content can be described by the equation: $y=-5,2869x+56,452$, $R^2=0,1699$. Between the variables there is negative correlation, if wind speed increases the methane content values decrease. Closeness of relationships between wind speed changes and methane content are moderate. Our proposals are the following: with the increase of wind speed the elements of the extraction system have to be coordinated in a way that the volume of the vacuum has to be increased until it levels off with the volume of the vacuum on top of the waste. Operators should take into account the volume of extraction and environmental parameters such as average temperature, precipitation intensity and wind speed in order to be able to plan the most favourable recovery of landfill gas and methane content.

The methane content of the landfill gas is influenced by the characteristic of wind speed intervals and the changes of wind direction. Our proposals are the following: at the surrounding areas at gas wells leachate must be returned in the waste and moisture content level must remain the same and within the range of gas wells covering and closing must be done in order not to let landfill gas into the air. With the increase of wind speed the elements of the extraction system have to be coordinated in a way that the volume of the vacuum has to be increased until it levels off with the volume of the vacuum on top of the waste. In the cases of gas wells we suggest a transition to a telemetry system with continuous control instead of a periodical regulation of valves.

It means that all the parameters about the quality of landfill gas, which are provided by the gas measuring points at the gas wells are stored on a computer.

The telemetry system would monitor the data sent by the meteorological station and the volume of extraction at the gas wells could be determined on the basis of that. With the usage of it the most favourable quality and quantity parameters can be guaranteed. Overall, we can say that the characteristic wind-speed intervals of the landfill affect the methane content of the landfill gas; due to the location of the gas wells the air coming upward on the waste dump results in a vacuum on top of the waste body, and almost pulls out the valuable landfill gas from the waste body, thus the methane content value will decrease, which causes operational problems.

References

[1.] Nagy V., Farkas F.: 2012. Exhaust gas tests using of biofuels in IC engines, Hungarian Agricultural Engineering, 24/2012, pp. 49-52, ISSN: 0864-7410

[2.] Sembery P., Tóth L.: 2004. Hagyományos és megújuló energiák, Szaktudás Kiadó, Budapest, p. 274-279

[3.] Hódi J.: 2009. Depóniagáz kutak problémái, megoldási lehetőségek XIX. Nemzetközi Köztisztasági Szakmai Fórum, Szombathely, 2009. április 21-23

[4.] Sallai L.: 2009. Cofermentation of organic waste of the pilot farm of SZTE MGK, Hungarian Agricultural Engineering N0 22/2009, HU ISSN 0864-7410

[5.] Tóth L. et al.: 2012. Alternatív energiaellátási rendszerek az agrárgazdaságban, Magyar Agrárkamara, Szaktudás Kiadó Ház, Budapest, ISBN 978-615-5224-22-5, 235.p 188-194pp. 208-215pp

[6.] Woperáné S. Á., Tanka S.: 2011. Hulladéklerakóban keletkező biogáz hasznosítása, Miskolci Egyetem, Tüzeléstani és Hőenergia Intézeti Tanszék, Anyagmérnöki Tudományok, Miskolc, 36/1. kötet. pp. 79–90

[7.] Molnár T.: 2007. Quantitative and qualitive analysis of the biogas production from the municipal solid waste, Hungarian Agricultural Engineering N0 20/2007, pp. 20-22, HU ISSN 0864-7410

[8.] Molnár T.: 2009. The impact of the weather conditions for the parameter of the production of landfillgas, Hungarian Agricultural Engineering N0 22/2009, pp. 91-94, HU ISSN 0864-7410

[9.] Molnár T.: 2012. Landfill gas quality and quantity parameter changes depending on precipitation intensity, Mechanical Engineering Letters, HU ISSN 2060 3789

[10.] Molnár T.: 2008. Landfillgas composition analysis, 50.th JubileeGeorgikon Scientific Conference, Keszthely 2008. szeptember 25-26, p. 165, ISBN 978-963-9639-31-7.

[11.] Loll U.: 2001. Biogaspotenziale im Klärschlamm und anderen biogenen Abfällen, KA Wasserwirtschaft, Abwasser, Abfall, 48. k. 10. sz. 2001. p. 1424-1429.

[12.] Stachowitz W. H.: 2004. „Berechnung" oder Abschätzungen von Gasproduktionsmengen Gasprognose

[13.] Tabasaran O.: 1981. Gas production from landfill. In: Bridgewater AV, Lidgren K, editors. Household waste management in Europe, economics and techniques. New York: Van Nostrand Reinhold Co.; 1981. p. 159–175.

[14.] Sváb J.: 1981. Biometriai módszerek a kutatásban, Mezőgazdasági Kiadó, ISBN 9632310136, p.50-51., Budapest

[15.] Bai A.: 2007. A biogáz. Szakkönyv. Társszerzők: Bagi Z., Bartha I., Fenyvesi L., Hódi J., Kovács K., Mátyás L., Mogyorósi P., Petis M. Száz Magyar Falu Könyvesháza Kht . ISBN 978 963 7024 30 6. Budapest, 2007. pp. 1-284

[16.] Bai A.: 2015. Helyi közlekedés és hulladékgazdálkodás. Magyar Energetika 22 (1) pp. 21-25 (2015)

[17.] Christensen, T. H. H., Kjeldsen P.: 1989. Basic biochemical process in landfills Sanitary Landfilling (ed.: CHRISTENSEN, TH.H.-COSSU, R.-STEGMANN, R.) Academic Press, pp. 29-48.)

[18.] Stachowitz W. H.: 2005. Grundlagen der Fassung und Entsorgung von Deponiegas, DAS – IB GmbH Stand: Juli 2005.

[19.] Stief K.: 1985. Anforderungen an die Wirksamkeit von Deponiebasisabdichtungen Deponiebasisabdichtung mit Kunstoffdichtungsbahnen, Beihefte zu Müll und Abfall, H.22. pp. 9-13.

HUNGARIAN AGRICULTURAL ENGINEERING
N° 27/2015 24-26
Published online: http://hae-journals.org/
HU ISSN 0864-7410 (Print) / HU ISSN 2415-9751(Online)
DOI: 10.17676/HAE.2015.27.24

PERIODICAL OF THE COMITTEE OF AGRICULTURAL AND BIOSYSTEM ENGINEERING OF
THE HUNGARIAN ACADEMY OF SCIENCES
and
SZENT ISTVÁN UNIVERSITY
Faculty of Mechanical Engineering

EXAMINATION OF VELOCITY DEPENDENT FRICTION OF STEEL PROBES

Author(s):
A. Csatár[1] – A. Varga[2]

Affiliation:
[1]Montavid Thermodynamic Research Group
[2]Szent István University, Faculty of Mechanical Engineering, Department of Mechanics and Technical Drawing

Email address:
csatar.attila@gek.szie.hu, varga.attila@gmgi.hu

Abstract

The phenomenon of friction reduces the efficiency of almost all machines in practice. For reduce the deficits we have to understand this phenomenon and we have to take it in all cases into consideration during design. Nevertheless in certain cases the descryption of a friction process is very difficult; because this depends on a lot of parameters. In case of polymers, granular materials or in geology the rate- and state dependent friction have great importance. In this paper velocity dependent friction of steel is examined with the help of a direct shear apparatus, which was developed in our earlier work.

Keywords

direct shear test, friction, time-dependent, velocity-dependence

1. Introduction

The friction is the resistance to relative motion between two or more substances. The relative motion can be created between masses of fluids, gases, solids, or combinations thereof. Since the friction and the effects of friction are so evident, the physicists have searched the fundamental causes of friction for thousands of years [1].

The phenomenon of friction reduces efficiency of the machines in practice. In order to reduce losses, we have to examine and understand this phenomenon. Friction cannot be neglected for the major part of mechanical engineering.

Coulomb was the first researcher, who examined the friction process about three centuries ago and he discovered that the kinetic friction does not depend on the shear velocity [2]. Later further researches showed that this phenomenon depends on several parameters, such as type of material, roughness, temperature. It is remarkable also, that friction may be velocity dependent. In some cases, due to the wide variety of parameters the description of a friction process is very difficult. In geology, mining- and earthquake science, in case of polymers, granular materials or other special materials the rate- and state-dependent friction (creep and relaxation) have great importance. Friction is a form of energy dissipation, therefore it is the subject of thermodynamics. However, only few researchers investigate the thermodynamic aspects of time dependent of friction [3, 4, 5]. The aim of our work was to examine velocity dependent properties of friction in case of steel with our previously developed direct shear testing apparatus. This shear apparatus is connected to the INSTRON 5581 type universal material testing machine and it is suitable for shearing with different (in certain cases very low) velocities and on different normal loads.

2. Velocity dependent experiments

The purpose of the multiple-velocity tests was to look for variations of shear strength as a function of velocity. A step increase of shear velocity results an immediate jump in frictional coefficient followed by displacement dependent decay and stabilization at a new steady-state friction. The reverse is seen if the shear speed is decreased (Figure 1.).

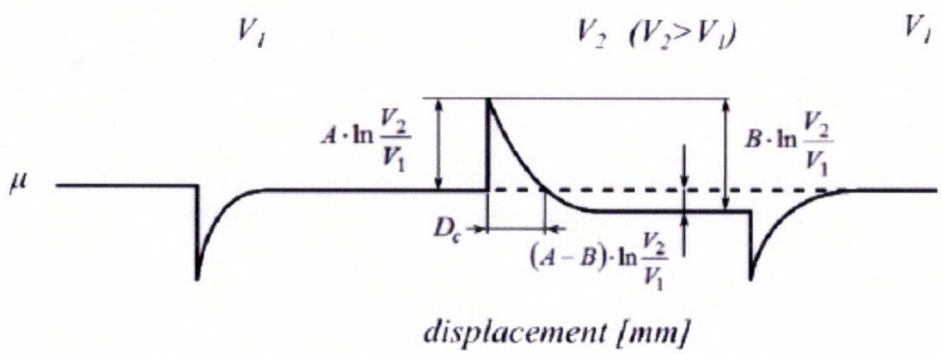

Figure 1. Effect of steps in shear speed on a friction coefficient

Dietrich and Kilgore [6] formulated an empirical law for fault tests. This formulation provides a descriptive framework for the interpretation of the transient shearing phenomenon. The coefficient of friction can be represented.

$$\mu = \frac{\tau}{\sigma} = \mu_0 + A \cdot \ln\left(\frac{V}{V^*} + 1\right) + B \cdot \ln\left(\frac{\Theta}{\Theta^*} + 1\right) \qquad (1)$$

where τ and σ are shear and normal stress V is a shear speed and Θ is a state variable. Parameters , A and B are experimentally determined constants and V* and Θ are normalizing constants [6]. A thermodynamic generalization of this empirical rate- and state-dependent friction law is given in [7]. In an ideal velocity stepping test, parameters A, B contain the graphical interpretation indicated in Figure 1 and μ0 represents the nominal coefficient of friction which for most materials ranges from 0.5 to 0.8. In practice, it is not possible to instantaneously step to a new constant sliding speed because of finite apparatus stiffness. Apparatus stiffness effects are readily modelled and cause the rounding of friction peaks and oscillations that are visible in Figure 1. In case of rocks, the values of the coefficients A and B generally vary between 0.005 and 0.015. [6]

3. Experimental measurements

The design was made on the basis of Dietrich's vertical shear apparatus [8]. In case of Dietrich's arrangement the displacement was vertical and the normal force was horizontal, still in our case the normal force is provided by an INSTRON 5581 type universal material testing machine, so it should be vertical thus the displacement should be horizontal. To keep the contact surface invariant during the shear process, one of the probes must be longer. We decided to use a box type layout because this apparatus must be suitable for shearing also granular materials, for this reason this must contain a fixed, loaded part and a moving part. These parts were suitable for fixing the probes. The shear force was measured by a load cell which is at the holding point of the fixed part; the displacement was measured by an inductive displacement transducer at the moving part. The displacement has been provided by a stepper motor (Figure 2.).

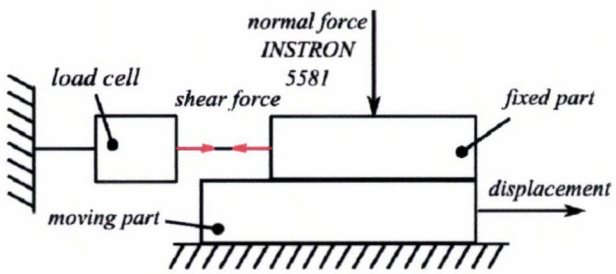

Figure 2. The sample assembly

To reduce the friction force between the moving part and the base-plate, linear bearings were used. Owing to the stepper motor and the control electronics very low shear velocity can be set. The rotation of the stepper motor is transformed to linear displacement by a screw shaft, this connects to the stepper motor with a cased coupling [9, 10].

4. Results

The usual experimental protocol for evaluating rate- and state-dependent friction changes the shear velocity in a stepwise manner under of constant normal stress. Multiple velocity tests were carried out with constant shear velocity for a predetermined displacement, then suddenly changed to a different velocity and held constant for a while and changed back to the first velocity again. The tests were carried out with two different speed settings, 4,4-43,6 and 10,1-79,1 μm/s, for steel probes. Additionally the different normal stress level was 200 kPa. During the tests the shear force and the displacement were measured and the shear diagrams were determined. The purpose of these multiple-velocity tests was to look the time dependent friction coefficient as seen in the earlier rock friction experiments of Dietrich. In these earlier works two different velocity effects were observed, the step increase of shear velocity results in an immediate jump in frictional coefficient followed by displacement dependent decay and stabilization at a new steady-state friction. The reverse is seen if the shear speed is decreased. This friction coefficient jump on the higher speed level and the decrease on lower speed level can be seen on the shear diagrams (Figure 3.).

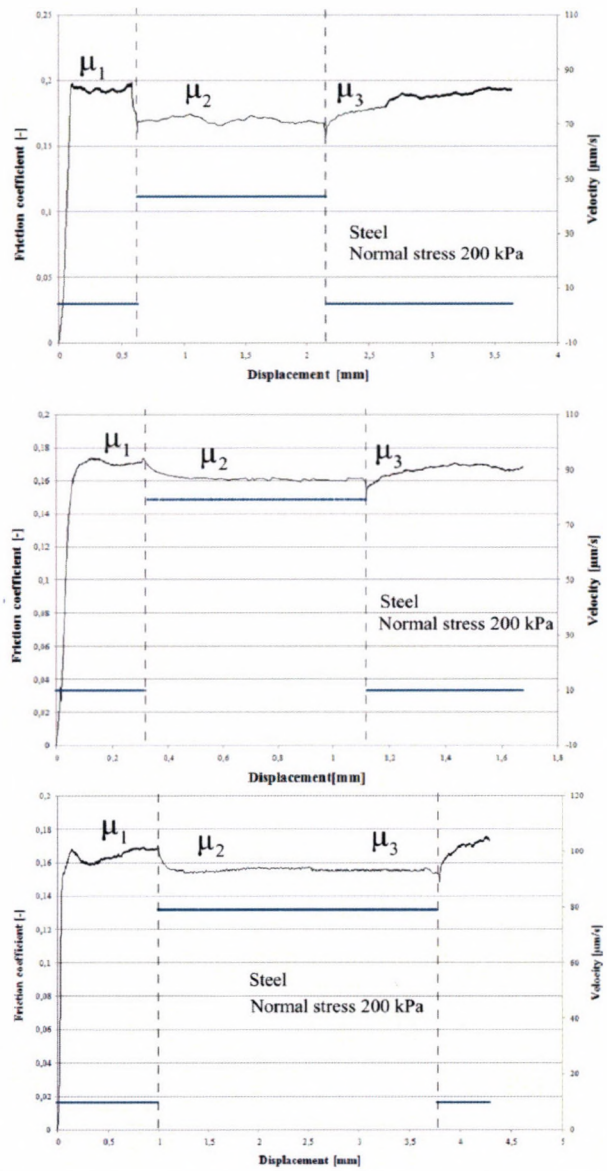

Figure 3. Displacement in function of time

Based on these diagrams and equation (1), the A and B parameters could be determined. The following table contains the results:

Table 1. Testing results

-	4,4-43,6 μm/s		10,1-79,1 μm/s	
	1st test	2nd test	3rd test	4th test
A	0,0045	0,0054	0,0013	0,0011
B	0,0173	0,0184	0,0063	0,0043

5. Conclusion

During our work, the measurements were carried out with two different velocity settings. Based on the results, this apparatus is suitable to examine rate- and state-dependent friction similar to the characteristics presented in the literature. We determined the constants which were needed to describe the phenomenon of friction in case of steel probes.

References

[1.] Dietrich J. H.: 1979. Modeling of Rock Friction I.: Experimental Results and Constitutive Equations, Journal of Geophysical Research, Vol. 84, pp. 2161-2168. http://dx.doi.org/doi:10.1029/JB084iB05p02161

[2.] Dowson D.: 1979. History of tribology, Longman, New York

[3.] Ruina A. L.: 1983. Slip Instability and State Variable Friction Laws, Journal of Geophysical Research, Vol. 88, pp. 10359-10370. http://dx.doi.org/doi:10.1029/JB088iB12p10359

[4.] Mitsui N., Ván P.: 2014. Thermodynamic aspects of rock friction, Acta Geodaetica et Geophysica, Vol. 49, pp.135-146. http://dx.doi.org/doi:10.1007/s40328-014-0048-6

[5.] Ván P.: 2010. A képlékenység termodinamikája. In: Fülöp T.(szerk.) Idő és térderiváltak anyagtörvényekben. Mérnök geológia Kőzetmechanika Kiskönyvtár 10, Műegyetemi Kiadó, Budapest, pp. 15-50.

[6.] Dietrich J. H., Kilgore, B. D.: 1994. Direct observation of frictional contacts: New insights for state-dependent properties, Pure and Applied Geophysics PAGEOPH, Vol. 143, pp. 283-302.

[7.] Ván P., Mitsui N., Hatano T.: 2015. Non-Equilibrium Thermodynamical Framework for Rate- and State-Dependent Friction, Periodica Polytechnica Civil Engineering, Online First paper 8249. http://dx.doi.org/doi:10.3311/PPci.8249

[8.] Dietrich, J. H.: 1981. Constitutive properties of faults with simulated gouge, Geophysical Monograph Series, Vol. 24, pp. 103-120. http://dx.doi.org/doi:10.1029/GM024p0103

[9.] Csatár A., Safranyik F., Bércesi G.: 2013. A NEW direct shear testing apparatus for the examination of the velocity- and timedependent friction, Hungarian Agricultural Engineering No 25; pp. 54-58; (ISSN 0864-7410)

[10.] Asszonyi, Cs., Kertész, P., Richter, R.: 1980. A kőzetmechanika anyagszerkezeti és reológiai alapjai, Veszprémi Akadémiai Bizottság, Veszprém, pp. 446.

HUNGARIAN AGRICULTURAL ENGINEERING
N° 27/2015 27-30
Published online: http://hae-journals.org/
HU ISSN 0864-7410 (Print) / HU ISSN 2415-9751(Online)
DOI: 10.17676/HAE.2015.27.27

PERIODICAL OF THE COMITTEE OF AGRICULTURAL AND BIOSYSTEM ENGINEERING OF
THE HUNGARIAN ACADEMY OF SCIENCES
and
SZENT ISTVÁN UNIVERSITY
Faculty of Mechanical Engineering

OPTIMAL PISTON'S DIAMETER RATIO IN FOUR PISTON CALIPER

Author(s):
Á. Horváth[1] – I. Oldal[2] – G. Kalácska[1]

Affiliation:
[1]Institute for Mechanical Engineering Technology, Szent István University,
2100 Gödöllő, Páter Károly street. 1. Hungary
[2]Institute for Mechanics and Machinery, Szent István University,
2100 Gödöllő, Páter Károly street. 1. Hungary

Email address:
adam.tamas.horvath@gmail.com, oldal.istvan@gek.szie.hu, kalacska.gabor@gek.szie.hu

Abstract

Researches of brakes have two ways: one direction is to increase the performance of brake and other direction is to increase life time of friction elements (brake disc, brake pad). In this study four pistons (side two) caliper were examined where optimal pistons diameter was defined. Pistons in caliper is different first piston (P1) according to a rotation direction diameters is smaller than second piston (P2) according to a rotation direction. Pressure distribution of brake pad's friction surface was examined to find optimal diameters of piston. Pistons diameter was changed where first piston's (P1) diameter is between 32-44 mm and second piston's (P2) diameter is between 32-64 mm. All case optimal diameter rations was defined which result that brake pad wear is consistent (not inclined). Optimal diameter is P1=44 mm and P2=56 mm where friction coefficient is 0,1 between brake pad and caliper. This construction gives consistent pressure distribution on brake pad friction surface.

Keywords

disc brake, brake pad, optimization, wear, FEM

1. Introduction

Nowadays researchers of vehicle examine how to increase different part's performance and how to make optimal working. Lot of agricultural vehicles have disc brake because working parameter is better than drum brake. [1] Most used brake is disc brake where it is the aim to increase the friction material's performance and to increase or to optimize life time of these parts. The aim of brake pad is to make consistent pressure distribution on friction surface. Consistent pressure distribution means that the total surface works and increases the braking performance and gives long life time to brake pad. Long life time depends on the friction material which gives high friction coefficient and wear is little. Coefficient of friction material was examined area where we checked the changing of friction coefficient and wear [2] when temperature is high [3] In this study we examined different material effect into brake pad and brake disc, how the coefficient of friction can change. [4] The other area of brake is brake's frequency, where researchers avoid the damaging frequency. [5] The other important aspect is the lifetime of brake pad and the life time of brake disc, because if the construction is not good, the brake pad and disc wear are very easy and life time is decreasing. If the wear is not right, that means the exploitage of brake pad is decreasing, it has to be changed early. It can happen that by a racecar the brake pad can't be used till the end of the race. Optimal wear depends on caliper construction where piston pushes the brake pad to brake disc. Several parameters effect on the wear. Söderberg et al examined commercial caliper (2 pistons per side) pressure distribution to define the pressure center of brake pad. [6]. This research does not examine high performance caliper pressure distribution in friction surface.

The aim of this study is to define optimal piston diameter in four pistons caliper. Pistons in caliper are different, according to a rotation direction first (P1) or second (P2) piston were defined where P2 piston's diameter is bigger than P1 piston's diameter. An optimal diameter ration results that brake pad's performance and lifetime can be increased.

2. Material and method

The brake system of vehicles is complex, where the different parts have different functions to provide safe working. Materials of parts depend on target what have to be accomplished. In case of disc brakes it is important that it has high performance and low weight (unsprung mass). This requirement effects the material which has low density and big capacity. Usually brake disc was made of gray cast iron and weight does not decrease significantly. In high performance car caliper and pistons were made of aluminium alloy (for example 7075t6), which has low density and different components increase the capacity. Other important parts are brake pads which friction on disc. Brake pads consist of two elements: one is steel plate which gives consistent pressure distribution. The other part of brake pad is friction material which makes braking torque with brake disc. Properties of materials are shown in Table 1.

Table 1. Properties of material

	Young modulus	Poisson's ration
Friction material	1 GPa	0.25
Steel plate	200 GPa	0.3
Caliper	82.4GPa	0.33
Brake disc	110 GPa	0.28

A simplified model was used to define the optimal diameter ratio of piston. This model is not a complex model, we only examined the brake pad and its context (caliper, brake disc, brake pad (steel plate and friction material) (Figure 1.).

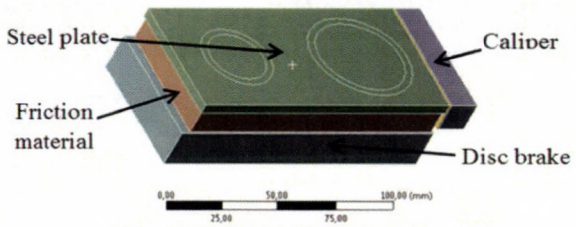

Figure 1. Examined model and parts

In this simplified model size of the brake pad's friction material 63×130 mm and friction material's thickness is 13 mm. The size of the brake pad's steel plate is 65×132 mm where thickness is 5 mm. Two pistons were pushing the brake pad to brake disc where piston's diameter was changed and pressure distribution on friction surface was examined. Piston model is only the contact surface on steel plate where 15 MPa pressure was defined. Piston's wall thickness is 3.5 mm in all cases of diameter. Diameter ration was changed to define the optimal construction where pressure distribution is consistent and brake pad's lifetime is longer. The piston's diameter is different because by braking the one side of brake pad is grazing on caliper and the other side is not. Disc brake pushes brake pad to caliper which makes friction on one side, but the other side of brake pad do not contact to other parts of caliper so there is no friction on other side. This is the reason why the piston is bigger in second place (P2) according to a direction of rotation and why is it smaller in first place (P1) according to a direction of rotation. (Figure 2.)

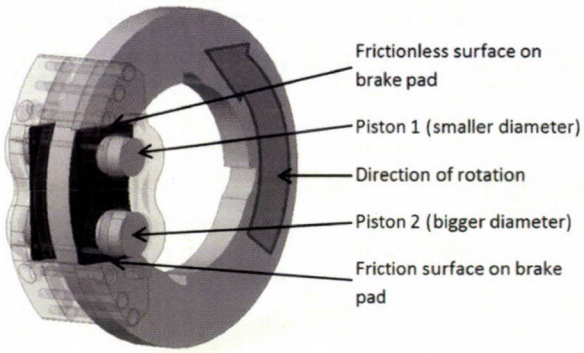

Figure 2. Examined parts of brake system name where piston's diameter is different

In this examination different diameter ration was used where first piston's diameter (P1) is fix and second piston's diameter (P2) was changed. The first piston's diameter is between 32 and 44 mm and second piston's diameter was changed between 32 and 64 mm. (Table 2.)

Table 2. P1 piston and P2 piston diameter where examined by optimal diameter ratio

P1 Diameter [mm]	Second piston (P2) according to the direction of rotation [mm]																
32	32	34	36	38	40	42	44	46	48	50	52	54	56	58	60	62	64
34		34	36	38	40	42	44	46	48	50	52	54	56	58	60	62	64
36			36	38	40	42	44	46	48	50	52	54	56	58	60	62	64
38				38	40	42	44	46	48	50	52	54	56	58	60	62	64
40					40	42	44	46	48	50	52	54	56	58	60	62	64
42						42	44	46	48	50	52	54	56	58	60	62	64
44							44	46	48	50	52	54	56	58	60	62	64

We used hexagonal mesh where element size was 2 mm with the aim we could get more suitable result. Our model has 10898 elements which means 35535 nodes in the model. We defined the connection between elements where two parts of brake pad (steel plate, friction material) have bounded connection which was used in real. Friction connection is between caliper and brake pad and brake pad and brake disc. 0.1 friction coefficient is between brake pad and caliper and 0.4 is between brake pad and disc. This friction coefficient (0.4) was used by Yaoqing and by other researchers. [7]

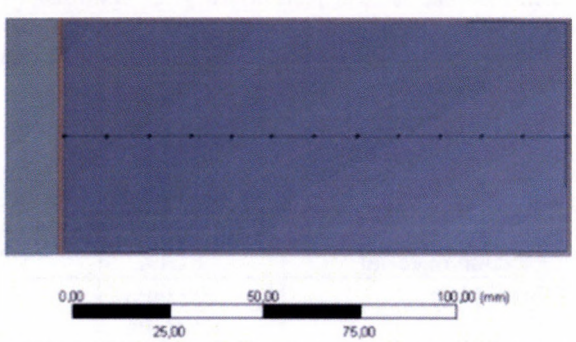

Figure 3. Examined points in center line of brake pad

3D model was made and examined pressure distribution on friction surface center line where pressure was defined in 13 points on centerline (Figure 3.)

Results show that in case of small diameter piston the pressure is low on the edge of brake pad so brake pad edge doesn't work and doesn't make suitable braking torque. By using of a big diameter piston, pistons center doesn't make suitable pressure on friction surface and the efficiency of brake pad is low. Diameters of pistons effect the friction surface distribution. When diameters of pistons are not suitable, wear of friction material isn't consistent which decreases the piston's lifetime. In this study optimal diameter ration was searched in four pistons caliper where brake pad wear was consistent because two pistons push both sides of the brake pad with the same force. Pressure distribution was defined in brake pad's center line to define optimal ration of diameter of pistons. Fig 5/a shows center line pressure where first piston's diameter (P1) was 42 mm and second piston's diameter (P2) was changed between 42 mm and 64 mm. When optimal diameters were defined, first and last point did not take into account because edge effect affects the results. Inside points (11 points) were used to define the optimal diameter ration (Figure 5/b).

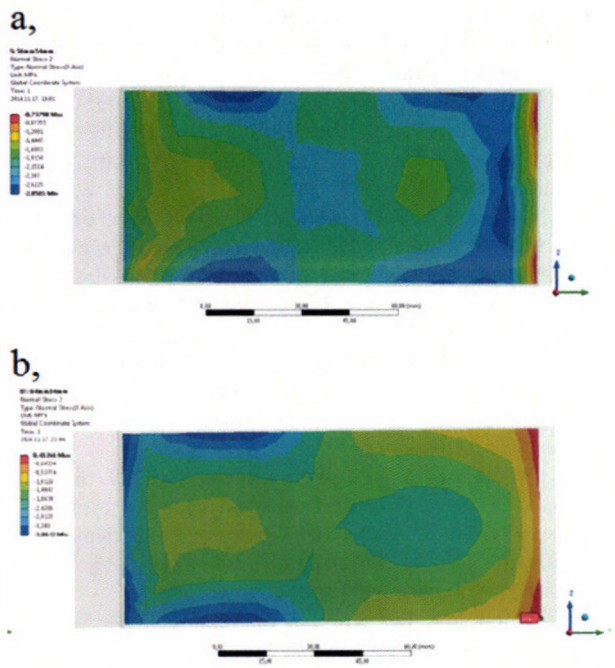

Figure 4. Pressure distribution when piston diameter is P1=54 mm and P2= 56 mm and b, when piston diameter is P1=34 mm and P2= 64 mm

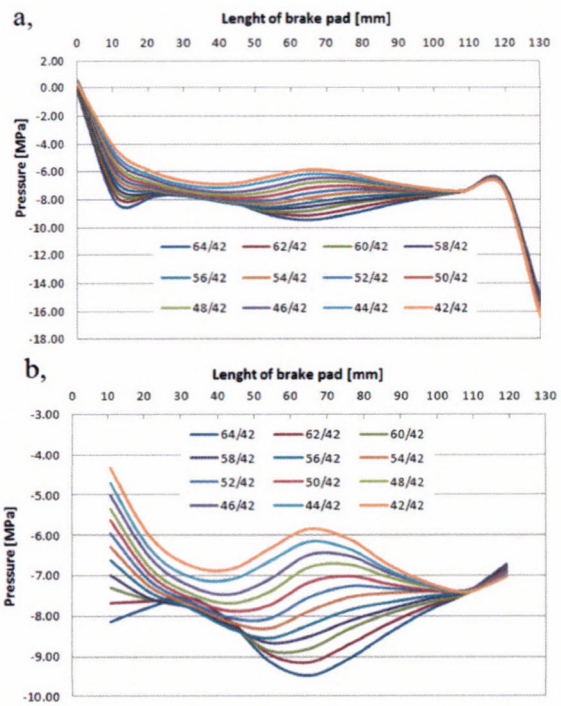

Figure 5. a, center line pressure along the entire length (13 points); b, center line pressure without outsides point (11 points)

Results show that pressure distribution depends on the piston's diameters which push the brake pad to brake disc. Furthermore pressure is lower in piston's center if there was a piston with big diameter used.

Figure of merit was made to compare the different construction to find the best diameter ration where pressure distribution is consistent. The figure of merit shows the difference between pressure and average of pressure (Figure 6.).

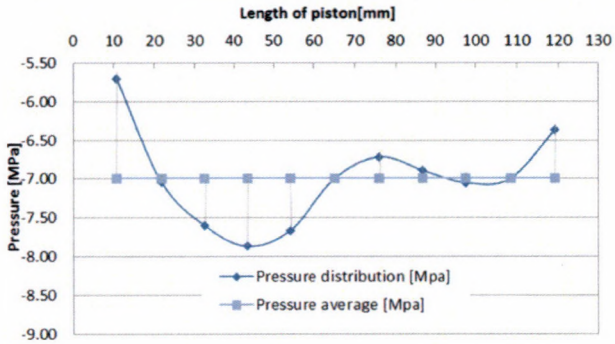

Figure 6. Definition of the figure of merit where P1=40 mm; P2=50 mm

Formula 1 helps to find the best construction which shows what diameters of ration give consistent pressure on center line of brake pad's friction surface. Smaller figure of merit shows which construction gives optimal wear of brake pad.

$$Q = \frac{s}{\bar{x}} \tag{1}$$

where Q is figure of merit, s is scatter of pressure and $\bar{x}$ is the average of pressure.

Figure of merit was defined by all different diameters of pistons and result is in figure 6. where first piston's diameter was 42 mm and second piston's effect was checked. This figure shows the change of figure of merit which depends on the diameter's ration (P1/P2) (Figure 7).

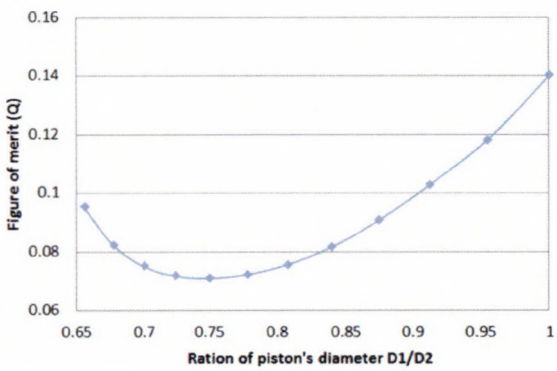

Figure 7. Figure of merit when ration of diameter was changed when first piston's diameter was 42 mm

Figure 8 shows different construction's (different piston's diameters) figure of merit. Results show that all constructions have an optimum point where brake pad's wear was consistent.

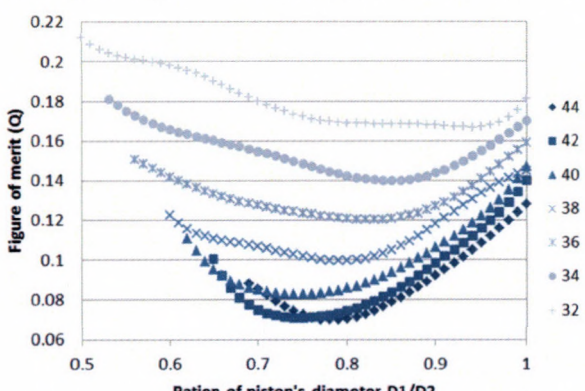

Figure 8. Different construction's figure of merit to define optimal ration of diameter

Results give which case gives optimal wear (smallest figure of merit) to increase the brake pad's lifetime because pressure distribution is consistent on center line of brake pad's friction surface. The best construction in this case is when first piston's diameter (P1) is 44 mm and second piston's diameter is 56 mm where figure of merit is 0.0698.

4. Conclusion

In this study optimal construction of piston's diameter was defined to make consistent wear of brake pad's friction surface. Pressure distribution of center line of piston was examined to find the best ration of diameter to increase brake pad's lifetime. In this study there was used a simplified model to check the piston's diameter effect to friction surface pressure distribution. Pistons of caliper are different. The diameter of the first piston (P1) according to a rotation direction is smaller than the diameter of the second piston (P2) according to a rotation. Diameter of the first piston was between 32 mm and 44 mm, diameter of the second piston was changed between 32 mm and 64 mm. Lots of cases were examined where an optimal diameter was defined, and we find the best diameter ration in all cases where pressure distribution was consistent. Figure of merit helped to compare the pressure distribution and we defined the best construction which gives long time of life. In this case we found the best construction when the diameter of the first piston (P1) was 44 mm and the diameter of the second piston (P2) was 56 mm, where figure of merit is 0.0698.

References

[1.] Horváth Á., Kalácska G., Oldal I.: 2015. Traktorokban alkalmazott fékdugattyú konstrukciója vizsgálata, Mezőgazdasági Technika, pp.2-4 ISSN 0026 1890

[2.] P.D. Neis P. D., Ferreira N. F., da Silva F. P.: 2014. Comparison between methods for measuring wear in brake friction materials Wear 319; pp. 191–199. http://dx.doi.org/doi:10.1016/j.wear.2014.08.004

[3.] Neis P. D., Ferreira N. F., Lorini F. J.: 2011. Contribution to perform high temperature tests (fading) on a laboratory-scale tribometer, Wear 271, pp. 2660-2664. http://dx.doi.org/doi:10.1016/j.wear.2010.12.023

[4.] El-Tayeb N. S. M., Liew K. W.: 2008. Effect of water spray on friction and wear behavior of noncommercial and commercial brake pad materials, Journal of materials processing technology 208, pp. 135-144. http://dx.doi.org/doi:10.1016/j.jmatprotec.2007.12.111

[5.] Lorang X., Foy-Margiocchib F., Nguyena Q. S., Gautier P. E.: 2006. TGV disc brakes queal, Journal of Sound and Vibration, 293 pp. 735–746. http://dx.doi.org/doi:10.1016/j.jsv.2005.12.006

[6.] Söderberg A., Sören Andersson S.: 2009. Simulation of wear and contact pressure distribution at the pad-to-rotor interface in a disc brake using general purpose finite element analysis software; Wear 267; pp. 2243–2251. http://dx.doi.org/doi:10.1016/j.wear.2009.09.004

[7.] Wu Y., Jin H., Li, Y., Ji Z., Hou S.: 2014. Simulation of temperature distributionin disk brake considering a real brake pad; Wear, Tribology Letters, 205–213. http://dx.doi.org/doi:10.1007/s11249-014-0400-6

HUNGARIAN AGRICULTURAL ENGINEERING
N° 27/2015 31-34
Published online: http://hae-journals.org/
HU ISSN 0864-7410 (Print) / HU ISSN 2415-9751(Online)
DOI: 10.17676/HAE.2015.27.31

PERIODICAL OF THE COMITTEE OF AGRICULTURAL AND BIOSYSTEM ENGINEERING OF
THE HUNGARIAN ACADEMY OF SCIENCES
and
SZENT ISTVÁN UNIVERSITY
Faculty of Mechanical Engineering

REALIZATION THE VOLUMETRIC FLOW CONTROL OF A DOMESTIC SIZE SOLAR COLLECTOR SYSTEM

Author(s):
I. Seres – P. Víg

Affiliation:
Department of Physics and Process Control, Szent István University, Páter K. street. 1., Gödöllő, H-2100, Hungary

Email address:
seres.istvan@gek.szie.hu, vig.piroska@gek.szie.hu

Abstract

The efficiency of the solar systems is influenced by numerous factors, and the control of the system is an important one among them. The usage of the flow control of solar liquid by influencing the rotational speed of the pump by a frequency controller has several advantages compared to the simple on-off switch regulation. To investigate these advantages the control system of a domestic size solar hot water system was changed this way in the Department of Physics and Process Control, Szent István University. In the paper the realization of the control is presented (installation, parameter setting of the used Altivar frequency inverter). The operation of the Labview control routine is described as well.

Keywords

solar energy, control, frequency regulation, efficiency, transient

1. Introduction

The first experiments with the solar applications started about 20 years before in the Department of Physics and Process Control, Szent István University, Gödöllő, Hungary, and since then a wide range of experimental equipment was installed for the different projects in the Department. Among them three type of solar collector (flat plate, vacuum tube and PV/T – hybrid photovoltaic and solar thermal) collects the heat for a domestic size hot water system, beside them a domestic size solar dryer, a transparent insulation wall and a 1 kWp photovoltaic system consist of the basics of the Department system.

At the University campus, there are some more, bigger units, operated by our Department staff, e.g. a 10 kWp grid connected photovoltaic system, a solar thermal system for heating the water of the swimming pool, and another one for the greenhouses of the horticulture unit of the University, a smaller, domestic size hot water system in the building of the experimental laboratories with vacuum tube collectors. The control of the mentioned systems are solved by computer based data logging systems, however we operate a few independent one.

2 The investigated system

The thermal units

The present paper is dealing with the household size hot water system, working at the Department. During the measurements this system was operated by a vacuum tube collector (15 heat pipe technology tubes), which is installed at the terrace of the department. The collector is oriented to South and it has an inclination angle of 45° to the horizontal (the inclination angle can be adjusted for several values as a seasonal optimum, but these measurement results were achieved by this value). The picture of the collector can be seen in Figure 1.

Figure 1. Solar collectors at the department, among them the vacuum tube collector (2nd), used or the experiments

Figure 2. The tube and valve system inside the research laboratory

The collector is connected to the inner units and the hot water tank by partly insulated 20 mm diameter copper tubes. As the research laboratory is relatively far from the terrace (location of the collectors), a relatively long (approximately 50 m = 2 · 25 m) tube system connects the collectors to the hot water tank. Inside the laboratory a relatively complicated valve system (Figure 2.) makes possible to route the hot water to the storage tank or to an experimental greenhouse scale-model (for heating its soil). There is an alternative possibility to circulate back the liquid to the outgoing tube if its temperature is not warm enough.

The storage tank is a 300 liter capacity, insulated tank (5 cm insulation) with double heat exchanger inside. The collector was connected to the heat exchanger located in the bottom part of the tank, the useful area of the heat exchange is 1 m2. In Figure 3 the storage tank and its schematic figure can be seen.

Figure 3. The photo and the schematic figure of the solar tank (3 temperature measuring points)

The data logging / control system

The data logging / controlling is realized by a PC based system. The system is set up by Adam data converter and communication units, which are communicate to each other and the computer by RS485 communication standard.

The used temperature sensors are partly Pt1000 Platinum thermal resistors (e.g. on the collectors in- and output sides, where high temperatures my occur), and partly NTC 10k thermal resistors (e.g. for the solar tank: top, middle, top, heat exchanger inlet and outlet point, fresh and hot water outlet point). The sensors are connected to the proper ADAM module (ADAM 4015 and ADAM 4015T), which modules send the data to the PC through an ADAM4060 RS485 communication module.

The communication software is an old development of an earlier member of the department staff, written in C, originally made for a win95 system. Now a new version of the software is developed under Labview, only the communication of this software with the ADAM modules has to be solved yet. The measured data are saved to the hard drive of the data logger with the time period, determined by the users of the software (typically every 30 s). The view of the screen during the data logging can be seen in Figure 4 [1].

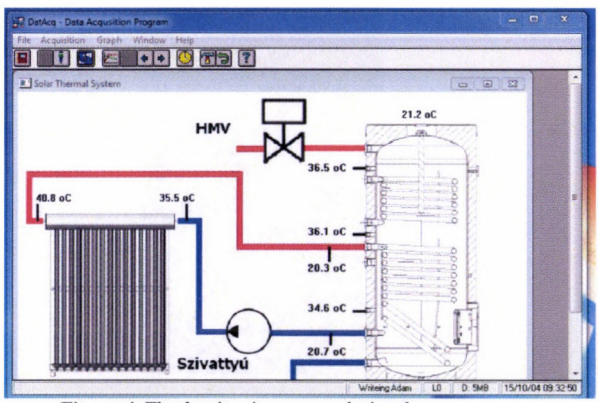

Figure 4. The data logging screen during the measurement

The used control method by the software the On-Off switch method was, such as the software was switching on or off the pump (through a relay) depending on the tank temperature is higher by 5 degree then the collector output or not.

The measured data, inducing the change

From the analysis of the measured data the next problem can be recognized. When the incoming solar power was not strong enough to maintain a stable temperature difference, bigger than the mentioned 5 Celsius between the collector output and the middle layer temperature of the storage tank, a continuous on-off switching could be seen in the system (Figure 5.). This state can occur during the morning, evening or partly cloudy conditions.

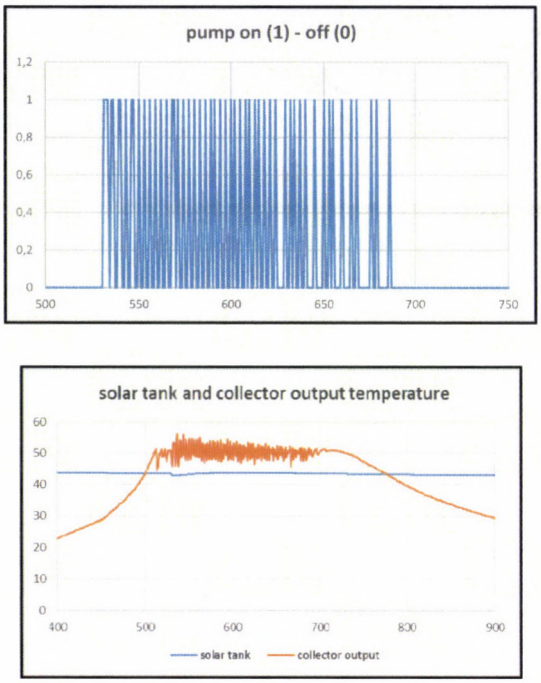

Figure 5. The data logging result in a cloudy day (2015 07.13)

The problem with this continuous on-off switching is that as the tubes are very long, the hot water could not get into the tank, but it was cooled back inside the tubes dissipating the energy to the surroundings, and heating the building. This case was shown for cloudy conditions, but similar effects can be seen for the morning and late afternoon periods, as well.

Modification of the control system for volmetric flow control

The idea we wanted to check is the regulation of the rotational speed of the solar pump, and in this way the regulation of the solar liquid flow velocity, thus the regulation of the flow rate (volumetric current) of the heat transporting medium. To achieve this first a simple lamp switch regulator (based on phase cut) was installed to the system, but with that the pump did not worked well together.

The frequency controller

Thus later on an Altivar 31 (Figure 6.) frequency controller was installed to the system [2]. The main properties of the used device are as follows (beside a lot of not so important properties for us):

- control range: 3 phase control in the range of 0 – 500 Hz
- power range: 0,18 kW– 2,8 kW
- acceleration and deceleration ramp time : 3 s (default, can be adjusted).

At the beginning a few sets has to be adjusted, e.g: as we used only one phase, the phase control function had to be tilted (checking the other two phases is tilted), and the rotation direction of the vector had to be defined (forward), and finally the control method had to be set [3].

Figure 6. The used Altivar31 frequency regulator

To control the pump, there are different options, it is possible to choose between presets values (changeable factory defaults), or with analog input, 0-10 V analog voltage or 4-20 mA current input.

In our case the voltage input was chosen in the regulator, and as the used DA unit was in the output range of 0 – 5 V, the high frequency, dedicated to the 10V input was set to 100 Hz. In this case, when 5 V of regulating voltage was sent to the unit, it was providing 50 Hz to the pump. In this way it was possible to regulate the frequency in the 0 – 50 Hz range, by the 0 – 5 V voltage interval.

Generating the control voltage

The next task was to generate the proper control voltage to the frequency regulator. As the necessary frequency is depending on the collector and tank temperatures measured by the computer, it was natural to use the data logging PC for this purpose. Theoretically there was an analog output voltage module installed in the data logging system, but it was used for different purpose.

As for data logging tasks different National Instruments hardware are in the department, as this task was quite simple, an USB6009 IO unit was used. It has two analog Input and output channels and 8 digital ones. For us the analog output was important, the output0 port was used for the task [4].

The physical setup of the USB6009 connected the frequency regulator can be seen in Figure 7.

Figure 7. The used hardware in operation

The software background: Labview

As the C# source code of the original data logging system was not available, a new routine had to be written for adjusting the proper voltage level of the USB6009 unit. To achieve this the Labview was used, from which the usage of the USB6009 is very simple [5].

The only problem had to be solved how to get the temperature data, measured by the old, C# based data logging system. As the parameter change was practically impossible without the source code, a not so elegant, but working method was used. The data logging system was writing to the hard disk the measured parameters, and the Labview was reading them out. to use for the control voltage.

The first time the refresh rate of the important data was 30 s, and the Labview was reading them back at the same rate, but as the two programs work independently, in some cases almost 60 s were the delay between the measurement and the voltage answer. For more fluent operation the refresh time was reduced to 10 s.

As the control measurements showed, that the pump operation is in the range of 2,5 V – 5 V / 25 Hz – 50 Hz interval (below 2,5 V/25 Hz the output power of the frequency inverter – which is changing by the frequency - was not enough to rotate the pump. So for the real control the 2,5 V – 5 V voltage range was used.

As the frequency inverter made the voltage of 0 – 5 V to the frequency of 0 – 50 Hz, and maximum rotation speed was planned if the temperature difference between the collector output and the solar tank is bigger than 5 Celsius, so the measured temperature difference was set as the control voltage for the frequency inverter, with the maximum value of 5 V. (If the temperature difference went above 5 degree, the voltage was limited to 5 V.)

However the measurement is going on 24 hours, the running of the control is reduced to the sonny intervals, the pump is shot down other time. The Labview code and the information screen during the operation can be seen in Figure 8.

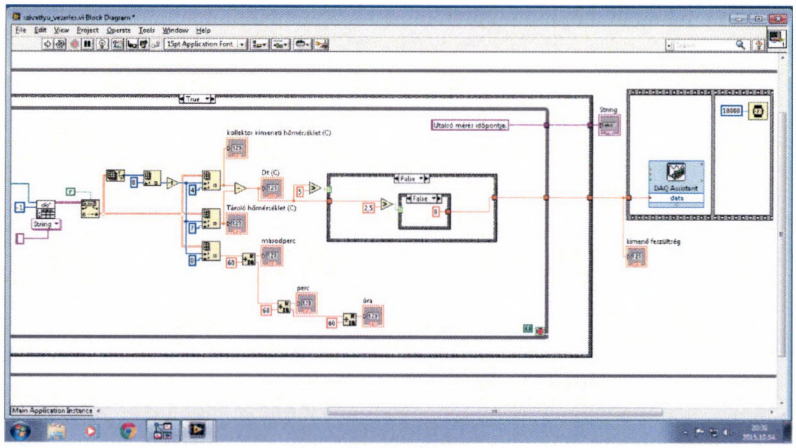

Figure 8. The code-part of the Labview routine

3. The effect of the modification

As the effect of the system change, smoother operation of the pump was predicted, which was checked from the measured value. Compared to the up and down jumping functions of the On-Off switch regulation, more smooth functions were expected. It was partly true (Figure 9.), however some more fine tuning in the morning and late afternoon should be done yet. The energetic consequences are shown in a separate paper.

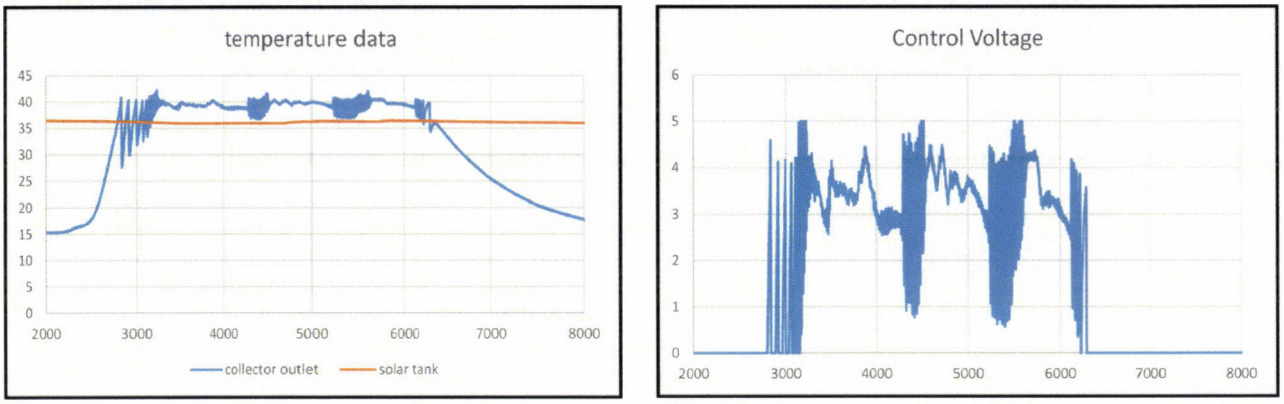

Figure 9. The temperature functions after the modification and the control voltage

4. Conclusion

During the operation of the solar thermal system in the Department of Physics and Process Control, Szent István University, it was observed, that in case of weaker solar radiation the heat absorbed by the collectors, cannot get inside the solar tank due to the very long tubes because of the used on-off regulation.

The control system was modified, as the solar pump rotational frequency is regulated as the function of the temperature difference. For the modification a Labview routine was developed, which generates a temperature difference voltage to a frequency inverter, supplying the pump.

However some graph on the effect of the modification is presented, the energetic consequences of the modification is presented in a separate paper.

Acknowledgements

The authors would like to thanks the help of the Schneider Electric Hungária Villamossági Zrt for the free replacement of our faulted frequency regulator, and in this way supporting the research.

References

[1.] Seres E. E., Farkas I., Biró A., Lágymányosi A., Buzás J.: 1998. Moduláris felépítésű adatgyűjtő rendszer, MTA

[2.] Schneider Electric 2004. Altivar31 Installation Manual, Schneider Electric, 06/2004

[3.] Schneider Electric 2004. Altivar31 Programing Manual, Schneider Electric, 05/2004

[4.] National Instruments (2005): User Guide and Specifications USB6009, National instruments

[5.] John Essick (2015): Hands-On Introduction to Labview for Scientists and Engineers, Oxford University Press, 2015, ISBN: 978-0-19-992515-5

HUNGARIAN AGRICULTURAL ENGINEERING
N° 27/2015 35-37
Published online: http://hae-journals.org/
HU ISSN 0864-7410 (Print) / HU ISSN 2415-9751(Online)
DOI: 10.17676/HAE.2015.27.35

PERIODICAL OF THE COMITTEE OF AGRICULTURAL AND BIOSYSTEM ENGINEERING OF
THE HUNGARIAN ACADEMY OF SCIENCES
and
SZENT ISTVÁN UNIVERSITY
Faculty of Mechanical Engineering

CORRELATION ANALYSIS OF BRANDS IN THE HUNGARIAN NEW TRACTOR MARKET

Author(s):
V. Medina – R. Tóth – M. Daróczi – Á. Bak

Affiliation:
Engineering Management Institute, Szent István University, Páter K. street. 1., Gödöllő, H-2100, Hungary

Email address:
medina.viktor@gek.szie.hu, toth.reka@gek.szie.hu, daroczi.miklos@gek.szie.hu, bak.arpad@gek.szie.hu,

Abstract

There are many tractor brands in Hungary. We examined whether are there any correlation among them. We set up a hypothesis that there is certain seasonality in the new tractor market in Hungary. We supposed also that the subsidies have a strong effect on the seasonality. For this reason we analysed the correlation of the nine most sold tractor brands in our paper. The research covers six years database and almost 100 thousand data. Based on the study we can declare certain seasonality in the new tractor market, which is influenced very much by the impact of state supports for investment. Although the whole tractor market has seasonality, the brands have a different correlation, because of the different marketing strategies of the brands.

Keywords

tractor brands, tractor market, correlation analysis, impact of support, Hungary

1. Introduction

The agriculture plays an important role in Hungary. Its competitiveness is determined by the level of the agricultural machinery [1, 2] The subsidies for investments can strengthen the competitiveness of the Hungarian agricultural sector [3]. For this reason the production is influenced very much by the supports. Presently the support system for investments is unpredictable. The producers aren't able to plan for long time, but the 35-45% subsidy is so high, the growers want to buy new machinery to utilize the EU money for reducing their costs.

Based on our hypothesis the tractor market can be characterized with seasonality. The sales have similar tendencies in every year. This market rhythm is usually disturbed by the supports for buying machines. The goal of our examination is to verify the hypothesis of the tractor market's seasonality and to show the effects of the subsidies.

2. Methods

The examination is based on the KEK KH data, which was collected, systemised and filtered by Datahouse Ltd. The data series from 2009 until 2014 was submitted by the Hungarian Association of Agricultural Tool and Machinery Distributors (MEGFOSZ). We elaborated the sheets containing almost 100 thousand data and systematized by brands to be able to analyse the correlations between the years.

It is expedient to typify the correlation between two variables with an index-number [4]. There are many such index-numbers, but the most popular is the Pearson correlation coefficient, which measures the tightness of the linear relation among the measurements. The coefficient is signed by r, its value is always between -1 and 1. If the points aren't situated along a linear, there isn't any correlation (r=0) or the correlation is weak (the value of r is closed to 0) If the points are situated along a linear r is closed to 1 or -1, in this case there is a strong correlation. If the points are directly on an increasing linear r=1, if on a decreasing linear r=-1. The correlation coefficient is symmetric, the two variables are commutable [4]. The weakness of the Pearson coefficient is that it isn't permitted to use it for part average, because it could show stronger relation than in deed.

If our data is measured not on interval scale but ordinal, then we can use the Spearman correlation coefficient. Its value is always between 1 and -1. The value 1 shows a perfect conformity between the X_i and Y_i rank number series. The value -1 means the two series are converse. If it is 0 there isn't any relation between the two rank series [5].

The Kendall's correlation coefficient is the alternative for Spearmann index to measure the correlation between two variables. To calculate it we use the natural order of the variables rank numbers. Its value is between 1 and -1. The meaning of the values is the same as in the case of Spearmann index. The calculation of spearman and Kendall coefficient is different, but the values are similar. Usually the Spearmann's coefficient shows more correlation than the Kendall's one [6, 7].

We used these three coefficients to verify and show the relation among years, brands and sales tendencies. The calculations were made by SPSS.

3. Results

The examination of the whole database with Pearson correlation coefficient shows significant correlation in some cases. The years 2009 and 2013 have value 0,687, the signification level value is 0,014, which is similar than the relation of years 2010/2013 and 2011/2012. The years 2011/2012 have a little less correlation, but with a signification level still below 0,05 (Table 1.). It was interesting the relation of the years 2009/2012, because the value

is 0,000 with a signification level 0,999. This means a completely independency. The year 2014 has a small negative correlation with the years 2009, 2010, 2013, although this correlation is not significant.

Table 1. Pearson correlation for the total tractor market

		2009	2010	2011	2012	2013	2014
2009	Pearson Correlation	1	,380	,518	,000	,687*	-,393
	Sig. (2-tailed)		,223	,085	,999	,014	,206
2010	Pearson Correlation	,380	1	,196	,323	,682*	-,267
	Sig. (2-tailed)	,223		,542	,306	,014	,401
2011	Pearson Correlation	,518	,196	1	,693*	,653*	,181
	Sig. (2-tailed)	,085	,542		,012	,021	,574
2012	Pearson Correlation	,000	,323	,693*	1	,393	,415
	Sig. (2-tailed)	,999	,306	,012		,206	,180
2013	Pearson Correlation	,687*	,682*	,653*	,393	1	-,118
	Sig. (2-tailed)	,014	,014	,021	,206		,715
2014	Pearson Correlation	-,393	-,267	,181	,415	-,118	1
	Sig. (2-tailed)	,206	,401	,574	,180	,715	

* Correlation is significant at the 0.05 level (2-tailed).
Calculations are based on KEKKH, Datahouse and MEGFOSZ data

The results of Kendall's correlation coefficient show an even stronger correlation at the year pairs 2009/2013, 2011/2012, 2011/2013. Comparing with the results of Pearson coefficient there was no significant the relation in the years 2010/2013. In the other cases there was even stronger correlation. The signification level decreased below 0,010. The values of Spearman's coefficient show even stronger correlation (Table 2). The main diverse value comes from 2014, because the correlation has negative value in four years.

Table 2. Kendall and Spearmann coefficient for the total tractor market

			2009	2010	2011	2012	2013	2014
Kendall's tau_b	2009	Correlation Coefficient	1,000	,273	,273	,107	,576**	-,242
		Sig. (2-tailed)	.	,217	,217	,630	,009	,273
	2010	Correlation Coefficient	,273	1,000	,030	,229	,333	-,182
		Sig. (2-tailed)	,217	.	,891	,303	,131	,411
	2011	Correlation Coefficient	,273	,030	1,000	,595**	,576**	-,121
		Sig. (2-tailed)	,217	,891	.	,007	,009	,583
	2012	Correlation Coefficient	,107	,229	,595**	1,000	,473*	,168
		Sig. (2-tailed)	,630	,303	,007	.	,033	,450
	2013	Correlation Coefficient	,576**	,333	,576**	,473*	1,000	-,061
		Sig. (2-tailed)	,009	,131	,009	,033	.	,784
	2014	Correlation Coefficient	-,242	-,182	-,121	,168	-,061	1,000
		Sig. (2-tailed)	,273	,411	,583	,450	,784	.
Spearman's rho	2009	Correlation Coefficient	1,000	,448	,462	,214	,755**	-,364
		Sig. (2-tailed)	.	,145	,131	,505	,005	,245
	2010	Correlation Coefficient	,448	1,000	,126	,322	,524	-,182
		Sig. (2-tailed)	,145	.	,697	,307	,080	,572
	2011	Correlation Coefficient	,462	,126	1,000	,725**	,755**	-,133
		Sig. (2-tailed)	,131	,697	.	,008	,005	,681
	2012	Correlation Coefficient	,214	,322	,725**	1,000	,673*	,287
		Sig. (2-tailed)	,505	,307	,008	.	,017	,365
	2013	Correlation Coefficient	,755**	,524	,755**	,673*	1,000	-,098
		Sig. (2-tailed)	,005	,080	,005	,017	.	,762
	2014	Correlation Coefficient	-,364	-,182	-,133	,287	-,098	1,000
		Sig. (2-tailed)	,245	,572	,681	,365	,762	.

**. Correlation is significant at the 0.01 level (2-tailed).
*. Correlation is significant at the 0.05 level (2-tailed).
Calculations are based on KEK KH, Datahouse and MEGFOSZ data

The examination of the whole database results a strong correlation among the years 2011, 2012 and 2013. In these three years we can see seasonality and there wasn't any impact of the subsidies. In 2009 was a support for buying agricultural machines to compensate the world crisis in 2008. In 2010 there was a very strong drop on the tractor market. This decline can explain the weaker correlation of the year 2010 with the others. In 2013 it was announced again a subsidy, which had an effect in 2014. This impact is manifested in the correlation coefficients, also with its negative values in previous years.

We made also the correlation analysis of 9 tractor brands. The results show some variation. The main similarity between global and brand seasonality we could see in the case of the year 2014, where the small negative correlation with 2009, 2010, 2011, 2013 was shown in almost all brands. The correlation between 2011 and 2013 was declared in the case of Case, Fendt, John Deere and New Holland. In the other cases were different correlations among the years (Table 3).

Table 3. Spearmann coefficient in the case of different tractor brands

Brand	Year	Coeff.	Sig.	Year	Coeff.	Sig.	Year	Coeff.	Sig.	Year	Coeff.	Sig.
Case	2009/2010	0,584	0,046	2010/2011	0,739	0,006	2010/2013	0,722	0,008	2011/2013	0,898	0,000
Claas	2011/2014	0,614	0,034	2012/2013	0,611	0,035	2013/2014	0,648	0,023	-	-	-
Fendt	2011/2013	0,504	0,046	2012/2013	0,609	0,035	2012/2013	0,609	0,035	-	-	-
John Deere	2009/2010	0,74	0,006	2011/2013	0,71	0,01	2012/2014	0,582	0,047	-	-	-
MTZ	2009/2010	0,757	0,004	2009/2013	0,643	0,024	2010/2013	0,839	0,001	2012/2013	0,643	0,024
New Holland	2010/2012	0,578	0,049	2011/2013	-0,711	0,01	2013/2014	0,747	0,005	-	-	-

Calculations are based on KEK KH, Datahouse and MEGFOSZ data

Analysing the correlation between years at different brands we can declare that the significant correlations are very variable in different years and brands. There were also three brands, where we couldn't find any relation between the years. The sales had no seasonality in the case of Landini, Massey Ferguson and Zetor.

4. Conclusion

Summarizing the results we can conclude that there is certain seasonality in the new tractor market, which is influenced very much by the impact of investment state supports. The years 2011, 2012, 2013 have significant correlation each other. These years were not disturbed by the subsidies. The years 2009, 2010 and 2014 have no correlations with other years because of the great influence of state supports. These clear relationships were not found in the case of brand examinations. The examined nine brands had different correlation in different years. This fact shows the effect of the different marketing activity of the brands. There is a variance between the global and brand seasonality. The different marketing strategies result varying intensity of sales and explain the deviations.

This publication is a result of a research work performed in the project called:
TÁMOP-4.2.1.D-15/1/KONV-2015-0007 Smart City: Innovatív kutatási hálózatok fejlesztése Gyula és Salgótarján városokban.

References

[1.] Magó L.: 2008a. A gépkihasználás fokozásával megvalósítható alacsony költségű gépesítési megoldások különböző üzemi méretű növénytermelő gazdaságokban, in Szerk.: Takács István „Műszaki fejlesztési támogatások közgazdasági hatékonyságának mérése" c. tanulmánykötet, Szent István Egyetemi Kiadó Gödöllő, p. 213-228., p. 244.

[2.] Magó L.: 2008b. Low Cost Mechanisation for Efficient Land Use in Small and Medium Size Arable Farms, Cereal Research Communications, Akadémiai Kiadó, Vol. 36: p. 1111-1114.

[3.] Magó L.: 2000. Relationship Between Farm Machine Requirement and Farm Size, Gazdálkodás, Scientific Journal on Agricultural Economics – English special edition Vol. XLIV., No. 1., p. 66-75.

[4.] Anderson D.: 1998. Statistics for Business and Economics, 7th edition, USA, South Western College Publishing, ISBN 0538875933

[5.] Flemming M. C. Nellis J. G. (1996): The Essence of Statistics for Business, 2nd edition, Hemel Hempstead, UK, Prentice Hall Europe, ISBN 013987779

[6.] Levin R, Rubin D. (1997): Statistics for Management, 7th edition, Englewood Clifs, NJ: Prentice Hall International, ISBN 0136067166

[7.] Vincze I., Varbanova M. (1993): Nemparaméteres matematikai statisztika, Akadémiai Kiadó,

HUNGARIAN AGRICULTURAL ENGINEERING
N° 27/2015 38-41
Published online: http://hae-journals.org/
HU ISSN 0864-7410 (Print) / HU ISSN 2415-9751(Online)
DOI: 10.17676/HAE.2015.27.38

PERIODICAL OF THE COMITTEE OF AGRICULTURAL AND BIOSYSTEM ENGINEERING OF
THE HUNGARIAN ACADEMY OF SCIENCES
and
SZENT ISTVÁN UNIVERSITY
Faculty of Mechanical Engineering

FORECASTING OF DISSOLVED OXYGEN IN THE RIVER DANUBE USING NEURAL NETWORKS

Author(s):
A. Csábrági[1] – S. Molnár[1] – P. Tanos[1] – J. Kovács[2]

Affiliation:
[1]Institute of Mathematics and Informatics, Szent István University, Páter K. street 1., Gödöllő, H-2100, Hungary
[2]Institute of Geography and Earth Sciences, Eötvös Loránd University, Pázmány Péter walkway 1/C., Budapest, H-1117, Hungary

Email address:
csabragi.anita@gek.szie.hu, molnar.sandor@gek.szie.hu, tanos.peter@gek.szie.hu kevesolt@iris.geobio.elte.hu

Abstract

The Danube is the second-largest river in Europe and the conservation of its water quality is very important because it influences the lives of millions people. The aim of this research is to predict one of the most important water quality parameters, dissolved oxygen, with the help of water pH, runoff, water temperature and electrical conductivity data. Multivariate Linear Regression (MLR), Back-propagation Neural Networks (BPNN) and General Regression Neural Networks (GRNN) were applied and their performances compared in this study. The most accurate prediction proved to be GRNN. This paper describes the influence of single input parameters on the prediction.

Keywords

River Danube, General Regression Neural Networks, Back-propagation Neural Networks, Dissolved Oxygen

1. Introduction

Dissolved oxygen is a very significant parameter in the condition of surface waters, and so its prediction by the help of general and easily measureable parameters is an important scientific question. The concentration of dissolved oxygen (DO) reflects the equilibrium or its lack between oxygen-producing processes (e.g. photosynthesis) and oxygen-consuming processes (e.g. aerobic respiration, nitrification, and chemical oxidation) and depends on many factors such as temperature, salinity, oxygen depletion, sources of oxygen and other water quality parameters [1]. The DO level is a measure of the health of aquatic systems. A certain minimum level of DO in water is required for aquatic life to survive [2].

Various models are used for the prediction of several parameters of surface waters, but in the last decade the techniques of artificial intelligence have been successfully applied as a forecasting method. In most research, the simply prediction of the concentration of dissolved oxygen was the aim [1, 3, 4, 5, 6, 7, 8, 9], while in a number of studies the prediction of biological oxygen demand (BOD) was the purpose [2, 7, 10] and, very rarely, models were applied to the estimation of chemical oxygen demand (COD) [7, 11]. MLP was applied by Rankovic et al. [3] for the modelling of DO in a reservoir, in Serbia, and in their next study [8] an adaptive network-based fuzzy inference system (ANFIS) model was used on the same dataset, but with fewer input variables. Ahmed [1] developed two models, an MLP and a radial basis function neural network (RBFN), for the prediction of DO in the Surma River (Bangladesh) using BOD and COD and the models were compared: the RBFN predicted better. Emamgholizadeh et al. [7] used three models (MLP, RBFN and ANFIS) and the MLP was the most efficient in predicting water quality variables (DO, BOD and COD) in the Karoon River, Iran. Basant et al. [2] predicted the DO and BOD in the Gomti River, India, using two models (partial least squares regression and MLP), and the performance of the MLP was better. MLP was developed by Dogan et al. [10] to predict the BOD in the Melen River, Turkey, and the COD was found to be more effective on the BOD estimation. The MLP with the Bayesian regularization training algorithm was successfully utilized by Wen et al. [4] to simulate the DO concentrations in the Heihe River, China, where the most effective inputs were determined as pH, NO3-N and NH4-N. Two applied models (MLR and GRNN) were compared by Heddam [9] and it was found that the best fit was obtained using GRNN model in prediction of DO in the Upper Klamath River, USA. Antanasijevic et al. [5] developed three models: MLP, GRNN and Recurrent Neural Network (RNN) for the modelling of DO in the River Danube, in Serbia at a single location, Bezdan, and the obtained results showed that RNN performed much better than the other methods. Only GRNN was used by Antanasijevis et al. [6] for the prediction of DO in the River Danube, in Serbia, at 17 sample sites, and various normalization and input selection techniques were compared and applied successfully.

The main objective of this study is to predict one of the most important parameters, dissolved oxygen, with the help of some easily measured physical and chemical variables of the River Danube using MLR and two types of neural networks (GRNN and BPNN). A further aim is to evaluate the results obtained and to apply sensitivity analysis to them, in order to determine which input variable(s) played a significant role in the prediction of output.

2. Material and methods

Water quality data set

There are 12 sampling sites in the section of the River Danube in Hungary, the Mohács station (Figure 1.) was chosen as a representative location, while the studied period was from 1998

to 2003. This complete river water quality data set was divided into two subsets. The data from 2003 were used as the test data set (26 data patterns, 17% of all available data), and the data from 1998-2002 were used as the training set (128 data patterns, 83% of all available data). The output variables corresponding to the input variables belonged to the same water sample, which was measured in the same time and at the same location. The same training and testing sets were used with every single model applied.

Figure 1. Hungarian section of the River Danube

Multivariate Linear Regression

Multivariate Linear Regression (MLR) is used to estimate the linear association between the dependent and one or more independent variables. MLR is based on least squares; and it expresses the value of the predicted variable as a linear function of one or more predictor variables:

$$y = \beta_0 + \beta_1 * x_1 + \beta_2 * x_2 + ... + \beta_i * x_i$$

where x_i is the value of the i_{th} predictor variable, β_0 is the regression constant, and β_i is the coefficient of the i_{th} predictor variable.

Back-propagation neural network

Artificial neural networks (ANNs) are basically parallel computing systems similar to biological neural networks. Among the various types of ANNs the multilayer perceptron (MLP) neural network structure is the most commonly used and is a well-researched basic ANN architecture. The MLP has generally three layers: input, output and one or more hidden layer(s). Each layer consists of one or more basic element(s) called a neuron or a node (or a processing unit). Nodes are connected to each other by links, synapses are characterised by a weight factor, which denotes the connection strength between two nodes. Each node in the input and inner layers receives input values, processes it, and passes it to the next layer. This process is conducted by weights [10], meaning that the hidden layer sums the weighted inputs and own bias value and uses the own transfer function to create an output value. Typical transfer functions are the linear, the sigmoid or the hyperbolic tangent function [12].

Back-propagation neural networks (BPNN) are multilayer feed-forward perceptrons (MLP) trained from the input data using an error back-propagation algorithm [5]. Back-propagation was proposed by Rumelhart et al. [13], and it is the most popular algorithm for the training of an MLP network [12]. This back-propagation algorithm has two steps. The first step is a forward pass, in which the effect of the input is passed forward through the network to reach the output layer. After the error is computed, a second step starts backward through the network [7] to correct the initial assigned weights of the input layer in such a way as to minimize the error. The term "feed-forward" means that a node connection only exists from a node in the input layer to other nodes in the hidden layer or from a node in the hidden layer to nodes in the output layer; and nodes within a layer are not interconnected to each other, there are not lateral or feedback connections. MLP using a BP algorithm is sensitive to randomly assigned initial connection weights [14]. The initialization of weights and bias values for a layer is conducted using Nguyen-Widrow method in the MATLAB environment [15], and these initial values are dissimilar on every single run, so after the training process different predicted values are obtained. Since these predicted values were significantly different, the MLP was trained sixty times at the same settings (number of neuron, input and target values, transfer functions and back-propagation algorithm etc.) and the average of these predicted values were taken into account.

In this study, the Levenberg-Marquardt algorithm is applied for adjusting the MLP weights [16] and the number of epochs was 1000. One hidden layer and a hyperbolic tangent sigmoid transfer function were used between the input and the hidden layer and a linear transfer function was employed between the hidden and output layers. Neural Network Toolbox of MATLAB was utilized for both ANNs.

General Regression neural network

GRNN was introduced first by Specht [17] as an alternative to MLP. GRNN is a modified form of the radial basic function neural network model. GRNN is a one-pass supervised learning network, and it is a universal approximator for smooth functions. GRNN is a four-layer feed-forward neural network, which is shown in Fig. 2. The first layer is fully connected to the second. Each input unit in the first layer corresponds to an independent variable in the model and the number of pattern neurons is equal to the number of data patterns. The training between the input layer and the pattern layer is performed by defining the weights (the center of the RBF functions) with the help of a special clustering algorithm such as the k-means algorithm [14] and estimates the Euclidean distance of the ith input vector (x_i) and the weight of the i^{th} input variable and the j^{th} pattern node (w_{ij}) where N is the number of input variables.

$$D_j = \sqrt{\sum_{i=1}^{N}(w_{ij} - x_i)^2}\,. \qquad (1)$$

Using the most popular RBF function, the Gaussian Kernel Function as an activation function, where σ is the smoothing factor or spread:

$$f(D_j) = \exp\left(\frac{-D_j}{2\sigma^2}\right). \qquad (2)$$

The smoothing factor is the only "unknown" parameter in the GRNN algorithm; it represents the width of the calculated Gaussian Kernel Function, and must be given before training the model.

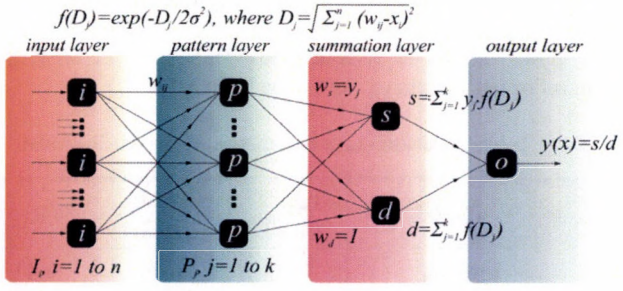

Figure 2. A schematic representation of GRNN, adopted from Antanasijevic et al. [6]

The number of neurons in the summation layer can be expressed as No+1, where No is the number of output neurons [6]. Since the model has only one output, each pattern layer unit is connected to the two neurons in the summation layer: the S-summation neuron and the D-summation neuron. The weights between the summation-neuron and output neuron are equal to the measured value of the output variable. The S-summation neuron computes the sum of the weighted outputs of the pattern layer (S) while the D-summation neuron calculates the unweighted outputs of the pattern neurons (D).

$$D = \sum_{j=1}^{K} f(D_j) \tag{3}$$

$$RMSE = \sqrt{\frac{1}{n}\sum_{i=1}^{n}(O_i - P_i)^2} \tag{4}$$

Finally, the output layer merely divides the S-summation neuron by the D-summation neuron [9].

Statistical forecasting of the models

The performance of the applied models can be assessed by several statistical error parameters. The root mean square error (RMSE), mean absolute error (MAE), and coefficient of determination (R2) were used to provide an indication of goodness of fit between the observed and predicted values. Expressions for these error parameters are given as follows:

$$RMSE = \sqrt{\frac{1}{n}\sum_{i=1}^{n}(O_i - P_i)^2} \tag{5}$$

$$MAE = \frac{1}{n}\sum_{i=1}^{n}|O_i - P_i| \tag{6}$$

$$R^2 = \frac{\left[\sum_{i=1}^{n}(O_i - \bar{O})(P_i - \bar{P})\right]^2}{\sum_{i=1}^{n}(O_i - \bar{O})^2 \sum_{i=1}^{n}(P_i - \bar{P})^2} \tag{7}$$

where n is the number of input samples; and O_i and P_i are the observed and predicted output value from the ith element, respectively. $\bar{O}$ and $\bar{P}$ denote their respective averages.

3. Results and discussion

Prediction by Multivariate Linear Regression

Equation (8) was obtained by the MLR from the input water quality variables, which represent the whole dataset (training set + testing set)

$$DO = 5.9198 * pH - 0.2101 * WT - 0.0053 * EC - 0.0002 * RF - 32.6353 \tag{8}$$

where pH is the water's pH value; WT is the water temperature (°C), EC is the electrical conductivity (μS/cm), and RF is the runoff (m^3/s).

Table 1 shows the performance evaluation of the MLR model in reference to training, testing and whole set.

Table 1. Performance parameters of the MLR model

MLR	RMSE (mg/L)	MAE (mg/L)	R^2
training	1.13	0.79	0.52
testing	1.73	1.24	0.45
whole	1.31	0.92	0.46

Prediction by Back-propagation Neural Network

The best performance with reference to the testing set was achieved by BPNN using z-score (normalizing so the inputs and targets have zero mean and unity standard deviation) and 5 neurons in the single hidden layer. These results, which are presented in Table 2, were the errors of sixty run's average.

Table 2. Performance parameters of the BPNN model – the error of sixty run's average

BPNN	RMSE (mg/L)	MAE (mg/L)	R^2
training	0.65	0.43	0.85
testing	1.57	1.28	0.57
whole	0.88	0.57	0.77

Prediction by General Regression Neural Network

The best performance with reference to the testing set was gained by BPNN applying z-score and 0.3 as smoothing factor, Table 3 depicts the obtained values of RMSE, MAE, R2 for the training, testing and the whole sets.

Table 3. Performance parameters of the GRNN model

GRNN	RMSE (mg/L)	MAE (mg/L)	R^2
training	0.47	0.27	0.93
testing	1.42	1.14	0.72
whole	0.72	0.41	0.85

Summarizing, the comparison of the results of the MLR and BPNN models with GRNN revealed that the GRNN performed better than the MLR and BPNN models in both training and testing.

Sensitivity analysis

Sensitivity analysis was applied to determine the relative significance of each input variable, namely which parameter played the most important role in predicting the DO. The optimal network architecture (GRNN) which provided the best performance was selected as a base and the evaluation process was conducted to eliminate only one input parameter in the data set. Table 4 gives the results of five networks, and each one demonstrates the extents, to which the eliminated variable would affect the network accuracy. As the results in the Table 4 show, the pH value was the most effective parameter in predicting DO, and the runoff had the weakest effect on the accuracy the prediction of DO.

Table 4. Sensitivity analysis of input variables eliminated separately

Combination	RMSE (mg/L)		MAE (mg/L)		R^2	
	Training	Testing	Training	Testing	Training	Testing
All	0.47	1.42	0.27	1.14	0.93	0.72
Eliminate pH	1.07	2.14	0.73	1.69	0.59	0.24
Eliminate EC	0.70	1.57	0.42	1.26	0.83	0.62
Eliminate WT	0.67	1.50	0.44	1.30	0.85	0.73
Eliminate RF	0.68	1.46	0.47	1.16	0.84	0.72

Following the application of sensitivity analysis by GRNN, the pH value of the applied input variables has the most significant influence on the prediction of the DO. This result is confirmed

by correlation coefficients. The highest correlation was obtained between the DO and pH (0.33), while the lowest was between the DO and RF (-0.16). The correlation coefficients between DO-WT and DO-EC were -0.29 and 0.25.

4. Conclusion

In this study, two types of the ANNs, namely (BPNN and GRNN) and MLR were applied to predict the DO in the River Danube, at a single location, Mohács, with water pH, temperature, electrical conductivity and runoff. In order to compare the two ANNs and MLR results, RMSE, MAE, and R2 were used as evaluation criteria. Based on the results obtained by training and testing of the ANNs, it was found that the GRNN model provided better predictions of DO than the BPNN, and so the use of GRNN is justified not only due to its better performance, but also on account of it quickness, as, in contrast to BPNN, it is a one-pass training algorithm that does not necessitate an iterative training process. A comparison of the ANNs with the conventional MLR shows that the ANNs demonstrated better performance indicators than the MLR when every model was trained and tested by the same data sets and input variables. Conclusions have shown that the two ANNs, and especially the GRNN are practical methods for predicting DO concentrations in a river.

References

[1.] Ahmed A. A. M.: 2014. Prediction of dissolved oxygen in Surma River by biochemical oxygen demand and chemical oxygen demand using the artificial neural networks (ANNs), Journal of King Saud University – Engineering Sciences, http://dx.doi.org/doi:10.1016/j.jksues.2014.05.001

[2.] Basant N., Gupta S., Malik A., Singh K. P.: 2010. Linear and nonlinear modelling for simultaneous prediction of dissolved oxygen and biochemical oxygen demand of the surface water – A case study, Chemometrics and Intelligent Laboratory System, Vol. 104, pp. 172-180. http://dx.doi.org/doi:10.1016/j.chemolab.2010.08.005

[3.] Rankovic V., Radulovic J., Radojevic I., Ostojic A., Comic L.: 2010. Neural network modelling of dissolved oxygen in the Gruza reservoir, Serbia. Ecological Modelling, Vol. 221, pp. 1239–1244. http://dx.doi.org/doi:10.1016/j.ecolmodel.2009.12.023

[4.] Wen X., Fang, J., Diao M., Zhang C.: 2013. Artificial neural network modelling of dissolved oxygen in the Heihe River, Northwestern China, Environmental Monitoring and Assessment, Vol. 185, pp. 4361-4371. http://dx.doi.org/doi:10.1007/s10661-012-2874-8

[5.] Antanasijevic D., Pocajt V., Povrenovic D., Peric-Grujic A., Rictic M.: 2013. Modelling of dissolved oxygen content using artificial neural networks: Danube River, North Serbia, case study, Environmental Science and Pollution Research, Vol. 20, pp. 9006-9013. http://dx.doi.org/doi:10.1007/s11356-013-1876-6

[6.] Antanasijevic D., Pocajt V., Povrenovic D., Peric-Grujic A., Rictic M.: 2014. Modelling of dissolved oxygen in the Danube River using artificial neural networks and Monte Carlo Simulation uncertainty analysis, Journal of Hydrology Vol. 519, pp. 1895-1907. http://dx.doi.org/doi:10.1016/j.jhydrol.2014.10.009

[7.] Emamgholizadeh S., Kashi H., Marofpoor I., Zalaghi E.: 2014. Prediction of water quality parameters of Karoon River (Iran) by artificial intelligence-based models, Int. Journal of Environmental Science and Technology, Vol. 11, pp. 645-656. http://dx.doi.org/doi:10.1007/s13762-013-0378-x

[8.] Rankovic V., Radulovic J., Radojevic I., Ostojic A., Comic L.: 2012. Prediction of dissolved oxygen in reservoirs using adaptive network-based fuzzy inference system, Journal of Hydroinformatics, Vol. 14, pp. 167-179. http://dx.doi.org/doi:10.2166/hydro.2011.084

[9.] Heddam S.: 2014. Generalized regression neural network-based approach for modelling hourly dissolved oxygen concentration in the Upper Klamath River, Oregon, USA, Environmental Technology, Vol. 35, pp. 1650-1657. http://dx.doi.org/10.1080/09593330.2013.878396

[10.] Dogan E., Sengorur B., Koklu R.: 2009. Modelling biochemical oxygen demand of the Melen River in Turkey using an artificial neural network technique, Journal of Environmental Management, Vol. 90, pp. 1229–1235. http://dx.doi.org/10.1016/j.jenvman.2008.06.004

[11.] Talib A. M. I. Amat M. I.: 2012. Prediction of chemical oxygen demand in Dondang river using artificial neural network, International Journal of Information and Education Technology, Vol. 2, pp. 259-261. http://dx.doi.org/10.7763/IJIET.2012.V2.124

[12.] Haykin S. 1998. Neural Networks: A comprehensive foundation, 2nd Ed., Prentice-Hall, Upper Saddle River, NJ.

[13.] Rumelhart D. E., Hinton G. E., Williams R. J. 1986. Learning internal representation by error back propagation, In: Rumelhart DE, and JL. McClelland (eds) Parallel distributed processing. MIT Press, Cambridge, MA, pp 318-362.

[14.] Kim S., Kim H. S.: 2008. Neural networks and genetic algorithm approach for nonlinear evaporation and evapotranspiration modelling, J. Hydrol., Vol. 351. pp. 299-317. http://dx.doi.org/10.1016/j.jhydrol.2007.12.014

[15.] Pavelka A. Procházka A.: 2004. Algorithms for initialization of neural network weights, Sbornik prispevku 11. Konference MATLAB, Vol. 2. pp. 453-459.

[16.] Marquardt D.: 1963. An algorithm for least square estimation of nonlinear parameters, Journal of the Society for Industrial and Applied Mathematics, Vol. 11, pp. 431-441. http://dx.doi.org/10.1137/0111030

[17.] Specht, D. F.: 1991. A general regression neural network, IEEE Transactions on Neural Networks, Vol. 2, pp. 568-576. http://dx.doi.org/10.1109/72.97934

HUNGARIAN AGRICULTURAL ENGINEERING
N° 27/2015 42-45
Published online: http://hae-journals.org/
HU ISSN 0864-7410 (Print) / HU ISSN 2415-9751(Online)
DOI: 10.17676/HAE.2015.27.42

PERIODICAL OF THE COMITTEE OF AGRICULTURAL AND BIOSYSTEM ENGINEERING OF
THE HUNGARIAN ACADEMY OF SCIENCES
and
SZENT ISTVÁN UNIVERSITY
Faculty of Mechanical Engineering

DEVELOPMENT OF BIODEGRADABILITY INDICATORS FOR MICROWAVE SLUDGE CONDITIONING

Author(s):
S. Beszédes[1] – P. Veszelovszki[2] – L. Ludányi[1] – G. Keszthelyi-Szabó[1] – C. Hodúr[1]

Affiliation:
[1]Department of Process Engineering, Faculty of Engineering, University of Szeged, Moszkvai blvd. 9, Szeged, H-6725
[2]Technical Institute, Faculty of Engineering, University of Szeged, Moszkvai blvd. 9, Szeged, H-6725

Email address:
beszedes@mk.u-szeged.hu, veszelov@mk.u-szeged.hu, ludanyi.lajos@gmail.com, szabog@mk.u-szeged.hu, hodur@mk.u-szeged.hu

Abstract

Microwave irradiation has a good potential to increase the ability of organic matter for biological degradation. Because of the strong disintegration effect of microwave irradiation on extracellular polymeric substances (EPS), which form complex sludge structure, and also on microbial cell walls has led to enhanced solubility of organic matters, given by the ratio of soluble to total chemical oxygen demand (SCOD/TCOD). From the aspect of the further utilization of sludge, the change of biochemical oxygen demand (BOD), which correlates the degradable organic matters of sludge under aerobic condition, can be considered advantageous. For comparison purpose, and for modeling and optimization of process, it is needed to create novel control parameters, by which can be measured the changes in organic matter fraction of sludge independently from the varying characteristic or different origin of raw sludge. Based on our results, it has established that in the range of 90-1050 $kJkg^{-1}$, and 0.5-5 Wg^{-1} for IMWE and MWPL, the surface fitted by constructed model can be characterized by a maximum value for BDI. Microwave treatment carried out over a certain value of MWPL and IMWE has resulted in lower biodegradability. Optimum range of IMWE and MWPL was concluded as 600-650 kJ and 2.5-3.0 Wg^{-1}, respectively, and both process parameters have significant effect on the change of BDI and SLI, as well.

Keywords

wastewater sludge, biodegradability, microwave pre-treatment

1. Introduction

Nowadays, because of the shortening of water resources, expectations for higher capacity and cleaning efficiency of wastewater purification technologies are growing. Notwithstanding of the technological development of wastewater treatment works the amount of sludge produced in these process is continuously increasing. Taking into consideration the environmental awareness and the more and more rigorous pollution control regulations, the research and development activity focuses on the sludge utilization processes. However the sludge utilization and valorization technologies require applying pre-treatments.

The sludge pre-treatment processes aim mainly the volume reduction to reduce the cost of transportation and storage, the destruction of pathogen microorganisms to decrease the microbial risk of sludge, the removal of the toxic components of sludge to reduce the environmental risk, or the enhanced degree of further utilization efficiency. Respect to the nowadays used industrial scale sludge handling technologies the thermal pre-treatments can be considered as the more commonly used processes. The advantageous effect of thermal pre-treatment on the sludge structure have been verified and utilized for decades [1]. The main aim for applying thermal pre-treatments is to reduce the odour load of sludge processing, to reduce the microbial risk of sludge disposal and to increase the organic matter removal efficiency of anaerobic digestion in industrial scale technologies

Previous investigations have been verified, that microwave irradiation is applicable in various waste and by-products handling technologies with high efficiency. Beside these advantages, it can be concluded, that the effects and efficiency of microwave processes are not enough deeply investigated and analyzed for many types of materials. It can be also established, that results of studies on microwave sludge conditioning obtained mainly from municipal sludge processing. The main advantages of microwave heating over the conventional heating methods are the following: rapid heat generation, volumetric heating, selecting heating mechanism in multicomponent system resulted from the different dielectric properties of components, and the very short process time demand due to the high energy intensity of microwave irradiation [2]. Application of MW irradiation combining with the oxidation process, such as ozonation, can also be considered to be promising technology as pre-treatment before AD of high organic matter containing but less degradable sludge [3].

Energy transfer carried by microwave irradiation affect the biodegradability of materials in two ways. Thermal effect is expressed in the increase of internal pressure of intracellular liquor caused by internal heating and rapid evaporation, which altogether can lead to cell wall disruption [4]. The non-thermal effect of high frequency electromagnetic field contributes to alter the structure of macromolecules with polarization of side chains and breaking of hydrogen bounds [5, 6]. High efficiency of MW treatments in the biomaterial processing and also on the rate of chemical reactions is often explained by the non-thermal effects of microwaves due to the direct interaction of electromagnetic field with molecules.

Thermal and a-thermal effects of the microwave (MW) irradiation play role in the „hot-spot" overheating phenomena,

and the different dielectric parameter of cell components led to selective heating manifested in the different thermal stress, which contributes in the intensive degradation of cell wall components such as cellulose and pectin [7]. MW pre-treatment has verified positive effects on cell wall destruction and releasing of organic matter into the soluble phase, but combining of it with addition of chemicals such as alkali, acid and oxidizer agents cause synergetic mechanism to accelerate the decomposition under aerobic and anaerobic condition., as well [8].

Despite the good potential of microwave irradiation for material processing and the promising results of the field of microwave research the adaptation of them in industrial scale processes has been not realized yet. Available scientific results and experiences from the microwave sludge conditioning are not enough to scale up the microwave process. Furthermore, beside these advantages, it can be concluded, that the effects and efficiency of microwave processes are not deeply enough investigated and analyzed for many types of materials.

Published scientific work and research reports in the field of microwave sludge processing find microwave irradiation as an efficient method to dehydrate the sludge, and to recover some valuable component, such as some metallic compound, and microwave irradiation is suitable as pre-treatments method before anaerobic digestion to increase the biogas yield. This advantageous and beneficial feature of microwave irradiation is caused by the effect of high frequency electromagnetic field on the secondary and tertiary structure of proteins, which can manifested in the decreased stability and the enhanced disintegration degree of sludge particles [9]. It has been also concluded, that the increment in the solubility of carbohydrate compounds of sludge was approximately 10-15% higher, than the improvement in protein solubilisation after microwave treatment [10].

Comparing of the results obtained from different studies has difficulties because of the different condition of experimental set-up, and the undefined or not exactly defined control parameters used for evaluation of microwave process. Therefore these observations are often led to incorrect conclusion, determined optimum parameters cannot be used for another material or equipment, and make complicated the scale up of processes. Additionally, the comparison of the efficiency of microwave operation and process parameters is difficult because the control parameters are undefined or the calculation methods are different, and the analytical methods are not standardized.

There are some studies concluded the increasing of microwave power has an increasing effect on the organic matter solubility [10, 11], nevertheless other studies summarized decreasing effect of the enhanced microwave power [12, 13]. Applying microwave treatment with high power intensity in open vessel systems, the agglomeration of partly dehydrated sludge particles are observable, because of the intensive evaporation from the surface of the sludge exposed to microwave irradiation. In this case, the change in sludge structure is considered irreversible, because the water addition after the microwave treatment is not able to resolve the organic matters [14].

It can be also noticed, that results of studies on microwave sludge conditioning obtained mainly from municipal sludge processing, which has lower organic and dry matter contant than the food industry sludge. It has been established, that microwave pre-treatments of municipal sludge enhance the organic removal efficiency of anaerobic digestion process [10] and increase the biogas production [13].

2. Materials and methods

Investigated wastewater sludge was originated from meat industry with a total solid (TS) content of 9.7 %, initial total COD of 105.9 kgm^{-3}, and soluble COD of 20.1 kgm^{-3}. Microwave experiments were carried out in a tailor made microwave sludge processing and measuring system developed at the Process Engineering Department of the University of Szeged Faculty of Engineering. Microwave equipment has a continuously irradiating magnetron with changeable power in the range of 50 W to 700 W operating at a frequency of 2450 MHz. Power of the continuously irradiating microwave magnetron is adjustable by varying of anode voltage through a transformer with variable voltage. To investigate the efficiency of the MW pre-treatment process the parameters studied were the microwave power level (MWPL), and the irradiated microwave energy (IMWE) (Equation 1). MWPL (Wg-1) was defined as the ratio of magnetron power to the quantity of treated sludge. MWPL and IMWE were calculated from the weight of sludge samples (m_{sl} [g]), the power of magnetron (P_m [W]), the irradiation time ($\tau\tau$[s]) and the percentage irradiation time period of magnetron (I [%]).

$$IMWE = \frac{P_m \times \tau \times I}{100 \times m_s} \quad [Jg^{-1}] \tag{1}$$

Carbonaceous biochemical oxygen demand (BOD) tests were carried out in a respirometric BOD system (BOD Oxidirect, Lovibond, Germany) thermostated at a temperature of 20±0.2°C (TS606, WTW). BOD analysis was according to the APHA5210D method. To ensure the consistency of the experiments, BOD seed microbe capsules (Cole Parmer, USA) were used for the measurements. The chemical oxygen demand (COD) was measured by the standardized colorimetric dichromate method using HACH test cuvettes, according to USEPA 5520D method. For the thermal digestion ET108 (Lovibond) thermoblock was used for 2 hours at 150°C. The COD was measured colorimetrically using PC Checkit photometer with inner calibration for COD measurement. The total chemical oxygen demand (TCOD) was measured from the total sludge matrix. The soluble organic matter content was given as the soluble chemical oxygen demand unit (SCOD). SCOD was determined after separation of soluble from solid fraction by centrifugation (RCF of 32000 g for 15 minutes, MPW-350 centrifuge) and pre-filtration (0.45 τm Millipore cellulose-acetate disc filter).

The solubility index (SLI) (Equation 2) and the biodegradation index (BDI) (Equation 3) are calculated from the total organic matter content (given by the TCOD), the soluble organic matters content (SCOD) and the biochemical oxygen demand (BOD), measuring them initially (0), at a given time (t) and from the parameters of maximum biodegradable sample (max).

$$SLI = \frac{\left(\frac{SCOD}{TCOD}\right)_t - \left(\frac{SCOD}{TCOD}\right)_0}{\left(\frac{SCOD}{TCOD}\right)_{max} - \left(\frac{SCOD}{TCOD}\right)_0} \quad [-] \tag{2}$$

$$BDI = \frac{\left(\frac{BOD}{SCOD}\right)_t - \left(\frac{BOD}{SCOD}\right)_0}{\left(\frac{BOD}{SCOD}\right)_{max} - \left(\frac{BOD}{SCOD}\right)_0} \quad [-] \tag{3}$$

3. Results and discussion

Our earlier results verified that MW pre-treatments have numerous advantages over the conventional heating, such as higher biogas yield and accelerated anaerobic decomposition. Increment of solubility and biodegradability depend on the

MWPL applied during microwave pretreatment and also on the irradiation time.

To analyze the effect of the two process parameters, i.e. IMWE (x_1) and MWPL (x_2), on the change of SLI and BDI response surface methodology (RSM) with CCF design was applied. Equations with significant terms remained showing that both of the factors have a linear and quadratic effect on the value of control parameters studied. Interaction among variables of IMWE and MWPL was not significant for BDI at the significance level of 0.05 ($\tau=\tau\%$), but it was significant for SLI. Multiple linear regression analysis of the experimental data yielded the following second-order polynomial equation:

$$SLI = 0.8085 + 0.301x_1 + 0.014x_2 + 0.0706x_1x_2 - 0.237x_1^2 + 0.036x_2^2 \quad [-]$$

$$BDI = 0.8921 + 0.071x_1 - 0.002x_2 - 0.298x_1^2 + 0.043x_2^2 \quad [-]$$

Results of the ANOVA for the quadratic model for BDI show a high degree of correlation between the predicted and observed values (R^2 value was over 0.9), the lack of fit values indicated that the lack of fits were not significant relative to the pure error at a level of 0.05. Results of RSM show that the degradation effects of MW pre-treatment were limited due to the demineralization effects. Results of response surface analysis show that MW pre-treatments enhance the SLI from 0.18 to above 0.9 at high IMWE and MWPL levels, but the increment of SLI was limited. Maximal SLI was obtained if irradiated MW energy reach IMWE value of 650 kJ and MW intensity was over MWPL of 2 Wg^{-1}, higher value of irradiated energy or higher intensity of MW treatment caused any further increment in the SLI (Figure 1.)

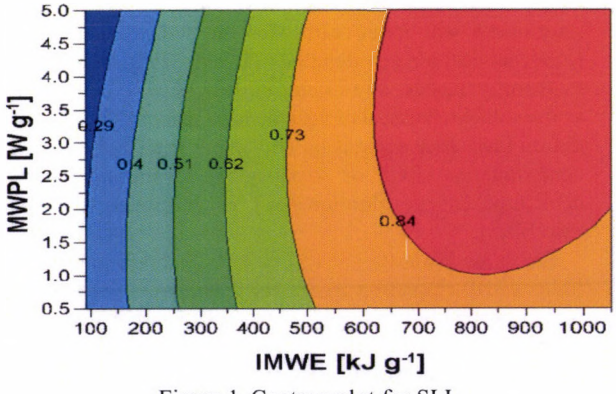

Figure 1. Contour plot for SLI

Trends of our experimental results are in good agreement with those reported by Ahn et al. [15] and Eskicioglu et al. [16], respectively; but our work was focused on the effects of different MWPL on sludge characteristic and the absolute value of differences in SLI was due to the different origin of processed sludge. Because of the strong disintegration effect of microwave irradiation on extracellular polymeric substances (EPS), which form complex sludge structure, and also on microbial cell walls has led to enhanced solubility of organic matters of food industry sludge. Degree of solubility was influenced by the preliminary treatment, increase in the absolute value of solubility was lower when secondary municipal sludge was used.

Contour plot for BDI indicate the optimum region for maximum biodegradability in IMWE range of 600-650 kJ/g, and MWPL range of 2.5-3.0 Wg^{-1}, respectively (Figure 2). Applying IMWE and MWPL at optimum level initial BDI for untreated sludge (0.21) enhanced to above 0.8 due to the microwave treatment.

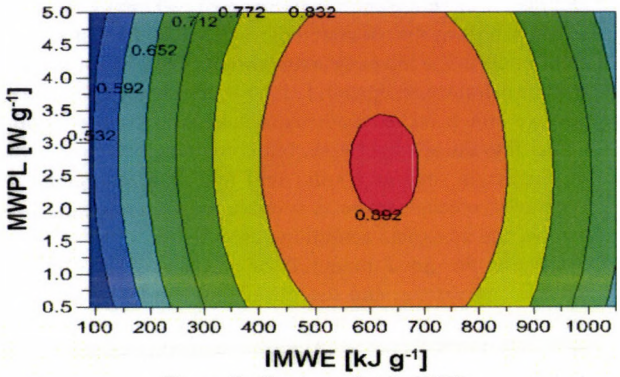

Figure 2. Contour plot for BDI

On the contrary to the results related to SLI, if the MW pre-treatment was carried out with higher intensity than the optimum region, or the irradiated energy was higher than that of it, a decreasing of BDI occurred. Results of RSM show that the degradation effects of MW pre-treatment were limited due to the demineralization effects. These effects play a significant role in the worsened biodegradability after high intensity MW irradiation of high water contented sludge. Additionally, in the materials containing carbohydrates and proteins, such as the investigated sludge, Maillard reactions can be take place under high temperature treatments which can manifested in an inhibited decomposition.

4. Conclusion

In present work the effects of MW pre-treatments on the biodegradability of organic matters, and biogas product from meat processing wastewater sludge (MPWS) were examined. To quantify the change in the solubility of organic matter of sludge and in the degree of biodegradability the solubilization index (SLI) and the biodegradation index (BDI) were developed. Defined SLI and BDI as control parameters, effects and significance of irradiated microwave energy (IMWE) and microwave power level (MWPL) were investigated with experimental design and response surface methodology (RSM).

Our results show, that MW pre-treatments could increase the biodegradability of organic matters of MPWS. However, over a certain value of MWPL and IMWE the degree of aerobic degradation and also the biogas production was worsened. Experimental results verified, that defined solubility index (SLI) and biodegradability index (BDI) is suitable to quantify the change of physicochemical characteristics and bioavailability of organic matter fraction of sludge. Based on the results of response surface modeling (RSM) optimum region for maximum biodegradability was determined in IMWE range of of 600-650 kJg^{-1}, and MWPL range of2.5-3.0 Wg^{-1}, respectively. It can be summarized, that the MW pre-treatments could be advantageous in numerous process based on biological transformation, such as activated sludge recycling processes, composting and anaerobic digestion.

Acknowledgements

This project was supported by the János Bolyai Research Scholarship of the Hungarian Academy of Sciences.The members of research group are thankful for the financial support provided by the Hungarian Scientific Research Fund (OTKA), under contract number K105021. This research was realized in the frames of TÁMOP 4.2.4. A/2-11-1-2012-0001 „National Excellence Program – Elaborating and operating an inland

student and researcher personal support system convergence program" The project was subsidized by the European Union and co-financed by the European Social Fund.

References

[1.] Neyens E., Baeyens J.: 2003. A review of thermal sludge pre-treatment processes to improve dewaterability. Journal of Hazardous Materials B, Vol. 98, pp. 51-67. http://dx.doi.org/10.1016/S0304-3894(02)00320-5

[2.] Clark D .E., Folz D., West J. K.: 2000. Processing materials with microwave energy. Materials Science and Engineering A287, pp. 153-158

[3.] Beszédes S., László Zs., Szabó G., Hodúr C.: 2009. Examination of the effect of microwave irradiation on the biodegradable and soluble fraction of organic matter of sludge. Annals of Faculty of Engineering Hunedoara-International Journal of Engineering, Vol. 7(4), pp. 87-90

[4.] Géczi G., Horváth M., Kaszab T., Alemany G. G.: 2013. No majdor differences found between the effects of microwave-based and conventional heat treatment methods on two different liquid foods. PLOS ONE Vol. 8(1), pp. 1-12 http://dx.doi.org/10.1371/journal.pone.0053720

[5.] Park B., Ahn J. H., Kim J., Hwang S.: 2004. Use of microwave pretreatment for enhanced anaerobiosis of secondary sludge. Water Science and Technology, Vol.50, pp.17-23.

[6.] Lakatos E., Kovács AJ., Neményi M.: 2005. Homogenious microwave field creation. Hungarian Agricultural Engineering, Vol. 18, pp. 80-81

[7.] Banik S., Bandyopadhyay S., Ganguly S.: 2003. Bio-effects of microwave-a brief review. Bioresource Technology, Vol. 87, pp. 155-159 http://dx.doi.org/10.1016/S0960-8524(02)00169-4

[8.] Beszédes S., László Zs., Szab, G., Hodúr C.: 2011. Effects of microwave pretreatments on the anaerobic digestion of food industrial sewage sludge. Environmental Progress and Sustainable Energy, Vol. 30, pp. 486-492 http://dx.doi.org/10.1002/ep.10487

[9.] Tang B., Yu L. F., Huang S. S., Luo J. Z., Zhuo Y.: 2010. Energy efficinecy of pretreating excess sewage sludge with microwave irradiation. Bioresource Technology Vol. 101(14), pp. 5092-5097. http://dx.doi.org/10.1016/j.biortech.2010.01.132

[10.] Appels L., Houtmeyers S., Dereve J., Van Impe J., Dewil R.: 2013. Influence of microwave pre-treatment on sludge solubilization and pilot scale semi-continuous anaerobic digestion. Bioresource Technology Vol. 28, pp. 598-603. http://dx.doi.org/10.1016/j.biortech.2012.11.007

[11.] Climent M., Ferrer I., Baeza M., Artola A., Vazquez F., Font F.: 2007. Effects of thermal and mechanical pretreatments of secondary sludge on biogas production under thermophilic conditions. Chemical Engineering Journal Vol. 133, pp. 335-342. http://dx.doi.org/10.1016/j.cej.2007.02.020

[12.] Park W. J., Ahn J. H., Hwang S., Lee C. K.: 2010. Effect of output power, target temperature, and solid concentration ont he solubilization of waste activated sludge using microwave irradiation. Bioresource Technology Vol. 101, pp. 13-16 http://dx.doi.org/10.1016/j.biortech.2009.02.062

[13.] Toreci I., Kennedy K, J., Droste R. L. 2009. Evaluation of continuous mesophilic anaerobic sludge digestion after high temperature microwave pretreatment. Water Resource Vol. 43, pp.1273-1284

[14.] Sólyom K., Mato R. B., Perez-Elvira S. I., Cocero M. J.: 2011. The influence of the energy absorbed from microwave pretreatment on biogas production from secondary wastewater sludge. Bioresource Technology Vol. 102(23), , pp. 10849-10854. http://dx.doi.org/10.1016/j.biortech.2011.09.052

[15.] Ahn J. H., Shin S. G., Hwang S.: 2009. Effect of microwave irradiation on the disintegration and acidogenesis of municipal secondary sludge. Chemical Engineering Journal Vol. 153, pp. 145-150. http://dx.doi.org/10.1016/j.cej.2009.06.032

[16.] Eskicioglu C., Kennedy K. J., Droste R. L.: 2006. Characterization of soluble organic matter of waste activated sludge before and after thermal pretreatment. Water Research Vol. 40, pp. 3725-3736 http://dx.doi.org/10.1016/j.watres.2006.08.017

HUNGARIAN AGRICULTURAL ENGINEERING
N° 27/2015 46-50
Published online: http://hae-journals.org/
HU ISSN 0864-7410 (Print) / HU ISSN 2415-9751(Online)
DOI: 10.17676/HAE.2015.27.46

PERIODICAL OF THE COMITTEE OF AGRICULTURAL AND BIOSYSTEM ENGINEERING OF
THE HUNGARIAN ACADEMY OF SCIENCES
and
SZENT ISTVÁN UNIVERSITY
Faculty of Mechanical Engineering

DEVELOPMENT OF A NOVEL MIXED FLOW DRYER DESIGN

Author(s):
F. Weigler – H. Scaar – G. Franke – J. Mellmann

Affiliation:
Department of Postharvest Technology, Leibniz Institute for Agricultural Engineering Potsdam-Bornim, Max-Eyth-Allee 100, Potsdam 14469, Germany

Email address:
fweigler@atb-potsdam.de, hscaar@atb-potsdam.de, gfranke@atb-potsdam.de, jmellmann@atb-potsdam.de

Abstract

Mixed flow dryers (MFD) are widely used in agriculture for the drying of various crops including maize and rice. As compared to other drying methods in the industrial drying, mixed flow dryers still have considerable potential for improving energy efficiency. The comparatively high primary energy consumption is mainly caused by uneven drying, which, in turn, is caused less by poor dryer control rather than by unfavorable dryer design. In order to optimize the processes in agricultural engineering, such as the mixed flow dryer, numerical methods are being increasingly used. Optimizing of the dryer geometry provides a high potential to further increase the efficiency of MFD.

Keywords

Mixed Flow Dryer, grain drying, numerical methods, experimental validation

1. Introduction

The majority of research papers published on mixed-flow drying were focused on how to increase the dryer performance and to save product quality, e. g. by improving the dryer control. Bruce [1] applied a multiple-bed computer simulation to model the dryer as a series of concurrent and counter-current elements. This model was successfully employed to predict the general behavior of the dryer and the influence of operating variables on dryer performance.

Early studies on the influence of different air duct geometries on the particle flow have been carried out by Maltry [2] and Klinger [3] using colored grains. However, their conclusions are just based on qualitative analyses. Chaabouni et al. [4] examined the bulk movement in MFD based on a residence time analysis with colored tracer particles. As they could demonstrate experimentally for the first time, the particles in the center of the dryer flow faster as particles close to the wall. To study segment processes and to mathematically model the MFD, relatively few work was done so far. Cenkowski, Miketinac, and Kelm [5] simulated and measured airflow patterns and isobars in a full-scale section of a conventional mixed-flow dryer. The differential equation system derived was solved using the finite element method. Even though a semi-empirical relationship for a static bed was implemented, the authors achieved an acceptable agreement with the measurements.

More recently, the number of papers related to basic research on MFD increased. Cao et al. [6] used a simulation model in order to investigate the effect of structural and operating parameters on the performance and energy consumption of a mixed-flow grain dryer. The conducted simulations were based on a two-dimensional dryer model which has been developed in a previous work. The authors put special emphasis into the study of the effect of structural parameters such as size and shape of air ducts, spacing between air ducts, number of rows of air ducts, and column height. As they revealed, small air ducts are better than large air ducts, amongst others.

Kocsis et al. [7] reported on experimental findings of the influence of air ducts and side walls on grain flow. Particle velocity and mass flow distributions were measured at a MFD test station equipped with a transparent acrylic glass front wall. As could be demonstrated the particle flow through the center of the dryer is faster than at the side walls. In order to investigate the bulk motion and thus the distributions of the particle velocity and the residence time in a MFD precisely, Iroba et al. [8] and Weigler et al. [9] developed two-dimensional models based on the Discrete Element Method (DEM). Using the discrete calculations particle trajectories in a mixed flow dryer were determined. The model predictions confirmed the experimental results obtained from particle flow measurements and certified that particles in the center of the dryer flow faster than those in the near wall regions. This phenomenon is known as core flow effect causing inhomogeneous particle flow. As a consequence, non-uniform drying occurs which is characterized by strong fluctuations of the grain moisture distribution over the cross section at the dryer outlet [10]. Particles having a higher velocity and lower residence time are under-dried, while particles with a lower velocity and, thus, a high residence time are over-dried. Therefore, it is necessary to optimize the geometry of the mixed flow dryer apparatus and to improve the drying process. In this way, drying costs and quality losses due to over-drying can be reduced and the formation of mold and toxins in storage due to under-drying can be avoided.

The present paper is aimed to evaluate the new developed design with respect to medium flow. For it, the experimental and numerical results obtained for the traditional and new design are compared with each other. The advantages and disadvantages of the new geometry are discussed.

The optimized dryer design should include the following enhancements:

- multi-stage product cross mixing,
- increasing the heat and mass transfer and thus,
- increasing the drying capacity,
- reduction of energy consumption,
- homogeneous drying conditions and thus,
- uniform product quality.

Through product-specific optimization of the novel dryer geometry and multi-stage product cross mixing drying performance compared to the traditional design can be significantly increased. The aim is to develop a high-performance dryer.

2. Numerical methods

The MFD which is analyzed consists of a vertical drying shaft, in which the inlet and outlet air ducts are horizontally arranged (Figure 1 and 2). The drying air flow is controlled by the staggered inlet and outlet air ducts. The material is charged from the top of the dryer and flows vertically downwards by gravity. The discharge device on the bottom of the dryer regulates the product mass flow rate.

Discrete Element Method (DEM)

The DEM describes the mechanical behaviour of bulk materials based on discrete structures (single particle). As compared to the finite element or finite volume method, the DEM works without any grid matrix. In the calculation the flow behavior of the bulk material is specified with Newton's law to the particles and a force-displacement law at the contacts between them. The mechanical behavior of an assembly of particles is described by tracing the movement of individual particles. The DEM was introduced by Cundall [11] and then applied to soils by Cundall and Strack [12]. It computes the particle flow numerically by an explicit time integration scheme with suitable boundary and initial conditions. In this work, a commercial software called PFC 2D© was used to simulate the solid mass flow in MFDs on a discrete way. To describe the real behavior of wheat particles, clumps were formed from spheres which are connected with each other. Every clump has an ellipsoidal shape and a length of 5.6 mm and a high of 3 mm. The mechanical properties of the clumps correspond to those of grains according to Mühlbauer [13].

Computational Fluid Dynamics (CFD)

The commonly used method for CFD calculations is the Finite Volume Method (FVM). This method calculates the fluid flux properties of the investigated system by the conservation laws for mass, momentum and energy. To discretize the differential equations, a grid matrix of the computational domain (called mesh) was created. Thereafter, boundary and initial conditions were defined for the borders of the domain, and the conservation equations were approximated to the mesh by the Gaussian Integral Theorem. When calculating the air flow in MFD, the bed was considered as a porous medium. The porosity of the bulk grain has been determined according to Matthies [14]. The specific pressure drop was determined using the Ergun equation based on measured values. For the inlet air ducts, an experimental determined flow velocity was used as initial condition for the air flow.

3. Experimental investigation

The experimental investigation of traditional and the newly developed geometries were performed on pilot-scale dryers at the Leibniz Institute for Agricultural Engineering. For this purpose, two traditional geometries were examined having the following geometric differences (see Figure 1 a, b):

- roof size
- roof number
- distance between the roofs.

The two dryers with traditional geometry consist of a vertical shaft with a height of about 2 m, a width of 0.6 m and a depth of 0.4 m. Roof-shaped ducts for inlet and exit air were uniformly arranged in the dryer shaft. Horizontal rows with half air ducts on the side walls alternate with those without half air ducts.

The traditional geometry 1 (see Figure 1a) is characterized by large roofs with a large distance between the roofs resulting in a low number of air ducts. As compared to industrial scale, this dryer has a reduced shaft dimension while maintaining the original roof size. Hence, it represents a sector of an industrial dryer. The traditional geometry 2 (see Figure 1b) is characterized by small roofs with a low distance between the roofs and a resulting high roof number. This dryer is a scaled (1:5) industrial dryer.

The dryer with the newly developed geometry (Figure 1c) consists of a vertically arranged dryer shaft with inclined walls. The direction of inclination of section changes from section to section. The dryer shaft has a height of about 2 m, width of 0.74 m, a total with a useful width of 0.6 m and a depth of 0.4 m. The air ducts are triangular in shape and arranged in horizontal rows. One section consists of 3 air duct rows. Each row consists of 6 full and 1 half air duct. The sections are alternately turned by 180°.

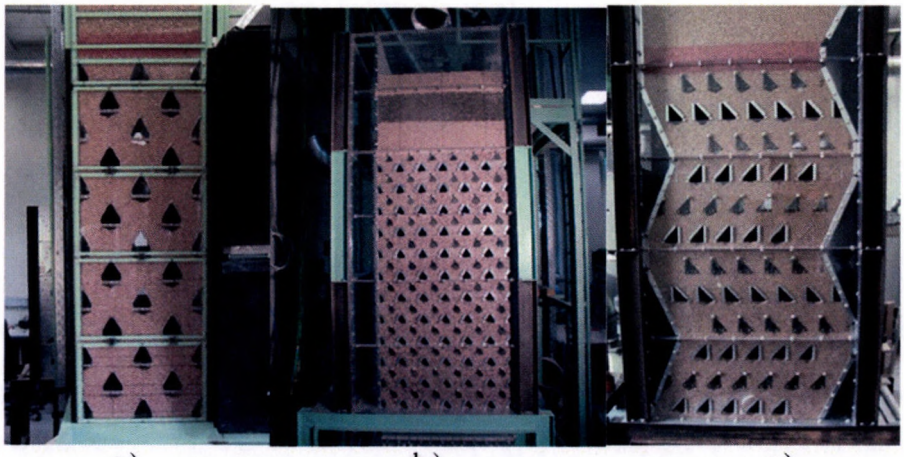

a.) b.) c.)

Figure 1. Experimental pilot scale dryers at ATB Potsdam:
a) traditional geometry 1, b) traditional geometry 2, c) newly developed geometry

The test dryers are equipped with a pneumatically operated discharge gate providing an even grain flow over the cross-section. The front wall of the grain flow study equipment is made of transparent acrylic glass (Figure 1) enabling to visually observe the movement of the particles. Coloured wheat was used as tracer particles. To measure the particle velocity profiles a digital video camera was employed. Wheat was used as bed material with an average moisture content of about 14 % w. b. and a bulk density of 780 $kg \cdot m^{-3}$.

At the beginning of the experiments, the dryer was completely filled with wheat and then emptied by using the discharge system. To observe the particle motion, a horizontal layer of coloured (red or black) wheat grains with a height of 150 mm was applied on top of the grain bed. The reproducibility of the experiments was confirmed by repeating the experiments. The tests were carried out to compare the particle flow profiles of the coloured particles.

4. Results

Figure 2 shows an experimental (a) and a numerical (b) discharge process observed and simulated at geometry 1, respectively, illustrating the resulting flow profile in the dryer. As can be clearly seen from the pictures, a pronounced particle velocity distribution was formed over the dryer width showing a so-called V-shaped profile. This means, the grains in the centre of the dryer flow faster than those near the side walls. This flow profile is caused by the interaction between the particles and the side walls with half air ducts. The big size of the roofs and the large spacing's between them favour the enormous forming of the profile.

As the simulated particle trajectories illustrate (Figure 2c), streaks of particles exist between the ducts without any cross-mixing over the dryer height. Considering the actual airflow distribution, this channelling and the different residence times between the centre and wall regions will result in a non-uniform moisture distribution at the dryer outlet.

Similarly, Figure 3 shows an experimental (a) and a numerical (b) flow profile obtained at geometry 2 of the test dryer. Again, two flow zones are visible in the dryer: a relatively wide core flow region in the center and the near wall regions with a pronounced velocity distribution. However, due to the smaller roofs and the lower spacing's between them, the core zone is more pronounced as compared to geometry 1 consisting of a more homogeneous flow profile. The near-wall flow profiles are due to the interaction of the grain with the dryer wall and the half air ducts. As the simulated particle trajectories illustrate (Figure 3c), streaks of particles exist between the ducts without any cross-mixing over the dryer height.

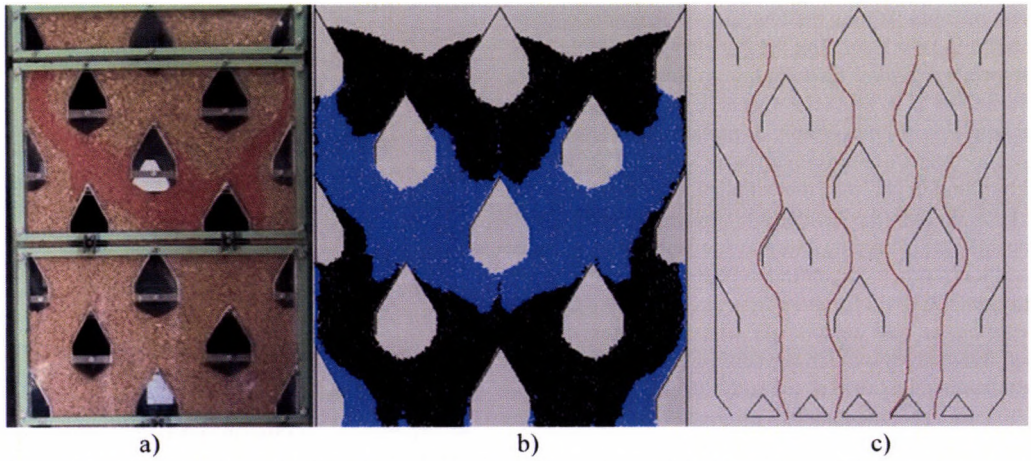

a) b) c)

Figure 2. Particle flow investigations for geometry 1: a) Experimental. b) Numerical. c) Particle trajectories.

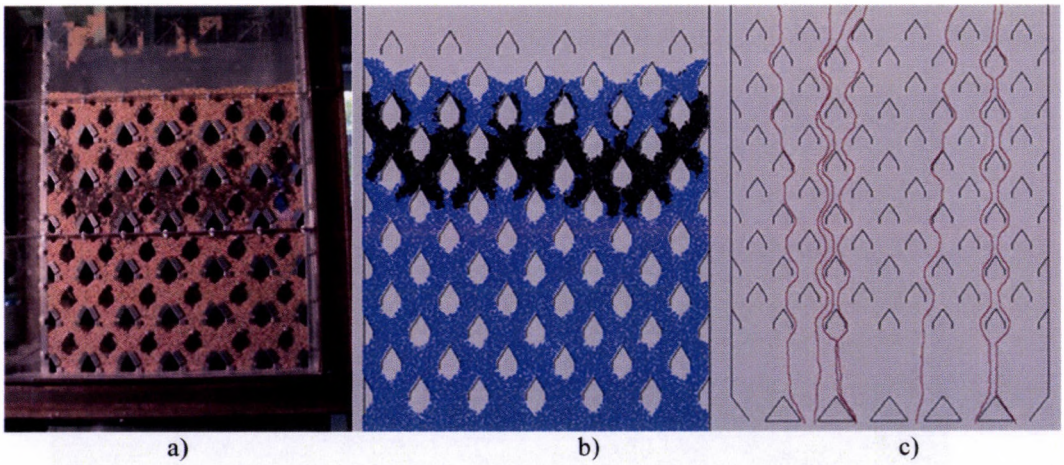

a) b) c)

Figure 3. Particle flow investigations for geometry 2: a) Experimental. b) Numerical. c) Particle trajectories.

As the particle flow investigations revealed, a flow profile also exists over the depth of the dryer. The tracer particles inside the dryer were observed to flow much faster than those at the transparent acrylic glass front wall. This means, that a flow profile was formed over the entire cross section of the dryer comparable to the core flow in a silo.

The numerical and experimental results obtained from the particle flow investigations revealed that wall friction has a large

effect on the grain flow in MFD. The results show that two regions exist: a near wall region and a central region. Grains in the center of the dryer have higher velocities and are delivered faster while grains close to the side walls have reduced velocities because of wall friction. As the comparison between simulated and experimental results showed as well, the Discrete Element Method can adequately predict the main features of particle flow. Therefore, it is possible to obtain particle trajectories from numerical studies.

The investigations of the air flow for the horizontal configuration shows, that the inlet air from an inlet-air duct will be distributed to the 4 surrounding outlet-air ducts, in which the air-stream to the lower outlet-air ducts is higher than to the upper one. The different residence times of the particles between center and wall region in the dryer result in a moisture distribution at the discharge device of the dryer. These effects were increased by the different flow velocities in the dryer.

5. Newly developed geometry

In the drying group of the Leibniz Institute for Agricultural Engineering Potsdam-Bornim (ATB), a new dryer geometry for the MFD [15] was developed (Figure 4a). The new geometry consists of a vertically arranged drying shaft with inclined walls and variable replaceable air ducts. The side walls of the dryer section are inclined to the vertical by a certain angle θ. This angle corresponds to the angle of inclination of the diagonals axes running through the centers of the roofs. The direction of wall inclination changes after each dryer section. Therefore, the direction of the particle flow paths varies from section to section. The particle trajectories are parallel to the diagonal rows of ducts, resulting in an alternating flow around hot inlet and cold exit air ducts (Figure 4b). This increases drying uniformity. The complementary angle of θ is greater than the angle of repose of most bulk materials, thereby, avoiding bridge formation at the side walls. In addition, the new apparatus design includes a multi-stage product cross-mixing. This is attained by a lateral displacement of the air duct rows at the interfaces between the sections. The multi-stage product mixing has multiple advantages: the drying potential of the air is by far better utilized, strains of moist particles are resolved, the drying conditions are homogenized and, hence, the drying efficiency is increased.

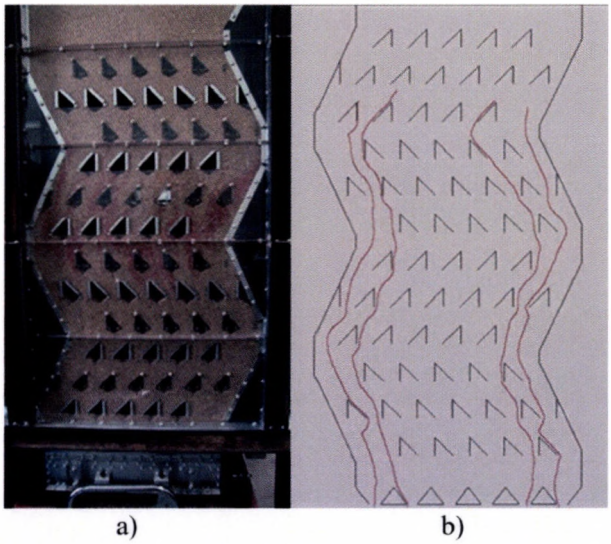

Figure 4. Particle flow investigations at the new geometry: a) Experimental. b) Particle trajectories.

With this arrangement, a systematic generation of regions with low particle velocity near the dryer walls is possible since the inclination increases the wall friction effect. If air ducts are removed in addition, regions with low air velocity occur near the wall. By adjusting particle and air velocities in the near-wall regions and in the center of the dryer, drying uniformity and particle moisture distribution are homogenized over the dryer cross section.

6. Conclusion

Experimental and numerical studies on particle flow were conducted to investigate the influence of design elements and to develop the new dryer design. As the results show, the particle flow distribution strongly depends on the dryer shaft and the discharge device. The experiments and simulation of the particle flow of two traditionally designed MFD with grain-shaped particles shows the expected behavior, that the particle flow through the center of the dryer has a higher velocity and lower friction effect. The long tail at the walls revealed the influence of wall friction and the half air ducts positioned directly at the side walls on the grain flow. As a consequence, grains have different residence times resulting in a non-uniform moisture distribution at the outlet of the dryer. Therefore, the shape and arrangement of the air ducts as well as the discharge device require further development to achieve a homogeneous particle flow distribution.

Against this background, our institute designed a new geometry for a MFD. The new design is characterized by sectional inclined side walls and triangular shaped air ducts. The zigzag pattern of the dryer and removable air ducts allow for creating regions with different particle and air velocities. In comparison with the traditional MFD geometry, thereby, we are able to generate regions with low air flow and low particle velocity near the dryer walls and regions with high air flow and high particle velocity in the center of the dryer. As a result, the drying conditions can be adjusted in different parts of the dryer. Hence, the drying process is homogenized. With the newly developed geometry, it is possible to locally adjust both particle and air velocities so as to counteract over-drying near the walls. The multi-stage product cross-mixing increases the drying efficiency. With a homogenized drying, energy can be saved and also the product quality can be improved. The new dryer geometry is further investigated in a succession project.

Acknowledgements

The authors gratefully thank the German Federal Ministry of Education and Research (BMBF) for funding this work (Project No. FKZ02PK2158).

References

[1.] Bruce D. M.: 1984. Simulation of Multiple-Bed Concurrent-, Counter-, and Mixed-Flow Grain Driers. Journal of Agricultural Engineering Research, 30, pp. 361-372. http://dx.doi.org/10.1016/S0021-8634(84)80037-2

[2.] Maltry W.: 1966. Einige Untersuchungen zur Aufklärung des Verhaltens von Getreide im Dächer-Schachttrockner. Archiv für Landtechnik 5(3), pp. 223–264

[3.] Klinger J.: 1977. Einige thermodynamische und strömungstechnische Untersuchungen zur Modellierung der Vorgänge in Dächerschachttrocknern für Getreidekörner; Ph.D. Dissertation, TU Dresden

[4.] Chaabouni M., Flick D., Techasena O.: 1992. Particles flow in industrial grain driers. Drying '92. In A. S. Mujumdar (Ed.), Proceedings of the 8th International drying Symposium (IDS'92),

Montreal, Canada, August 2-5, 1992 (pp. 1409 - 1418). Amsterdam: Elsevier Science Publishers B.V.

[5.] Cenkowski S., Miketinac M., Kelm A.: 1990. Airflow Patterns in a Mixed-Flow Dryer. Journal of Canadian Agricultural Engineering, 32, pp. 85-90.

[6.] Cao C. W., Yang D. Y., Liu Q.: 2007. Research on Modeling and Simulation of Mixed-Flow Grain Dryer. Drying Technology, 25, pp. 681-687. http://dx.doi.org/10.1080/07373930701290951

[7.] Kocsis L., Teodorov T., Mellmann J., Gottschalk K., Mészáros C., Farkas I.: 2008. Analysis of Grain Flow Experiments in a Mixed-Flow Grain Dryer. In Proceedings of the 17th World Congress of International Federation of Automatic Control (IFAC). Seoul, Korea, July 6-11, 2008, pp. 1608-1612.

[8.] Iroba K. L., Mellmann J., Weigler F., Metzger T., Tsotsas E.: 2011. Particle velocity profiles and residence time distribution in mixed-flow grain dryers. Granular Matter 13, pp. 159–168. http://dx.doi.org/10.1007/s10035-010-0222-7

[9.] Weigler F., Scaar H., Mellmann J.: 2012. Investigation of particle and air flows in a mixed flow dryer. Drying Technology 30 (15), pp. 1730–1741. http://dx.doi.org/10.1080/07373937.2012.703742

[10.] Mellmann J., Iroba K. L., Metzger T., Tsotsas E., Mészáros C., Farkas I.: 2011. Moisture Content and Residence Time Distributions in Mixed- Flow Grain Dryers. Biosystems Engineering 109, pp. 297–307. http://dx.doi.org/10.1016/j.biosystemseng.2011.04.010

[11.] Cundall P. A. 1971. A computer model for simulating progressive large scale movements in blocky rock systems, Proceedings of the symposium of the international society of rock mechanics (Nancy France), Vol. 1, Paper No. II-8

[12.] Cundall P. A., Strack O. D. L.: 1979. A discrete numerical model for granular assemblies, Geotechnique, 29(1), pp. 47-65. http://dx.doi.org/10.1680/geot.1979.29.1.47

[13.] Mühlbauer W.: 2009. Handbook of Grain Drying; AgriMedia Verlag: Clenze, Germany, 2009.

[14.] Matthies H. J.: 1956. Der Strömungswiderstand beim Belüften landwirtschaftlicher Erntegüter. Aus den Arbeiten des Institutes für Landmaschinen der Technischen Hochschule Braunschweig

[15.] Mellmann J., Weigler F., Scaar H., Teodorov T.: 2011. Dächerschachttrockner zur Trocknung von Schüttgut (Mixed-flow dryer for drying of bulk solids). European patent, EP 11180103

HUNGARIAN AGRICULTURAL ENGINEERING
N° 27/2015 51-55
Published online: http://hae-journals.org/
HU ISSN 0864-7410 (Print) / HU ISSN 2415-9751(Online)
DOI: 10.17676/HAE.2015.27.51

PERIODICAL OF THE COMITTEE OF AGRICULTURAL AND BIOSYSTEM ENGINEERING OF
THE HUNGARIAN ACADEMY OF SCIENCES
and
SZENT ISTVÁN UNIVERSITY
Faculty of Mechanical Engineering

COMPARISON OF GALA MUST APPLE QUALITY GROWN ON DIFFERENT TREE TRELLISES

Author(s):
Gy. Csima[1] – Zs. Varga[1] – G. Ficzek[2] – I. G. Gyökös[2] – Z. Láng[1]

Affiliation:
[1]Technical Department, Faculty of Horticultural Sciences, Corvinus University of Budapest, Villányi street 29-43., H-1118
[2]Department of Pomology, Faculty of Horticultural Sciences, Corvinus University of Budapest, Villányi street 29-43., H-1118

Email address:
gyorgy.csima@uni-corvinus.hu, zsofia.varga@uni-corvinus.hu, gitta.ficzek@uni-corvinus.hu, imregergo.gyokos@uni-corvinus.hu, zoltan.lang@uni-corvinus.hu

Abstract

The aim of this project was to compare the effect of different trellises (slender spindle, V-system and an experimental Y shape trellises) on some quality parameters of fresh market `Regal Prince´ (Syn. Gala Must) apples, which were grafted on M.9 dwarfing rootstocks. It was found that the Y-shape trellis has grown the largest and most uniform size apples meanwhile the yield per hectare was similar to that of V system. The higher cover color coverage rate, which increases the selling price, the less firmness, the higher solid (sugar) content, the earliness are in favour of Y-shape trellis.

Keywords:

trellis, apple size, quality, yield, 'Regal Prince'

1. Introduction

The increasing competition in the market and the changing preferences of consumers are resulting in increased demand for excellent quality apple (Malus × domestica Borkh.) fruits [1]. In the main apple producing countries of the world 'Gala' is favored by both growers and consumers, but in the European apple producing countries the size and color of fruits do not develop until the optimal harvest date, which often causes trouble. Because of this the harvest is often delayed, nevertheless it have negative effect on fruit quality (flesh firmness, storability), and it increases the risk of fruit crack [2].

Use of trellises enable advantageous limb structure of branches (optimal assimilation) in one (or more) plane(s), so prevent damages due to strong wind and increase early production. It is important to note, that the position of fruits inside the canopy basically affects fruit development, especially the development of size and color [3]. And last, but not least, the use of trellises make easier the chemical plant protection and handling of plants (pruning, thinning, etc.), ease the automation of irrigation and fertilization and enables the mechanization of harvesting [4, 5, 6, 7]. Higher returns due to early production of high density apple orchards are breaking even in 6-7 years compared to 10-12 years for traditional plantations. The trellises are usually constructed in "V" shape [8], but it seems to be the most successful a single plane of posts with 2-4 wires. The effect of different canopy shapes to yield were compared in preview studies in case of 'Golden Delicious' [9], 'Royal Gala' [9, 10]; and Jonagold' [11].

2. Materials and methods

Experimental plantation

Experiments were started in 2007 in Hungary on a newly planted orchard plot in the near of Soroksár on 0.1755 ha on the experimental farm of Corvinus University of Budapest. The aims were to reduce manpower demand by using special tools and machines in delicious quality apple plantation and also to grow larger and more uniform size fruits.

The plantation was divided in three plots. In the first plot 'Regal Prince' (Syn. Gala Must) saplings on M.9 rootstock were grown on V-system (V shaped) trellis on 0.054 ha, in the second one the same type apple saplings were grown on slender spindle (I shaped) trellis on 0.054 ha and in the third plot also Gala Must saplings were grown on a new trellis, called Y shaped (Figure 1) on 0.0675 ha. To distinguish the trellises the slender spindle trellis by I, the V-system was marked by the letter V and the new trellis by Y. In case of Y-shape trellis the consoles of with incline in 20 grade to the horizon were fitted on both sides of the central poles. The saplings fixed on Y canopy to the wires alternately to the left and right (see Figure 1.).

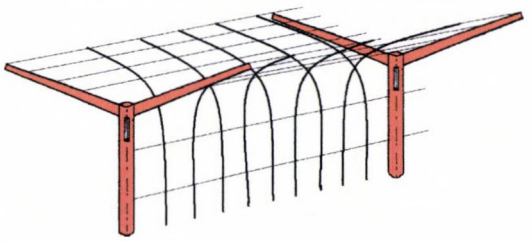

Figure 1. Schematic view of experimental Y-shape trellis system

In each plot 3 rows of 50 m length was planted, with row distances of 3.6 m, 3.6 m and 4.5 m respectively. This last one because of the post width of 2.9 m at the Y shaped trellis (Figure 2., right). Plant distances in the row were 50 cm for Y shape canopy and V-system and 100 cm for slender spindle trellis. (see Figure 2.). The saplings were fixed to the wires in all trellises. Figure 2 shows the arrangement of saplings in the row of Y canopy.

Figure 2. Slender spindle, V-system and Y shaped trellises after plantation in 2007

To be able to compare the three growing systems, in each plot the same treatment was applied for all trees (mulching, spraying, nutrition, irrigation, etc.). The tools and machines - a new top and bottom boom sprayer with droplet collecting plat, a mower adaptor for pre-pruning and a tractor town harvesting platform - were already tested [12, 13]. In this paper the value and yield of apples grown on the three trellis system are compared.

Yield measuring started already in the second year. Seven years after plantation, in the 2014 season, between 22.08. and 02.09 a series of tests were carried out including the measurement of main geometrical sizes, size distribution, fruit masses, basic and cover color, rupture stress, as well as total soluble solid (Brix%) and acid content of the fruits. Yield per tree and per hectare was also measured for each trellis.

Performed tests

For the estimation of yield fruits were harvested from the 5% of the saplings from each type of trellises. All the picked fruits were taken in view. For the quality characterization 34 apples were picked randomly from each row (3) of each type of trellises (3), which gave 102 fruits from each type of trellises and altogether 34*9=306 fruits from the plantation.

On each fruit the largest and smallest meridian diameter as well as fruit height was measured in mm with a 0.01 mm resolution Mitutoyo CD-15DC digital caliper. The harvested apples were sorted in 4 diameter groups: 75 mm and above; between 65 mm and 75 mm; between 55 and 65 mm, and smaller than 55 mm to find the distribution pattern for the three trellises.

The basic and cover color stimulus components (X, Y, and Z) of the harvested samples were measured with a Colorlite sph 850 spectrophotometer on each fruit. From he recorded data the L*, a* and b* values were calculated according to CIE 1976 color measurement standards [14]. The basic and cover color was compared in case of each trellis.

The fruit firmness was measured on the half of the samples, both on sunny and shady side of the apples with an Effegi FT-011 manual penetrometer [15] with a cylinder probe of 7/16" (approximately 11,09 mm) diameter.

From each row 17 apples were milled and mixed with a juicer. From the juice the total titratable acidity with three times of repetition for each row was determined in % malic acid with 0,1 n NaOH solution based on MSZ EN Nr 12147:1998 Hungarian Standard.

The total soluble solids (Brix%) was determined based on CODEX ALIMENTARIUS 3-1-558/93 formula using ATAGO PR-101 type digital refractometer in Brix% with three repetitions. The total soluble solid content can be corresponds to the sugar content, which is one of main taste characters. The consumer preference of fresh apple is determined by harmonious taste, which depends principally on sugar/acid ratio [16, 17]. So the ratio of total soluble solid content to total titratable acid content was calculated. If this ratio is under 15, the apple contains too much acid and or little sugar, so it is not comfortable for consumers. If this ratio value is high, above 25, the apple is sweet, but it contains very few acids, so it will lose its taste during storage, it is good only for fresh consumption.

3. Results and discussion

The fruit size distributions of the 34-34 apples from each row of each trellis (Figure 3.) clearly shows that the characteristic mean diameter of fruits harvested from experimental Y-shape trellis are significantly bigger, than in case of V-system and slender spindle trellis.

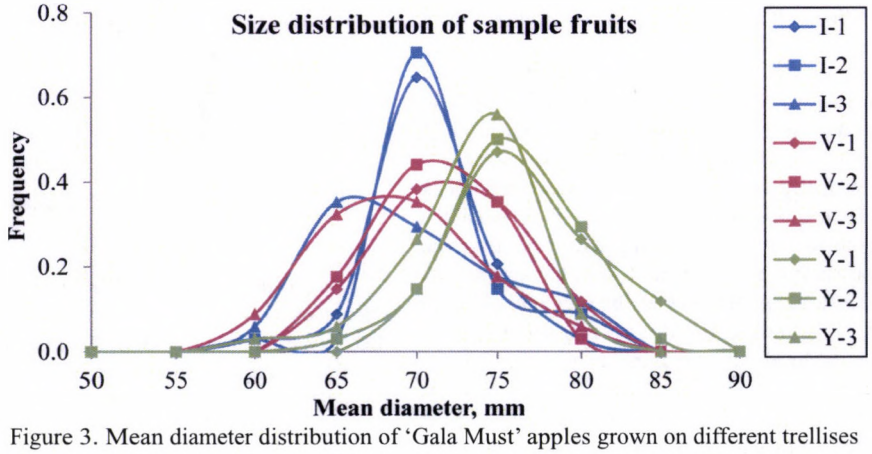

Figure 3. Mean diameter distribution of 'Gala Must' apples grown on different trellises

All the harvested apples were classified by mean diameter into four groups before storing and selling: <55 mm (for juice); 55-65 mm; 65-75 mm; and >75 mm. The size distribution of the harvested quantity (approximately 6 tones from the whole experimental plantation) is shown on Figure 4. From the illustrated data clearly seems, that the size distribution of Y-shape trellis is more homogenous between the three rows, than in case of V-system trellis. The slender spindle trellis also resulted uniform fruit size apples, but those apples were smaller, than the fruits grown on Y-shape trellis. Furthermore on Y-shape trellis the ratio of diameter sizes 55-65 mm and size under 55 mm to other size groups were the least.

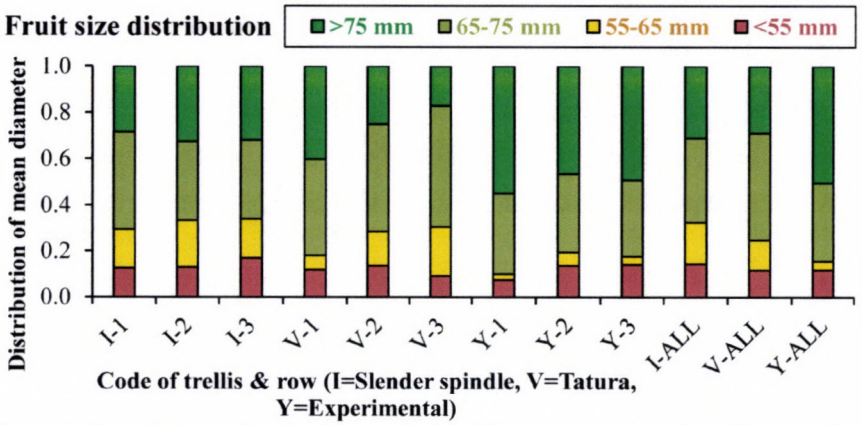

Figure 4. Mean diameter size distribution of 'Gala Must' apples grown on different trellises

The change of specific yields of applied trellises between 2008 and 2014 are illustrated on Figure 5. According to our results, on the V-system trellis the yield is clearly higher, than on slender spindle trellis contrary the results of Mika and Piskor [18], who found no significant difference between V-system and super spindle. The estimated specific proceeds were calculated also for 1 ha area for the three trellises as illustrated on Figure 6. The value of V-system is a little higher than that of Y shape trellis. The reason for the handicap of Y-shape canopy is, despite higher yield per trees and better fruit quality, the larger growing area of it (larger row distances)

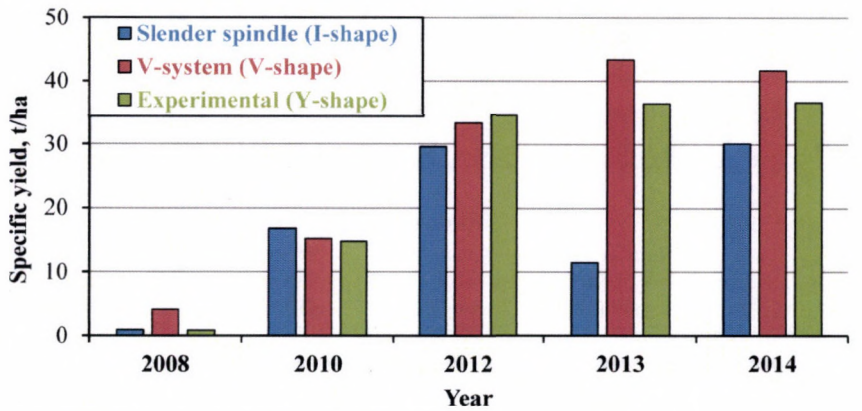

Figure 5. Change of specific yields of 'Gala Must' apple grown on applied trellises between 2008 and 2014

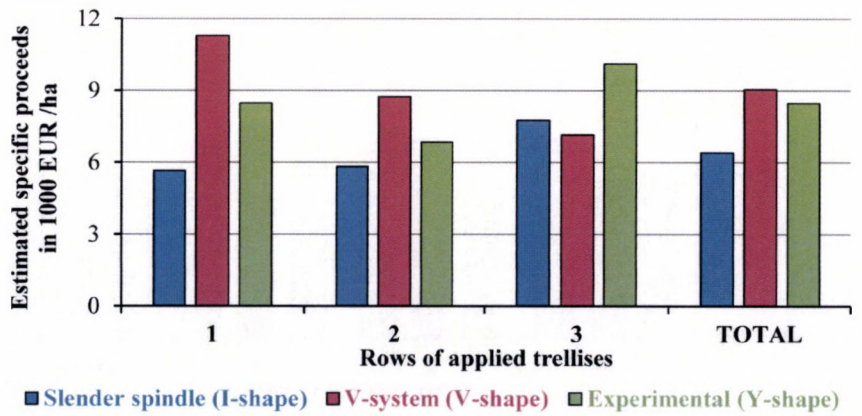

Figure 6. Estimated specific proceeds of applied trellises for 1 ha plantation area (based on the moderate HUF-EUR exchange rate of the Hungarian National Bank for term 09.01.2014. – 12.31.2014.: 1 EUR = 312.24 HUF)

The CIE L*, a* b* color parameters (Figure 7.) shows the little, not significant difference between apples growing on the mentioned trellises. The same base color was evidence of applying the same apple cultivar clone. The little differences in cover color refer to different degree of maturity.

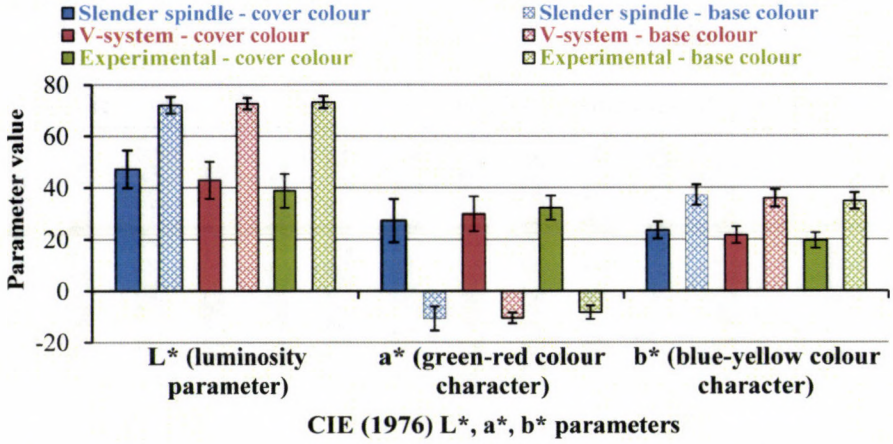

Figure 7. CIE (1976) L*, a*, b* color parameters of 'Gala Must' apples growing on different type of trellises.

Comparing the rupture stress data results (Fig. 8.), it is clear, that the fruits grown on Y-shape trellis are in average a little softer, compared to the other two trellises. Due to the beneficial canopy design of Y-shape trellis the fruits get more sunshine and light, so the fruits can be harvested earlier.

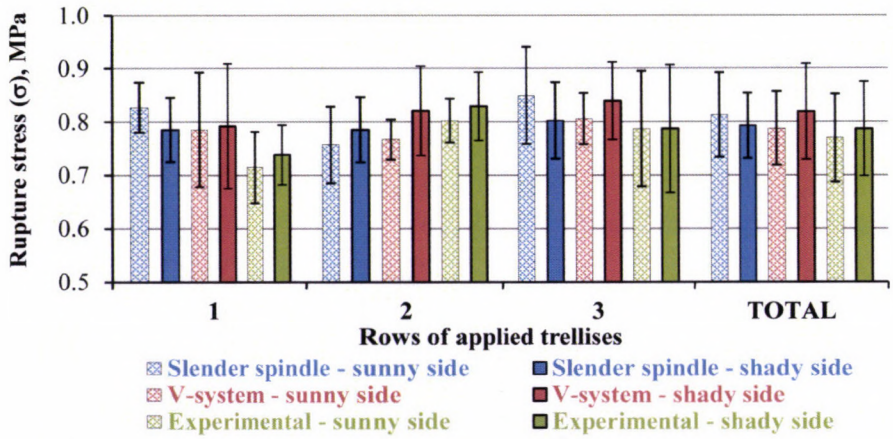

Figure 8. Rupture stress on sunny and shady side of Gala Must apples grown on different type of trellises.

The ratio of total soluble solid content (which corresponds to sugar content) to the total titratable acid content is a good marker for characterizing the taste of apple. The parameter values was about the same for the tested apples, as it seen on Figure 9. There was a little size, but clear difference between the trellises, which referred also to the degree of maturity.

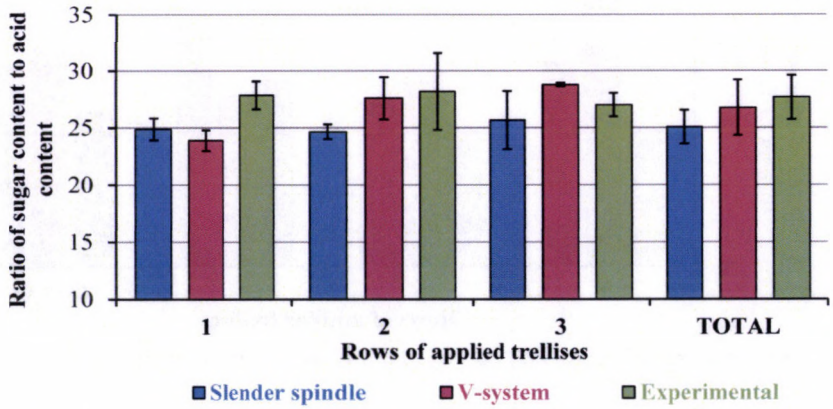

Figure 9. Ratio of sugar content to the acid content of 'Gala Must' apples grown on different type of trellises

4. Conclusion

As a result of the 2014 tests the characteristic mean diameter of Gala Must fruits harvested from Y-shape trellis are significantly larger, the size distribution is more homogenous between the rows, compared with the results on slender spindle and V-system trellis. The specific yield in t/ha in 2014 and in most of the previous years was the highest on V-system, followed by the Y-shape trellis. The explanation for this is the larger row distance of Y trellis. The higher cover color coverage rate, which increases the selling price, the less firmness, the higher solid (sugar) content, the earliness are in favor of Y trellis. The experimental Y shape trellis is a good choice for apple growers who want to produce high value apples with less manpower demand.

References

[1.] Ficzek G., Ladányi M., Radeczky Zs., Tóth M.: 2013. Healthcare values and potential uses of the new Hungarian apple varieties on the basis on fruit analysis, International Journal of Horticultural Sciences, Vol. 19., pp. 25-28.

[2.] Iglesias I., Alegre S.: 2006. The effect of anti-hail nets on fruit protection, radiation, temperature, quality and profitability of 'Mondial Gala' apples, Journal of Applied Horticulture, Vol. 8., pp. 91–100. p.

[3.] Stajnko D., Rozman Č., Pavlovič M., Beber M., Zadravec P.: 2013. Modeling of 'Gala' apple fruits diameter for improving the accuracy of early yield prediction, Scientia Horticulturae, Vol. 160., pp. 306–312. http://dx.doi.org/10.1016/j.scienta.2013.06.003

[4.] Robinson T. L. 2006. Modern apple training systems, The University of Vermont, 2006.

[5.] Fenyvesi L., Fenyvesi D.: 2008. Optimization of a Supporting Device for Mechanical Harvesting, Acta Horticulturae, Vol. 768, pp. 423-430.

[6.] Hegybíró M., Kurtán S., Láng Z., Nagy S., Wieser A.: 2013. Special Technical Knowledge in Horticulture. In: Németh Zámboriné, É., Sárosi, Sz., Horváth, L.: Modern Horticulture. Corvinus University of Budapest, Faculty of Horticultural Science, 2013.

[7.] Robinson T., Hoying S., Sazo M. M., DeMarree A., Dominguez L.: 2013. A Vision for Apple Orchard Systems of the Future, New York Fruit Quaterly, Vol. 21., pp. 11-16.

[8.] Robinson T. L.: 1998. V-Shaped Apple Planting Systems, Acta Hort. (ISHS), Vol. 513. pp. 337-348. http://dx.doi.org/10.17660/ActaHortic.1998.513.40

[9.] Widmer A., Krebs C.: 2001. Influence Of Planting Density And Tree Form On Yield And Fruit Quality Of 'Golden Delicious' And 'Royal Gala' Apples, Acta Hort (ISHS), Vol. 557. pp. 235-242. http://dx.doi.org/10.17660/ActaHortic.2001.557.30

[10.] Hampson C. R., Quamme H. A., Brownlee R. T.: 2002. Canopy Growth, Yield, and Fruit Quality of 'Royal Gala' Apple Trees Grown for Eight Years in Five Tree Training Systems, HortScience, Vol. 37., pp. 627-631.

[11.] Licznar-Małańczuk M.: 2006. Training system and fruit quality in the apple cultivar 'Jonagold', Journal of Fruit and Ornamental Plant Research, Vol. 14. pp. 213-218.

[12.] Láng Z., Kurtán S., Nagy S., Serelegi K., Sinóros-Szabó B.: 2009. Mechanization of fresh market apple production based on a special trellis, Hungarian Agricultural Engineering, Vol. 22., pp. 31-33.

[13.] Láng Z., Serelegi K.: 2010. Apple Production Trials on a Y Shaped Trellises. AgEng2010, the International Conference on Agricultural Engineering, Clermont-Ferrand, France, 6-8. September, 2010, Full paper on PD, Ref 282, 1-4

[14.] Voss D. H.: 1992. Relating colorimeter measurement of plant color to the Royal Horticultural Society Colour, Horticulturer Science, Vol. 27. pp. 1256–1260.

[15.] Abbott J. A.: 1999. Quality measurement of fruits and vegetables, Postharvest Biology and Technology, Vol. 15. pp. 207-225. http://dx.doi.org/10.1016/S0925-5214(98)00086-6

[16.] Vangdal E. 1985. Quality criteria for fruit for fresh consumption, Acta Agriculturae Scandinavica, Vol. 35. pp. 41–47.

[17.] Harker F. R., Marsh K. B., Young H., Murray S. H., Gunson F. A.. Walker S. B.: 2002. Sensory interpretation of instrumental measurements 2: sweet and acid taste of apple fruit, Postharvest Biology and Technology, Vol. 24. pp. 241–250. http://dx.doi.org/10.1016/S0925-5214(01)00157-0

[18.] Mika A., Piskor E.: 1997. Growth and cropping of dwarf 'jonagold' ('jonica') apple trees planted at the density ranged from 2,000 to 10,000 per ha and trained as slender spindle, super spindle and V-system, Acta Hort. (ISHS), Vol. 451., pp. 473-478. http://dx.doi.org/10.17660/ActaHortic.1997.451.54

HUNGARIAN AGRICULTURAL ENGINEERING
N° 27/2015 56-60
Published online: http://hae-journals.org/
HU ISSN 0864-7410 (Print) / HU ISSN 2415-9751(Online)
DOI: 10.17676/HAE.2015.27.56

PERIODICAL OF THE COMITTEE OF AGRICULTURAL AND BIOSYSTEM ENGINEERING OF
THE HUNGARIAN ACADEMY OF SCIENCES
and
SZENT ISTVÁN UNIVERSITY
Faculty of Mechanical Engineering

PRECISION PLOT SEEDER FOR MEDICINAL AND AROMATIC PLANTS – CONCEPT, DEVELOPMENT AND OPTIMISATION

Author(s):
Z. Gobor[1] – H. Heuberger[2] – R. Rinder[2]

Affiliation:
[1]Institute for Agricultural Engineering and Animal Husbandry (ILT), Bavarian State Research Center for Agriculture (LfL), Vöttinger Str. 36, Freising, D-85354, Germany
[2]Institute for Crop Science and Plant Breeding (IPZ), Bavarian State Research Center for Agriculture (LfL), Am Gereuth 2, Freising, D-85354, Germany

Email address:
zoltan.gobor@LfL.bayern.de, heidi.heuberger@lfl.bayern.de, rudolf.rinder@lfl.bayern.de

Abstract

A novel precision plot seeder for medicinal and aromatic plants was designed and built. Based on the system design-oriented development as well as the implemented state-of-the-art hardware and software solutions, it was possible to identify the problems in the early phase of the design process, to create multiple design variants, to overcome the lack of cross-disciplinary knowledge and consequently achieve savings in associated labour and material costs. The electrification should provide more accurate seed placement and continuous regulation of seed rates and row length for each row, as well as the option to generate detailed documentation about the sowing process.

Keywords

Precision plot seeder, experimental practice, digital prototyping, system based designs

1. Introduction

The Food and Agriculture Organisation of the United Nations (FAO) projected that if current patterns in food consumption will persist, 60 percent more food will need to be produced to meet the needs of the growing earth population that is expected to top the nine billion mark in 2050. Changes towards more sustainable production are required including investments in research, development and dissemination of the technologies and information in order to improve efficiency and reduce waste and pollution. The increase of the resource use efficiency, cutting the use of fossil fuels and reducing direct environmental degradation are some of the important components which can improve sustainable development in the agricultural sector [1]. Further development of methods and techniques in the field of experimental practice can positively affect the process of achieving these requirements.

The sowing equipment used in experimental practice require high degree of modularity to use it for as many crop species as possible and to be able to assess as many issues as possible within the experimental research with respect to the optimisation of the seeding process. A prerequisite is an even distribution of the defined amount of seeds over the predetermined length of a trial plot. Depending on the explicit research question, the distances between the rows, which number can vary, need to be exactly retained. Above all an accurate and steady sowing depth, an important parameter for the optimum germination [2, 3], needs to be maintained for each row on the entire plot length and ideally should be carried out automatically. The mechanisation within the experimental praxis started in second half of the twentieth century and the backgrounds and requirements for sowing equipment have been listed and evaluated by Kemp [4], Cameron et al. [5] and Hergert [6]. In that time, considerable savings in time and labour were anticipated from the newly developed machinery in regarding the manual sowing.

Medicinal and aromatic crops belong to high value specialty crops and are often established on fields by sowing. The species vary in grain size, thousand seed weight, required seed rates, shape and surface textures, strength of the bran and composition of the grain sizes. These parameters particularly affect the performance of the single-grain seed drills, as well as seeders equipped with a cone-belt distributor. Experiments with fine-grained aromatic and medicinal plants in which conventional seeders were used provided inadequate results [3].

The most of the modern agricultural machines are based on the functional principles presented in the past. However, the implementation of a powerful and often inexpensive electronics offered an expeditious development of new concepts, improvement in quality and efficiency, as well as introduction of newer, smarter ways in operator-machine interaction.

Considering the facts above and state of the art in both, the sowing technology and mechatronics, as well as the practical experiences of the employees of the Bavarian state research center for agriculture (LfL) within the field of sowing of medicinal and aromatic plants, an electrically driven precision plot seed drill was designed and built within the scope of a research project [7]. During the development the even lateral and longitudinal distribution of seeds, including fine-grained seeds regardless of the soil type and terrain configuration were particularly emphasised. Furthermore, a modular design was striven for allowing quick adaptation for sowing in shallow cultivation or rather on high dams with variable adjustable number of rows and row spacings. Additional task was to carry out the development harmonized with the Machinery Directive 2006 /42 / EC which inter alia regulates the technical requirements for electronically controlled machines. According to this topic, programmable control systems are primarily addressed within the regulation, because security strategies may be needed for agricultural and forestry mobile machines as well [8].

2. Material and methods

In the first phase a digital prototype of a sowing aggregate has been created using Autodesk Product Design Suite. The digital prototype was prepared for examining the characteristics under different conditions. In order to evaluate the functionality and assure optimisation already in the early phase of the development, kinematic simulations of the important mechanisms and force analysis has partly been carried out (see Figure 1). In the following phase a single module with a modified cone belt distributor (Fa. Wintersteiger) was built and as a mechanically driven functional model tested under real conditions. The objective was to compare the effects of a new design with the conventional coulter system. In parallel, electric actuators, sensors and controller were selected and tested under laboratory conditions to prepare the module for electrification. The electrification itself was based on a software-oriented and modular approach and the implementation of off-the-shelf, reusable components, in order to increase the efficiency of the system design. One of the biggest challenges within the field of machine development is the adoption of embedded technologies. The modular approach helps on the one hand to develop reusable components, but on the other hand significantly affects the way of the design process. Inter alia the modularity of the mechanical system needs to be reflected within the controller architecture. Although the traditional programmable logic controllers (PLCs) still play an important role within implementation in machine control systems, a decision was made to implement an embedded controller. The aim was to improve the flexibility, to assure the advantage of condition monitoring, to provide possibilities for easier upgrading than on systems with fixed logic (adaptability in term of changing I/O requirements), as well as to use advanced control techniques based on machine vision, and motion control capabilities, if necessary. The developed embedded controller is based on single-board RIO (sbRIO) platform [9] and electronic expansion circuit board for signal conditioning developed at the institute. Speed and resource trade-offs are typical issues related to programmable gate Array (FPGA)-based implementations. Generally, FPGA takes the benefits of the high execution speeds on FPGA targets but the software design requires minimisation of the resource consumption. Even with trends like multi-core, a processor-based solution will never get the parallelism offered by FPGAs [10].

Figure 1. Digital prototype (left); example of a simulation with digital prototype (middle) and physical prototype of the precision plot seeder for medicinal and aromatic plants of the LfL with five electrically driven seeding units and passive compensation of the slope inclination (right)

The complexity and the increasing number of questions and hypothesis within experimental praxis which are expected to be answered or tested require an ever increasing amount of field data. Inter alia data related to the presetting of the machine for each actual sowing scenario can be valuable, if possible shortcomings and impacts of those parameters on the expected sowing quality should be analysed. For example definition of the optimal parameters, setting and assessing the accuracy and efficiency with high temporal and longitudinal motion resolution can deliver completely new insights. Since development of a new seeder was aimed, the implementation of sbRIO offered the advantage of capturing and storing of all states, sensor and control signals with a correspondingly high sampling rate for later analysis, like in previous projects [11, 12]. On such a way comprehensive documentation of the sowing process is secured. The control software was created using NI LabVIEW Developer Suite (Real-Time (RT) and FPGA modules).

The functionality of modern machines relies on an ever greater share of control software. Because of the increasing complexity the control software must be tested at an early stage of development to avoid risk of errors in the field. Conventional design methods in mechanical engineering provide only limited software testing opportunities before the physical machine is available. The fact, that a truly multidisciplinary approach to embedded system design requires not only simulation capability within domains of mechanical, control, electrical engineering and embedded computing but also synergistically combines these disciplines [13], is well known. As the cost of computing decrease and the amount of data increase, the likelihood that applications will fail due to numerical errors accumulate. Hence, a not fully deterministic testing software (model) running under Windows which emulates the physical system was created. The aim was to replicate the operating modes and use simulated signals in order to allow demonstration of the operating sequences to the user, test of the software prior to actual commissioning including intentionally implemented failures. In a further step a more rigorous full hardware-in-the-loop (HIL) testing was carried out whereas the sensors and actuators where implemented on a test bench, to test determinism and the dynamic performance of the prototype. Finally, test under real condition were carried out and documented.

3. Results

After development of a digital prototype and optimisation based and simulation five aggregates were built. The frame of an existing vegetable planter for small seeds (Gaspardo) was used and the newly developed aggregates adapted for individual and quick setup on it. The base frame of each aggregate and the carrier of the cone-belt distributor are designed to compensate the transversal and longitudinal slope based on a gyro mechanism. Additionally, a quick adaptation for sowing in the seedbed or on dams with different heights is provided. Special mechanism for automatic triggering of the lifting device, as well as at the

individual and manual setting of the sowing depth and the coulter pressure for each unit are the most interesting feature of the novel seeder. The currently manual adjustment of the position of the gyro mechanism, of the sowing depth and of the coulter pressure can be automated. As furrow openers the practice-proven double disc coulters of the company Lemken were chosen (see Figure 1). The control electronics is housed in a robust enclosure, which at the same time has the functionality of the control panel and human-machine-interface (HMI). The control buttons and status indicators assure simple and clear structured control.

Each cone belt distributor is coupled to a stepper motor PD6-N89 - Plug & Drive (Nanotec). Stepper motors with drives are one of the most commonly used solutions for motion control. An accurate positioning without implementation of a feedback device such as encoder was possible. Depending on the used mode, up to 12800 steps per revolution can be configured. The main advantage is that a high torque can be reached already by relatively low rotational speeds. Additional advantage of the implemented motors is the method of its control. It can be carried out via network using an RS485 or CANopen protocol, or by providing the position, speed, or torque signals using separate digital inputs.

The electric drives, encoder MNI20 (Pepperl+Fuchs) and the controller were chosen and combined with the aim to provide high longitudinal sowing resolution. For the used vegetable planter which tires have a diameter of 680 mm one micro step of the drive corresponds to a motion of the seeder smaller than 1 mm in longitudinal direction. The main reason of choosing such a high accuracy is to minimise the losses of the expensive seed and to achieve higher accuracy in the longitudinal distribution. The speed of the stepper motor which drives the cone belt distribution is dynamically calculated based on the speed of the tractor and the length of the trial plot.

Typically, in case the software should intelligently respond to a stimulus such as sensor signals or HMI, using of state machines is the most powerful aspect in LabVIEW [14]. Since by using this design pattern the program execution is no longer linear, the part of the code which will be executed depends on the inputs from HMI or sensors (asynchronous discrete-time events), or the results of the current execution. Traditionally, FPGA design were limited to hardware designers, but using LabVIEW FPGA control systems designers are supported with enough "system-level" abstraction in order to deploy their designs to FPGAs [10]. Thus, a combination of an FPGA and RT software to control the sequences of the sowing cycle was developed in the form of a state machine, allowing to extend its functionality without restrictions. In the RT software sowing parameters (e.g. length of the trial plot, desired number of motor steps within one sowing cycle) can be read from the XML configuration file which is stored on a USB memory card. If required, all states of the digital inputs and outputs (I/O-s) and variables can be transmitted via FIFO from the FPGA software in RT software, to store them into a log file for further off-line analysis. One of the main drawbacks to use state machines is the difficulty to follow the program flow and because of this, debugging and tracing of errors can be in some cases tricky, particularly in time critical application where execution highlighting is not an option [14]. Thus, several models on a sub-system and system level were developed to carry out testing. The simulation models included the behaviour model, reproducing the logical behaviour of the machine and the kinematics model visualising the movement behaviour of the machine (see Figure 2).

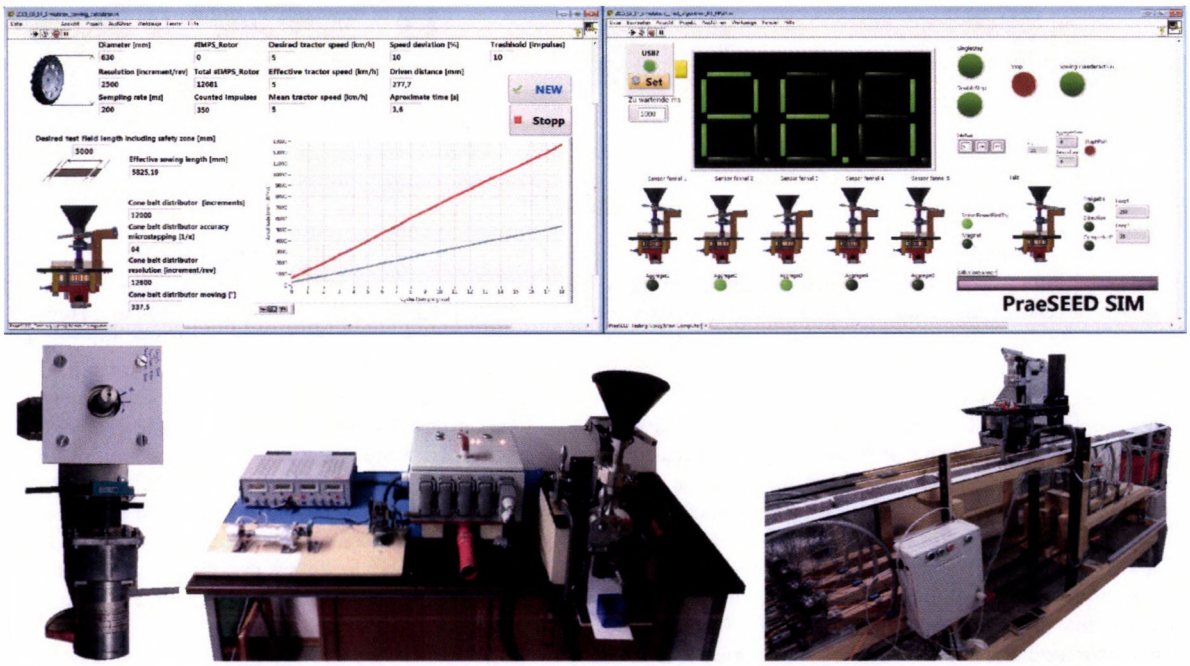

Figure 2. Front panel of the not fully deterministic testing software (simulation model) running under Windows which calculates the number steps (position) of the cone belt distributor depending on the simulated inputs (top left); front panel of the simulation model reproducing the logical behaviour of the seeder with visualisation of the movement behaviour (top right); sub-system level HIL test of the stepper motor (bottom left); HIL test of the system (bottom middle); testing of the longitudinal distribution on test bench (bottom right)

This method can be either used during development or for later revisions or bug fixes, just as well in cases when the access to the physical system or the real-time target is not possible nor desired. Applications written in G rely on more than just the compiled LabVIEW source code, meaning that it is impossible for each version of LabVIEW to produce the same numerical results as in a prior version [15, 16]. Running the same application on different platforms, also if same version of LabVIEW is used, can generate irregularities in numerical results [14]. Hence it is necessary to carry out software testing before the commissioning. Considering

the fact that the most system design errors are introduced in the original specification, but aren't found until the test phase, the early verification and validation techniques based on the models and virtual testing helped to detect the errors timely. Therefore, virtual commissioning of the control algorithm and FPGA and RT part of the software have been done by software in the loop (SIL) tests in virtual environment before uploading to the controller. (see Figure 2 top right). Further, the HIL simulation was carried out using a system-level model, which included the embedded system algorithm and the operating environment in form of a real-time simulator delivering inputs and receiving outputs from the embedded system as the real system would (see Figure 2 bottom middle). Using HIL simulation it was possible to test and verify the real-time performance of the embedded system. The main advantage of this method was a possibility to verify the logical behaviour in real time, to test operation and failure conditions that are difficult to physically replicate and to check and optimise the control software. For example the simulation showed that a manual or visual inspection may reveal the outage of one or more of the connected fennels in every sowing cycle, but this solution is suboptimal considering the number of rows and number of experiments which usually needs to be carried out in a short time consecutively. Thus, the controlling algorithm was designed to carry out self-diagnostic and if there is no outage indication, the control algorithm can move into the next stage without causing damage within the hardware or impeding the consistent transversal distribution.

Virtual commissioning allowed to test the performance under different scenarios and recognise the problems in the development stages which resulted in less debugging during the commissioning phase. In the post-processing phase of the virtual commissioning the testing results were analysed in order to implement changes and document the possible problems and differences in relation to the real installation on the prototype. Unfortunately, the experiences from practice showed that during the implementation phase additional errors and difficulties can occur which have not been detected within modelling and simulation phase because during the commissioning of a real installation mostly different topics merge. Particularly, new concerns can be induced: trough installations - requiring clarification of the components functionality; since the fact that software is always the last thing installed and its development during the commissioning is common; trough parameterisation and optimisation of the software during this phase; through errors caused by unintended network communication; as well as the acceptance test and the introduction of the novel product to the operators and the service personnel.

4. Conclusion

Historically, engineers of different disciplines worked in their departments on specific task, carrying out sequential development and making design decisions independently, resulting in longer development cycles. Today, considering the mechatronic approach the streamline is parallel development and collaboration of several teams on design, prototyping, and deployment. The fundamental aspect is to create virtual prototypes in order to explore the machines before they are built. In conventional manufacturing the commissioning is usually one of the last steps before the machine is delivered to the customer. In case, shortcomings are first realised in this phase of the project, design correction are required, causing sometimes exponential increase of the costs and undesirable changes in the time schedules.

The digital prototype enabled both the functional test of the newly developed mechanisms and assemblies, as well as analyses based on simulation. Possible design deficits were minimised through optimisation based on analysis of gained results and significantly reduced the time for the development and assembling the prototype. The tests showed a high stability and robustness of the mechanics and provided basis for the further development including electrification of the prototype (Figure 3.). The electrification was carried out based on a software-oriented and modular approach, using off-the-shelf reusable components. Thus, the efficiency of the system design was enhanced.

Using simulations with created system models, which included the FPGA and RT software models, additional insight were gained about the system behaviour, the human machine interface (HMI) and the physical and environmental aspects of the sowing process. System models allowed defining different simulation scenarios and documenting of the behaviour of the control algorithm and its systematic analyses. The analysis can reflect the completeness and integrity of the software regarding of requirements and also can be used for further design refinement. During the development design of reusable components including mechanical parts and software was aimed, in order to create and test mechatronic components in terms of modules or parts of a test bench which can be used in further projects. Both, the SIL and the HIL test allowed optimisation of the HMI based on the operators' feedback, as well as the possibility to learn the operations and how fault conditions are indicated and handled within a safe simulation environment.

The experiments under controlled conditions and virtual commissioning, only partially led to successful commissioning within the implementation phase, because only observations in a finite number of predefined and generally simplified scenarios can be carried out under such conditions. Hence, enough data needs to be collected during field tests under uncontrolled conditions to possibly identify the problematic scenarios which may not have been considered during the machine development or rather the design of simulations. By this means events and effects which couldn't be anticipated or observed previously could be explained.

Figure 3. Testing of the precision plot seeder for medicinal and aromatic plants of the LfL with electrically driven seeding units and passive compensation of the slope inclination

Acknowledgements

The authors thank to all involved employees of the Institute for Agricultural Engineering and Animal Husbandry, the Institute for Crop Science and Plant Breeding and experimental stations of the Bavarian State Research Center for Agriculture for the excellent cooperation.

References

[1.] OECD/FAO 2012. OECD-FAO Agricultural Outlook 2012-2021, OECD Publishing and FAO. http://dx.doi.org/10.1787/19991142

[2.] Ziegler K., Göbel E., Schmittmann 0., Schulze Lammers P.: 2012. Precision seed drill tests in Germany 2009-2011. International sugar journal 114/1367, 795-803

[3.] Meinhold T., Blum H., Budde M., Damerow L., Schulze Lammers P.: 2013. Partial Process-Analysis of the Sowing Process for Fine Seeds. Conference proceedings Land. TechnikAgEng 2013, 8.9. Nov. 2013 Hannover, 189-195.

[4.] Kemp, D. C.: 1966. A brassica plot seeder. Journal of Agricultural Engineering Research, 11 (2). pp. 135-147. http://dx.doi.org/10.1016/S0021-8634(66)80051-3

[5.] Cameron D., Milner J. B., Carruthers J.: 1967. An automatic self-propelled seed drill for cereal plots. Journal of Agricultural Engineering Research, 12 (2), 142-146. http://dx.doi.org/10.1016/S0021-8634(67)80008-8

[6.] Hergert G. B.: 1969. A spaced-plant seeder for cereal plots. Canadian Journal of Plant Science, 49, 642-644.

[7.] Gobor Z., Heuberger H., Rinder R.: 2014. Entwicklung und Optimierung einer Präzisionssämaschine für Heil- und Gewürzpflanzen (Feinsämereien). Mitteilung der Gesellschaft für Pflanzenbauwissenschaften Band 26 ISSN:0934-5116 pp.323-324

[8.] Zeltwanger, H.: 2013. Safety and security requirements in mobile machines, Proceedings, 1st international Mobile Machine Control (MMC) conference, Nuremberg, Germany, 12-13. Jun 2013, CAN in Automation GmbH, pp. 01-7 - 01-12

[9.] National Instruments 2014. OEM OPERATING INSTRUCTIONS AND SPECIFICATIONS NI sbRIO-9605/9606 and NI sbRIO-9623/9626/9633/9636

[10.] Kassas Z. M.: 2011. Methodologies for Implementing FPGA-Based Control Systems. Proceedings of the 18th IFAC World Congress; Milano, Italy. 28 August–2 September 2011

[11.] Gobor Z.: 2013. Data acquisition and automated data analysis in prototype development - Testing of the prototype for automated attachment of the supporting wires in hop gardens. 1st international Mobile Machine

[12.] Gobor Z.: 2015. Development of a diagnostic tool for performance analysis during the testing of agricultural implements. SCILABTEC 2015 7th International scilab user conference. Paris 21-22.05.2015

[13.] MacCleery B., Kassas Z. M.: 2008. New mechatronics development techniques for FPGA-based control and simulation of electromechanical systems. Proceedings of the 17th IFAC World Congress; Seoul, Korea. 6–11 July 2008

[14.] Bitter R., Mohiuddin T., Nawrocki M.: 2007. LabVIEW: Advanced Programming Techniques, Second Edition, CRC Press, Boca Raton London New York

[15.] Farkas I., Rendik Z.: 1997. Intermittent thin layer corn drying, Drying Technology, Vol. 15, pp. 1951-1963. http://dx.doi.org/10.1080/07373939708917340

[16.] Schmidt D.: 2010. An Introduction to Floating-Point Behavior in LabVIEW. National Instruments Corporation.

CONTENTS OF NO 27/2015